UNIVERSITAT POLITÈCNICA DE VALÈNCIA

DEPARTAMENT DE QUÍMICA

The Ro/SSA Complex in Systemic Lupus Erythematosus Patients

Ph.D. THESIS

Submitted by

Noelle Mariane do Nascimento

Ph.D. Supervisors:

Prof. Dr. Ángel Maquieira Catalá
Prof. Dr. Rosa Puchades Pla
Prof. Dr. David Giménez Romero

Valencia, febrero de 2017

ÁNGEL MAQUIEIRA CATALÁ, and ROSA PUCHADES PLA, PhD. in Chemistry and professors at the *Universitat Politècnica de València*, and DAVID GIMENEZ ROMERO, PhD. in Physical-Chemistry at the *Universitat de València*

CERTIFY:

That the work "*The Ro/SSA Complex in Systemic Lupus Erythematosus Patients"* has been developed by Noelle Mariane do Nascimento under their supervision in the Instituto Interuniversitario de Reconocimiento Molecular y Desarollo Tecnológico (IDM) at the *Universitat Politècnica de València*, as a thesis Project in order to obtain the PhD. degree in chemistry at the *Universitat Politècnica de València*.

Valencia, February of 2017

Prof. Dr. Ángel Maquieira Catalá Prof. Dr. Rosa Puchades Pla Prof. Dr. David Gimenez Romero

The LORD is my shepherd; I shall not want. He maketh me to lie down in green pastures: he leadeth me beside the still waters. He restoreth my soul: He leadeth me in the paths of righteousness for his name's sake. Yea, though I walk through the valley of the shadow of death, I will fear no evil: for thou art with me; thy rod and thy staff they comfort me. Thou preparest a table before me in the presence of mine enemies: thou anointest my head with oil; my cup runneth over. Surely, goodness and mercy shall follow me all the days of my life: and I will dwell in the house of the LORD for ever.

Para Deus e minha família, de onde emanam os verdadeiros sentimentos.

Acknowledgements

Firstly, I would like to thanks God for all the details and the opportunity. Besides my family (standing out my husband Seiti, my sister Lóren, my mother Rosangela, my father José and grandpas (Sônia, Morisa, Santana and Ana *in memoriam*), and Marcos and Neusa Santana) and friends (they know who they are, highlighting Carolina, Camila and Alex), I would like to thanks Angel Maquieira, David Giménez Romero and Rosa Puchades Plá. Specially I would like to thanks the "Ferrao family", Eva Brun that helped me to keep going, and Sergi Morais, for all the knowledge and respect.

Fortunately, I have been working with nice people, Sergi Morais and Eva Brun: Thank you very much. Sergi, thank you for the patience. Eva, thank you to heard me when I needed. You are my friend! And I hope to maintain this friendship for ever.

Julia Atienza, Marichu, Nuria Pastor, thanks for the "mona" every monday, and to supply the laboratory, respectively. Pilar Aragón, also thank you! Carmen, thanks for the clean laboratory! Miguel Angel, thanks for the humility, that's a virtue. Luis Tortajada, I wish you all the best in your life. Interestingly, as researcher, you go step-by-step, so for sure you will go far. Patricia Noguera, you are very fun. Prof. Dr. Angel Maquieira and Prof. Dr. Rosa Puchades, thank you to form the team that I have been working. I recognize that you both are responsible for all projects and that it requires dedication and it is not easy.

Of course that I could not finish this acknowledge, from the part of the professors and colleagues without to talk about Prof. Dr. Maria José Bañuls. The respect and the treatment, it is also a virtue. So, thank you all!

Well, from the lab, I need to highlight Regina Niñoles, which have been working in the past. Thank you to be so active and to work hard! Miquél and Daniel, besides to work well, I feel the potential that you both have, so, I desire success in your life. Pilar and Gabi, thank you for the good moments. Paulina Dobosz, thank you for the inspiration. Augusto Juste, thank you for the help. Ahmed Ali, Maria Jose (from Andalucia), Zeneida, Sara Martorell, Sara Santiago and Jose Luiz, thank you. Victoria Gonzalez, it is a pleasure to have you in my side. Your respect is striking. There was important people that passed, for example Anda Gabriela and from the master degree program, Tabita Ana. Also, thank you UPV, UV, La Fe hospital, Generalitat Valenciana for the Grisolia/Santiago scholarship and projects.

Thank you all. Those years were very important and marked my life. Now, I feel that this cycle is finished. A very important cycle.

Thank you all

Abstract

In this work the involved mechanisms between Ro/SSA complex, composed also by the tripartite motif 21α (TRIM21α) and trove domain 2 (TROVE2) proteins, with respect to systemic lupus erythematosus (SLE) autoantibodies is studied. The work is divided in three chapters: I- Structural basis for the Functional Mechanism of TRIM21α in Systemic Lupus Erythematosus ; II- Functional mechanism of the TROVE2 RNA-binding protein in Systemic Lupus Erythematosus and III- Label-free piezoelectric biosensor for determination of circulating autoantibodies for Systemic Lupus Erythematosus Diagnosis.

Samples of lupic patients and health subjects were kindly provided by La Fe hospital, accordingly the required protocols. After its extraction and purification, the immunoglobulin samples were obtained to study in vitro protein interactions and the involved mechanism by using a quartz crystal microbalance with dissipation factor attributions, and dual polarization interferometry. Techniques such, polarization modulation infrared interferometry, x-ray photoelectron interferometry and contact angle measurement were used in order to characterize surfaces. Pre-steady-state analysis revealed an antibody bipolar bridging involved in both TRIM21α and TROVE2 proteins.

Identification of the main immunodominant human linear epitope for TRIM21α was finely mapped using a series of overlapping synthetic polypeptides with a size of 21 amino acids. The epitopes recognized by autoantibodies for this protein spanned the linear sequence from the aminoacid 151 to 183, and a conformational epitope for SLE patients and healthy subjects, respectively. Sera of lupic patients was targeted by SLE epitope, allowing health subjects to be discriminated. Major Histocompatibility Complex Class-II binding peptide prediction results corroborated the sequence as the immunodominant linear epitope, mostly coded as the HLA DRB1*1304 allele for SLE patients, and HLA DRB1*0806 for controls. The subdominant epitope corresponded to the PRY-SPRY domain, recently known as mammalian Fc receptor. Finally, the TRIM21α protein structure was determined by a new homology modeling, never before presented.

From the TROVE2 protein, the major linear epitope recognized by autoantibodies correspond to the sequence from the aminoacid 160 to 210 for healthy subjects. However, the major epitope in SLE serum is undiscovered. We suggest that the difference between epitopes could correspond to a majority necrosis-induced specificity in SLE patients, and an apoptotic via in healthy subjects. TROVE2 showed the ability to bind to Fcs, depending on alkaline earth cations in solution. The results suggest that the TROVE2-TRIM21α binding is a calcium-dependent protein interaction linked through the *MIDAS*-like motif in the vWFA-like domain.

Finally, a pratical consequence of all study was the development of label-free biosensing method, based in microbalance technology, for in vitro diagnostics of systemic lupus erythematosus patients, allowing the premature sensing of autoantibodies against TRIM21α and TROVE2 protein, in advance of the clinical illness symptoms appear.

Resumen

En este trabajo se ha estudiado el mecanismo involucrado entre el complejo Ro/SSA, compuesto también por las proteínas *tripartite motif 21* (TRIM21α) y *trove domain 2* (TROVE2) con respecto a autoanticuerpos de pacientes que tienen lupus eritematoso sistémico, en comparación con autoanticuerpos de personas sanas. El estudio comprende tres capítulos: I- Base Estructural para el funcionamiento de *TRIM21α* en Lupus Eritematoso Sistémico; II- Mecanismo Funcional de la proteína enlazante *TROVE2 RNA* en Lupus Eritematoso Sistémico y III- Biosensor piezoeléctrico sin marcaje para la determinación de autoanticuerpos circulantes para el diagnóstico del Lupus Eritematoso Sistémico.

Las muestras de pacientes lúpicos y personas sanas fueron proporcionadas por el hospital La Fe de acuerdo con los protocolos establecidos. Tras una etapa de extracción y purificación de las inmunoglobulinas fueron estudiadas la interacción de proteínas *in vitro* utilizando una microbalanza de cristal de cuarzo con atribución de factor de disipación e interferometria de polarización dual. Técnicas de caracterización como espectroscopía infrarroja de reflexión-absorción por modulación de la polarización, espectroscopía fotoelectrónica de rayos-x y análisis de ángulo de contacto fueron utilizadas con la finalidad de caracterizar superficies. El análisis del estado pre estacionario ha revelado un mecanismo de puente bipolar para las dos proteínas, TRIM21α y TROVE2.

Tras su identificación, fue mapeado el epítopo inmunodominante linear para TRIM21α, utilizando una serie de polipéptidos sintéticos superpuestos de 21 aminoácidos. Los epitopos reconocidos por autoanticuerpos para esta proteína abarca la secuencia lineal a partir del aminoácido 151 hasta el 183 para epitopos de pacientes lúpicos y sujetos sanos, respectivamente. El suero de pacientes lúpicos fue reconocido por los epitotopos de SLE, permitiendo la discriminación de pacientes sanos. Los resultados de la unión del Complejo Mayor de Histocompatibilidad clase II con el péptido de unión corroboraron la secuencia cómo el epítopo lineal inmunodominante, codificado como el alelo HLA DRB1 * 1304 para pacientes con LES y HLA DRB1 * 0806 para los controles. El epitopo subdominante corresponde al dominio PRY-SPRY, recientemente conocido receptor Fc de mamífero. Finalmente, la estructura

de la proteína TRIM21α fue determinada utilizando un nuevo modelo de homología no presentado antes.

De la proteína TROVE2, el epitopo lineal immunodominante reconocido por los autoanticuerpos corresponde a la secuencia que pudiera corresponder del aminoácido 160 hasta 210 para sujetos sanos. Sin embargo, el epitopo mayoritario en sueros lúpicos no fue determinado. Se sugiere que la diferencia entre los epitopos se corresponde mayoritariamente a una necrosis-inducida en pacientes lúpicos, y a una vía apoptótica en pacientes sanos.

TROVE2 presentó la habilidad de unirse a Fcs dependiendo de los cationes alcalinos presentes en la disolución. Los resultados sugieren que la unión TROVE2-TRIM21α es dependiente de la interacción con calcio vinculada a través del motivo MIDAS en el dominio vWFA.

Finalmente, una consecuencia práctica de todo el estudio fue el desarrollo de un biosensor libre de marcaje para diagnóstico *in vitro* de lupus eritematoso sistémico, permitiendo la detección prematura de autoanticuerpos anti TRIM21α y anti TROVE2, varios años antes de la aparición de los síntomas clínicos de la enfermedad.

Resum

En aquest treball s´ha estudiat el mecanisme involucrat en el complex Ro/SSA, compost per les proteïnes tripartite motif 21 (TRIM21α) i trove domain 2 (TROVE2) respecte a autoanticossos de pacients que tenen lupus eritematós sistèmic, en comparació amb autoanticossos de persones sanes. L´estudi es divideix en tres capítols: : I- Base Estructural per al funcionament de TRIM21α a lupus eritematós sistèmic; II- Mecanisme Funcional de la proteïna enllaçant TROVE2 RNA en lupus eritematós sistèmic i III-Biosensor piezoelèctric sense marcatge per a la determinació d'autoanticossos circulants per al diagnòstic del lupus eritematós sistèmic.

Les mostres de pacients lúpics y persones sanes van ser amablement proporcionades per l'hospital La Fe d'acord amb els protocols establerts. Després d'una etapa de purificació adequada, el *pool* de mostres de immunoglobulines va ser estudiat les interaccions *in* vitro de les proteïnes utilitzant una microbalança de cristall de quars amb atribució de factor de dissipació i interferometria de polarització dual. Tècniques de caracterització, como ara espectroscòpia de infraroja de reflexió-absorció per modulació de la polarització, espectroscòpia fotoelèctrica de rajos X i anàlisi d'angle de contacte van ser emprades amb per tal de caracteritzar les superfícies. L´anàlisi de l´estat preestacionari ha revelat un mecanisme de pont bipolar que involucra les dos proteïnes, TRIM21α i TROVE2.

Una vegada identificat, va ser mapat l'epítop immunodominant lineal per a TRIM21α emprant una sèrie de polipèptids sintètics superposats de 21 aminoàcids. Els epítops reconeguts per autoanticossos per a aquesta proteïna engloben la seqüència lineal a partir de l'aminoàcid 151 fins al 183 per a epítops de pacients lúpics y subjectes sans, respectivament. El sèrum de pacients lúpics va ser reconegut pels epítops de SLE, fet que va permetre la discriminació de pacients sans. Els resultats de la unió del Complexe Major de Histocompatibilitat classe II amb el pèptid de unió van corroborar la seqüència com l'epítop lineal immunodominant, codificat com l'al·lel HLA DRB1 * 1304 per a pacients amb LES i HLA DRB1 * 0806 per als controls. L'epítop subdominant correspon al domini PRY-SPRY, recentment conegut receptor Fc de mamífer. Finalment, l'estructura de la proteïna TRIM21α va ser determinada utilitzant un nou model d'homologia no presentat abans.

De la proteïna TROVE2, l'epítop lineal immunodominant reconegut pels autoanticossos correspon a la seqüència que pogués correspondre l'aminoàcid 160 fins al 210 per a subjectes sans. No obstant això, l'epítop majoritari en sèrums lúpics no va ser determinat. Es suggereix que la diferència entre els epítops es correspon majoritàriament a una necrosis induïda en pacients lúpics i a una via apoptòtica en pacients sans.

TROVE2 va mostrar l'habilitat de unir-se a Fcs en funció dels cations alcalins presents en la dissolució. Els resultats suggereixen que la unió TROVE2-TRIM21α depèn de la interacció amb calci vinculada a través del motiu MIDAS en el domini vWFA.

Finalment, la conseqüència pràctica de tot l'estudi va ser el desenvolupament d'un biosensor sense marcatge per al diagnòstic in vitro de lupus eritematós sistèmic, el qual permet la detecció prematura d'autoanticossos cap a les proteïnes TRIM21α i TROVE2 anys abans de l'aparició dels símptomes clínics de la malaltia.

Resumo

Neste trabalho são estudados os mecanismos envolvidos entre o complexo Ro/SSA, composto também pelas proteínas *tripartite motif 21α* (TRIM21α) e *TROVE domain 2* (TROVE2), com relação aos autoanticorpos de lúpus eritematoso sistêmico (SLE). O trabalho está dividido em três capítulos: I- Análise *in vitro* e *in silico* do reconhecimento molecular entre autoanticorpos de lúpus e Receptor Fc TRIM21α; II- Evidência *in vitro* de complexos imunes TROVE2 com pontes bipolares na patogênese do lúpus eritematoso sistêmico e III- Biossensor piezoelétrico livre de marcagem para prognóstico e diagnóstico de lúpus eritematoso sistêmico.

Amostras de pacientes lúpicos e indivíduos sanos foram gentilmente fornecidos pelo hospital La Fe, de acordo com os protocolos necessários. Após sua extração e purificação, as amostras de imunoglobulina foram obtidas para estudar as interações protéicas *in vitro* e o mecanismo envolvido, utilizando-se uma microbalança de cristal de quartzo com atribuições de fator de dissipação e interferometria de polarização dupla. Técnicas como a interferometria infravermelha de modulação de polarização, interferometria fotoelétrica de raios X e medição de ângulo de contato foram utilizadas para caracterizar superfícies. A análise pré-estado estacionário revelou um ponteamento bipolar de anticorpos envolvido em ambas proteínas, TRIM21α e TROVE2.

A identificação do epítopo principal imunodominante humano para TRIM21α foi finamente mapeada utilizando uma série de polipeptídeos sintéticos sobrepostos com um tamanho de 21 aminoácidos. Os epítopos reconhecidos pelos autoanticorpos para esta proteína abrangem a sequência linear do aminoácido 151 a 183 e um epítopo conformacional para os enfermos de SLE e indivíduos saudáveis, respectivamente. Os autoanticorpos de pacientes lúpicos visaram epítopos proteicos, permitindo que indivíduos saudáveis fossem discriminados. Os resultados da predição de peptídeo de ligação utilizando Complexo de Histocompatibilidade Maior Classe II corroboraram a sequência como o epítopo linear imunodominante, codificado na maior parte como o alelo HLA DRB1 * 1304 para doentes com LES e HLA DRB1 * 0806 para os controles. O epítopo subdominante correspondeu ao domínio PRY-SPRY, recentemente conhecido como receptor Fc de mamífero.

Finalmente, a estrutura da proteína TRIM21α foi modelada por homologia, nunca antes apresentada.

Com a proteína TROVE2, o epítopo linear principal reconhecido por autoanticorpos corresponde à sequência do aminoácido 160 a 210 para indivíduos sanos. No entanto, o principal epítopo no soro de SLE é desconhecido. Sugerimos que a diferença entre epítopos poderia corresponder a necrose induzida em pacientes com LES e uma via apoptótica em indivíduos sanos.

TROVE2 mostrou a capacidade de se ligar a Fcs, dependendo de catiões alcalino-terrosos em solução. Os resultados sugerem que a ligação TROVE2-TRIM21α é uma interação de proteína dependente de cálcio ligada através do motivo de tipo MIDAS no domínio semelhante ao vWFA.

Finalmente, uma das conseqüências práticas de todo o estudo foi o desenvolvimento de um método de biossensibilidade livre de marcagem, baseado na tecnologia de microbalança, para o diagnóstico *in vitro* de pacientes com lúpus eritematoso sistêmico, permitindo a detecção precoce de autoanticorpos contra a proteína TRIM21α e TROVE2, antes da aparição de sintomas clínicos.

Publications

Noelle M. do Nascimento, Isidro Monzó, Roberto Tejero, Jesús V. de Julián–Ortiz, Jorge Escorihuela, José L. Lopez–Paz, Elena Grau García, Jose A. Román–Ivorra, Rosa Puchades, Angel Maquieira, Sergi Morais and David Gimenez–Romero. In vitro and in silico analysis of the molecular recognition between lupus autoantibodies and TRIM21α Fc Receptor. *Submitted to Plos One*

Augusto Juste–Dolz, Noelle M. do Nascimento, Isidro Monzó, Elena Grau García, Jose A. Román–Ivorra, Rosa Puchades, Angel Maquieira, Sergi Morais and David Gimenez–Romero. In vitro evidence of bipolar-bridged immune TROVE2 complexes in the pathogenesis of systemic lupus erythematosus. *Submitted to PNAS*

Noelle M. do Nascimento, Augusto Juste–Dolz, Elena Grau-García, Jose A. Román–Ivorra, Rosa Puchades, Angel Maquieira, Sergi Morais, David Gimenez–Romero. Label-free piezoelectric biosensor for prognosis and diagnosis of Systemic Lupus Erythematosus. *Biosensor & Bioelectronics*, 90 (2017) 166-173.

Patent

Noelle M. do Nascimento, David Gimenez–Romero, Elena Grau García, Augusto Juste–Dolz, Angel Maquieira, Sergi Morais, Rosa Puchades and Jose A. Román–Ivorra. Elucidación de estados de transición y patrones de reconocimiento molecular mediante la función $\partial\Delta\Gamma/\partial\Delta Q$ y su aplicación a la detección de enfermedades. Submitted.

Congresses

Noelle M. do Nascimento, Sergi Morais, Isidro Monzó, Roberto Tejero, Jesús V. de Julián–Ortiz, Jorge Escorihuela, José L. Lopez–Paz, Elena Grau García, Jose A. Román–Ivorra, Rosa Puchades, Angel Maquieira and David Gimenez–Romero. TRIM21α Structure and its Mechanism Acting in Systemic Lupus Erythematosus Patients and Healthy Subjects. X International Workshop on Sensors and Molecular Recognition,Valencia, 7-8 June, 2016. ISBN 978-84-617-5330-7

Augusto Juste–Dolz, Noelle M. do Nascimento, Sergi Morais, Isidro Monzó, Roberto Tejero, Jesús V. de Julián–Ortiz, Jorge Escorihuela, José L. Lopez–Paz, Elena Grau García, Jose A. Román–Ivorra, Rosa Puchades, Angel Maquieira and David Gimenez–Romero. Mecanismo Funcional de la Proteína *TROVE2* en Pacientes Lúpicos. X International Workshop on Sensors and Molecular Recognition,Valencia, 7-8 June, 2016. ISBN 978-84-617-5330-7

Augusto Juste–Dolz, Noelle M. do Nascimento, Sergi Morais, Elena Grau García, Jose A. Román–Ivorra, Rosa Puchades, David Hervás Marín, Angel Maquieira & David Gimenez–Romero. A Novel Biosensor for Diagnostic and Monitoring of Systemic Lupus Erythematosus. X International Workshop on Sensors and Molecular Recognition,Valencia, 7-8 June, 2016. ISBN 978-84-617-5330-7

N. M. do Nascimento, Sergi Morais, Isidro Monzó, Roberto Tejero, José L. Lopez–Paz, Elena Grau García, Jose A. Román–Ivorra, Rosa Puchades, Angel Maquieira and David Gimenez–Romero. Mapeado de las Interacciones TRIM21-Autoanticuerpo en Pacientes Lúpicos. XLII Congreso Nacional de la Sociedad Española de Reumatologia, Barcelona, 18-21 May, 2016.

do Nascimento NM, Monzó I, Tejero R, Morais S, López-Paz JL, Grau García E, Román Ivorra JA, Puchades R, Maquieira A, Giménez Romero D. Mapping TRIM21α-autoantibody Interactions in Systemic Lupus Erythematosus Patients. 10th European Lupus Meeting, Venice, 5-8 October, 2016

do Nascimento NM, Monzó I, Tejero R, Morais S, López-Paz JL, Grau García E, Román Ivorra JA, Puchades R, Maquieira A, Giménez Romero D. Mapping TRIM21α-autoantibody Interactions in Systemic Lupus Erythematosus Patients. ACR/ARHP Annual Meeting, Washington DC, 11-16 November, 2016

N. M. Nascimento, S. Morais, J. Escorihuela, R. Puchades, A. Maquieira and D. Gimenez–Romero. Biosensing Autoantibodies for the Diagnosis of Systemic Lupus Erythematosus. IX International Workshop on Sensors and Molecular Recognition. Valencia, 6-7 july, 2015. ISBN: 978-84-608-2360-5

N.M. Nascimento, D. Gimenez-Romero, I.S. Monzó, R. Tejero, S. Morais, R. Puchades and A. Maquieira. Predicting the idiotype IgG-Ro52 molecular recognition in lupic patients. IX International Workshop on Sensors and Molecular Recognition. Valencia, 6-7 july, 2015. ISBN: 978-84-608-2360-5

N.M. Nascimento, I.S. Monzó, M.A. Gonzalez–Martínez, S. Morais, R. Puchades, A. Maquieira, D. Gimenez–Romero. Apotope recognition by serum autoantibodies in Systemic Lupus Erythematosus. Biophysics of Proteins and Surfaces: Assembly, Activation, Signalling. Madrid, 13-15 october, 2015

Noelle M. Nascimento, Sergi Morais, Rosa Puchades, Ángel Maquieira, David Gimenez–Romero. Monomerization Strategies for Purification of Anti-Ro52 Polyclonal Antibodies. VIII International Workshop on Sensors and Molecular Recognition. Valencia, 3-4 july, 2014. ISBN: 2014.978-84-697-1302-0

Noelle M. do Nascimento, David Gimenez–Romero, Sergi Morais, Rosa Puchades, Angel Maquieira. Desarrollo de un Sistema Biosensor para la detección de Enfermedades Autoinmunes. Encuentro de Estudiantes de Doctorado, UPV, Valencia-Spain, 12 june 2014

N. Nascimento, D. Gimenez Romero, A. Maquieira Catala, R. Purchades. Estudio de la red idiotipo–antiidiotipo en pacientes con lupus eritematoso sistémico. VII International Workshop on Sensors and Molecular Recognition. Valencia,4-5 july, 2013. ISBN: 978-84-695-8811-6

Noelle M. do Nascimento, David Gimenez–Romero, Sergi Morais, Rosa Puchades, Angel Maquieira. Estudio de las Interacciones de la red idiotipo–Antiidiotipo del Lupus Eritematoso Sistémico mediante Interferometria de Polarización Dual (DPI). XXXIV Reunión Bienal de la Real Sociedad Española de Química (RSEQ), Santander, 15-18 septiembre 2013

N. do Nascimento, D. Giménez-Romero, S. Morais, M.A. González–Martínez, J.L. López–Paz, A. Maquieira, R. Puchades. Dual Polarization Interferometry for Sensing the Idiotype–Antiidiotype Network. XVII European Conference on Analytical Chemistry. (EUROANALYSIS). Warsaw, 25-29 august, 2013

Abbreviations

AA	Amino Acid
AC	Alternating Current
APC	Antigen Presenting Cell
ANA	Antinuclear Antibodies
CA	Contact Angle
DILE	Drug-Induced Lupus Erythematosus
DNA	Deoxyribonucleic Acid
DPI	Dual Polarization Interferometry
dsDNA	Double-stranded DNA
DVD	Digital Versatile Disc
ELISA	Enzyme-Linked Immunosorbent Assay
Fab	Fragment Antigen-Binding
Fc	Fragment crystalizable
HLA	Human Leukocyte Antigen
hYRNPs	Cytoplasmic Ribonucleoprotein Particles
Hz	Hertz
IgA/D/E/G/M	Immunoglobulin A, D, E, G, M
IRF3/5/7	Interferon Regulatory Factor 3, 5, 7
IRRAS	Infrared Reflection-Absorption Spectroscopy
ITGAM	Integrin Alpha M
Ka	Absorption Rate Constant
Kd	Dissociation Rate Constant
K63	Ubiquitim K63 ligase
L1/L2	Linker1/Linker2
MHC	Major Histocompatibility Complex
MIDAS	Metal Ion-dependent Adhesion Site
Poh1	Proteasomal subunit 1
QCM	Quartz Crystal Microbalance
QCM-D	Quartz Crystal Microbalance with Dissipation monitoring

RBCC	Ring B Box Coiled Coil
RNA	Ribonucleic Acid
Ro/SSA	Ro protein/Sicca Syndrome A Type
SAM	Self-Assembly Monolayer
SLE	Systemic Lupus Erythematosus
Sm	Smith
SRS	Somatostatin Receptor Scintigraphy
SSA	Sicca Syndrome type A
STAT4	Signal Transduction and Activator of Transcription 4
TNF-alpha	Tumor Necrosis Factor alpha
TRIM21	Tripartite Motif Family 21
TRIM21α	Tripartite Motif Family 21 alpha
TRIM21β	Tripartite Motif Family 21 beta
TROVE2	Trove Domain Family 2
Ube2V2	Ubiquitin-conjugating enzyme E2 variant 2
Ub2w	Ubiquitin-conjugating enzyme 2W
U1RNP	U1 Ribonucleoprotein
vWFA	von Wilebrand Factor A
XPS	X-ray Photoelectron Spectroscopy

Content

1. General Introduction

1.1 Immune System

1.1.1 Innate and Adaptive Immunity

The immune system is responsible for protecting animal bodies from invading pathogenic organisms and other disturbing agents. It is able to generate an enormous variety of cells and molecules capable of specifically recognize and eliminate the invader. These cells and molecules act together in a dynamic network separated in specific recognition and response.[1,2] There are a less specific (innate) and a more specific (adaptive) levels of the immune system. They function as a highly interactive and cooperative manner, generating the production of a combined response more effective than either branch could produce by itself.[3] The Table 1 presents the principal differences between them.

Table 1 Principal differences between innate and adaptive immune systems [1-3]

Non Specific Immunity (Innate)	Specific Immunity (Adaptive)
Response is not antigen dependent	Response is antigen-dependent
Not antigen specific	Antigen specific
There is immediate maximal response	There is an interval time between exposure and maximal response
No immunologic memory	Exposure results in immunologic memory

The innate immunity provides a first line of natural defence, manifested without infection. It can be described at physiological level, including the vigorous mucociliary clearance mechanism, and anatomically, as the skin, that retards the entry

of microbes and the growth of pathogens due to the acidic pH (between 3-5) present in certain regions of the body.[1]

An important example of the innate immune system action is the inflammatory process. This contribute to the production of fluids that have cells (exuded from the vessels) whose function is to eliminate the invader, through phagocytosis, where the pathogen is digested, or endocytosis, where the pathogen is internalized and breached down.[4]

The innate immune system relies upon a limited repertoire of receptors to detect invading pathogens, but compensates for this limited number of invariant receptors, targeting conserved microbial regions that are shared by large groups of pathogens. Speed is a defining characteristic of the innate immune system, due to the capacity of an immediately protective inflammatory response, thought the hematopoietic cells, including macrophages, dendritic cells, mast cell, neutrophils, eosinophils, natural killer cells and natural killer T cells. In addition to hematopoietic cells, innate immune responsiveness is a property of the skin and the epithelial cells lining the respiratory, gastrointestinal and genitourinary tracts. Moreover, innate immunity plays a central role in activating the subsequent adaptive immune response.[2]

The adaptive immunity, contrasting the innate immune system, act as the first response of the body when it is infected. This system responds with a high degree of selectivity and permits it to distinguish differences among antigens. This specific recognition is capable to detect subtle differences between pathogens and can discriminate between foreign molecules and cells of the body.[3] When activated, there is a high production of molecules against antigens allowing this to recognize a unique antigen, being a key characteristic of this system. Once recognized, a memory effect is developed, that is, if a second contact occurs with the same antigens, a heightened state of immune activity will act immediately. Because of this attribute, the immune system can confer life-long immunity to many infectious agents after an initial encounter.[5,6]

The adaptive immune system involves T and B lymphocytes (the two major populations of lymphocytes) and antigen-presenting cells. The lymphocytes leave the bone marrow, circulate in the blood and lymphatic system, and reside in various lymphoid organs. They produce and display antigen-binding cell-surface receptors and define immunologic attributes of specificity, diversity, memory, and self/nonself recognition.[3]

T lymphocytes are produced in bone marrow and migrate to the thymus to mature. During its maturation, the T cell comes to express a unique antigen-binding molecule on its membrane. T-cell receptors can recognize only the antigen that is bound to cell-membrane proteins. B lymphocytes mature within the bone marrow and after that, each expresses an unmatched antigen-binding receptor on its membrane. This antigen-binding or B-cell receptor is a membrane-bound antibody molecule. These secreted antibodies are the major effectors molecules of humoral immunity.[1, 6]

Certain immune components play important roles in both types of innate and adaptive immunity.[4] As illustrated in Figure 1, virus/bacteria gain access to the body through a bruise in the skin, trespassing the innate barrier defence. To avoid contamination, an increased level of chemokines and microbial peptides are produced. The peptides control the infection, by killing directly the pathogen and giving chemotactic information for cells (phagocytes, dendritic cells), providing the activation of the adaptive immune system. It leads an adaptive immune response by causing chemotaxis of memory T cells. These factors increase the expression of the correspondent vascular adhesion molecules. Besides, the level of innate immune cells and memory T cells increase in the inflamed area. The dendritic cells and phagocytes engulf the pathogens.[6] The already activated phagocyte of the innate immune system leads to triggering the respiratory burst and eliminate engulfed organisms, while activated dendritic cells carry the antigenic peptides. These cells enter to the lymph node and present the antigens to the naïve and central memory T-cells. It generates the proliferation of T cells specific for pathogen-associated antigens, producing the CD4 T helper cell and CD8 cytotoxic killer T cells.

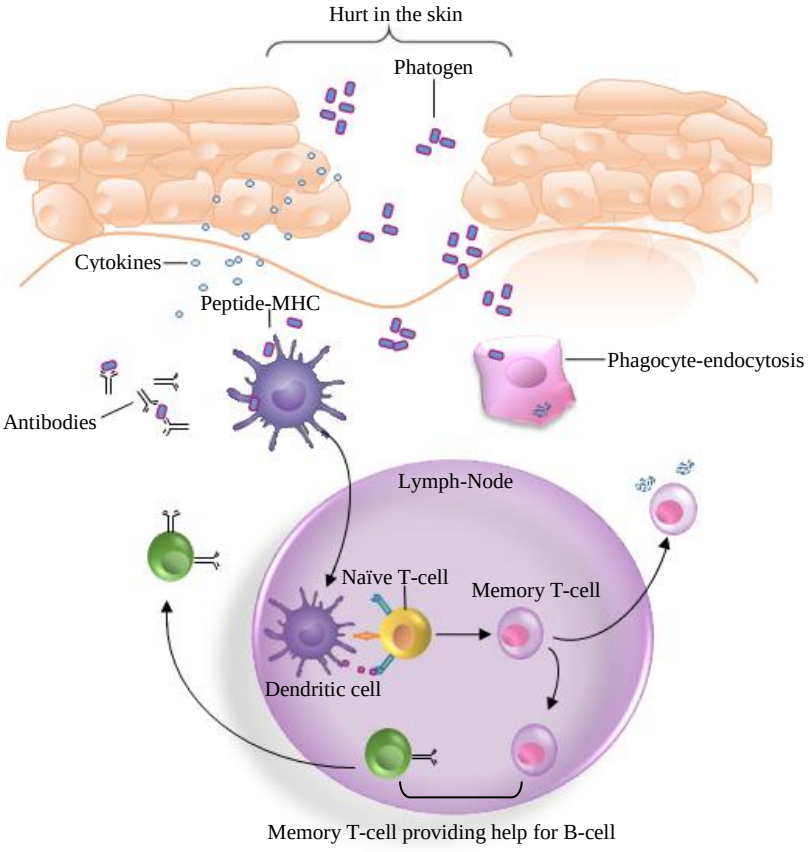

Figure 1 Action of innate and adaptive immune systems in response to bacterial infection of the skin.

CD8 T cells destroy pathogens and CD4 help to induce the production of pathogen-specific antibodies, through the major histocompatibility complex, whose function is indirectly connected to the antibody production, as explained in the next section. These antibodies can directly neutralize pathogens, binding to its surface and starting the complement cascade, which in turn, initiates the lysis of the pathogen and further enhances phagocytosis of the organism by the deposition of complement-

derived opsonins. In addition, antibodies bind to innate system phagocytes via interaction with Fc receptors. Thus, antibodies lead to enhance phagocytosis and highly efficient antigen presentation to T cells, increasing adaptive T cell responses. These collaborations of the innate and acquired immune systems generate multiple levels of defence, ideally leading to clearance of the pathogen and immunogenic substances.[5]

1.1.2 Major Histocompatibility Complexes

As previously described, major histocompatibility complexes (MHCs) have an important function in the innate immune system, being responsible to present peptides of extracellular origin to CD4 T cells that, after to receive this information, start the production of antibodies. The structure of the MHCs are one of the most extensively studied regions in the human genome because of the contribution of multiple variants at this locus in autoimmune, infectious and inflammatory diseases, and in transplantation.[7] The MHC class II can be found on chromosome 6 in the human genome and is composed of two glycoproteins, a α-chain of molecular mass 30–35 kDa and a β-chain of 26–30 kDa. They have the capacity to deliver intracellular signal and present a characteristic restriction in their expression, encountered primarily on cells of the immune system such as macrophages and B cells, justifying its polymorphism and diversity of allelic variants.[1,4] For humans, they are known as Human Leukocyte Antigens (HLA), involving three classes of HLA class II molecules, the DP, DQ and DR. Each of them can be presented having an A or B domain. The most widely studied is the HLA-DR, being the HLA-DRA almost identical and HLA-DRB diverse, and to the major binding selectivity.

The main function of the MHC class II molecules is to present processed antigens, which are derived primarily from exogenous sources, to the cluster of differentiation cell T-lymphocytes. Thereby, they are critical for the initiation of the antigen-specific immune response. Besides antigen presentation, evidences showed

that ligation of MHC class II molecules also activates intracellular signalling pathways, frequently leading to apoptosis. Constitutive expression of MHC class II molecules is confined to professional antigen-presenting cells (APC) of the immune system. In nonprofessional APCs, MHC class II molecules can be induced by a variety of immune regulators.[8]

The mechanism of action of the MHC Class II is well established and its function leads to an adaptive immune response. When the body detect the presence of an exogen antigen, this is taken up by endocytosis. After the degradation process and the peptide action of elimination, as presented above, the MHC Class II interact with the antigen. The antigen presenting cells, that displays antigens-MHCs bound on their surfaces, activate the pathogen-recognition and the Th cells start to be produced. These cells are responsible for the generation of different cytokines that stimulate the B cells to produce also different class and types of antibodies.[1,4,8]

1.1.3 Antibodies

Antibodies play an important role in the adaptive immune system. When the body is infected, one of the responses of the specific defence is the production of them.[1-6] In spite of the firsts antibodies appearing after an infection are the immunoglobulin M (IgM), further stimulations may lead the production of IgG, IgA, IgE and IgD, isotypes of immunoglobulins.[1]

The most abundant antibodies was found to be the IgG types, divided in four subclasses (IgG_1, IgG_2, IgG_3 and IgG_4), being IgG_1 the most common of the IgGs, comprising about 70% of total IgG. Quantitatively, IgG is the major antibody isotype present in humans and widely recognized as a therapeutic agent for primary immunodeficiency, infectious diseases or autoimmune diseases.[9] Due to the plentiful of type G immunoglobulins, this study is focused on this kind of antibodies.

The basic structure of an antibody comprises two identical light chains and two identical heavy chains linked together by disulphide bonds. Each chain can be

of κ or λ type. The firsts amino acids of the terminal regions of a light or heavy chain varies among antibodies of different specificities, being classified as V_L regions for light chains and V_H regions for heavy chains. The antigen binding fragment is called Fab fragments, were there is an antigen-binding activity. The other fragment was classified as Fc fragment (crystallisable fragment), a common part for all IgG antibodies, divided in two constant domains, called C_H2 and C_H3.[10] IgGs contains a diversity of sugars bonded especially in the C_H2 domain. At medical point of view, these sugars are important due to the nature of IgG, pro or anti-inflammatory.[11]

The Figure 2 shows the four types of IgGs and their differences. The characteristic of the subclasses of IgGs are the amino acid content of the heavy chains and the ratio of κ to λ light chains. The major structural differences are found in the hinge region in terms of the number of residues and interchain disulphide bonds. This region links the two Fab arms to the Fc portion of the IgG molecule, providing flexibility. In addition, it forms a structure connected between the two heavy chains. To interact with differently spaced epitopes, the Fab arms comprises flexibility, helping the Fc region to adopt different conformations. The disulphide bonds in the middle hinge region covalently link the heavy chains.[1,6]

Fabs from the IgG_1 is freely flexible, permitting rotation about their axes of symmetry and movement within a sphere centred at first of two interchains disulphide bridges. IgG_2 comprise a shorter hinge than IgG_1 and the residual glycine in this region, combined with their shortness, decreases the rotation and the lateral movement of the Fabs. IgG_3 has elongated and inflexible hinge region, whit its Fabs having a rotation and wave rate similar to those in IgG_1. Finally, the IgG_4 hinge region is shorter than the IgG_1, their flexibility is between the IgG_1 and IgG_2 and presents little rotation around the hinge region.[10 -14]

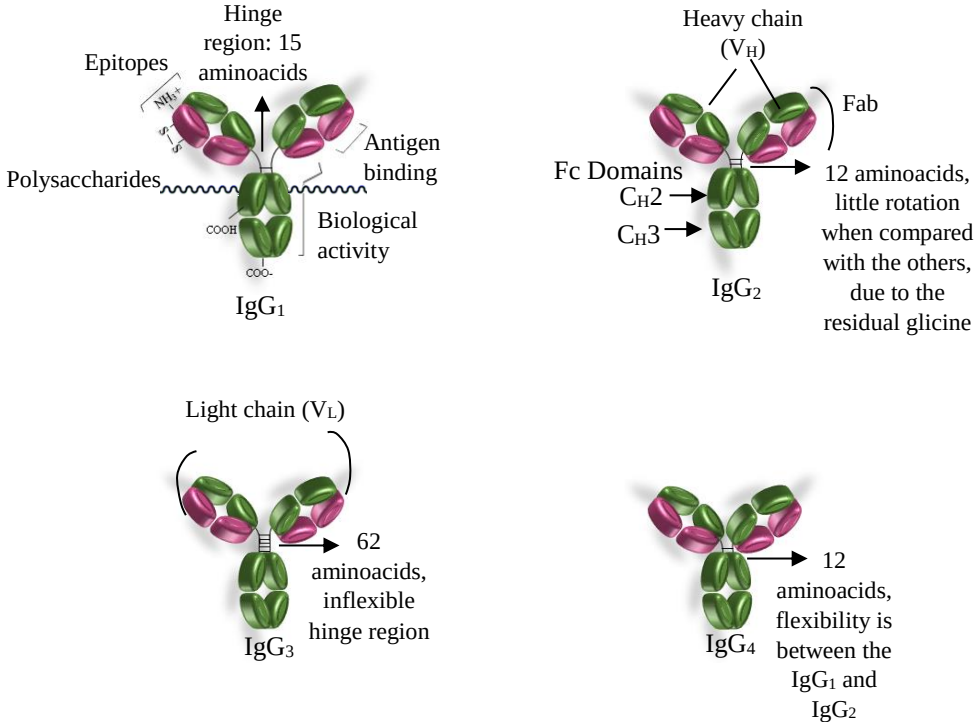

Figure 2 Antibodies subclasses structures of IgGs isotypes

The idiotypic determinants (antigenic determinants) present in each individual antibody arise from the sequence of the heavy- and light-chain variable regions. Each individual antigenic determinant of the variable region is called idiotope. In some cases, an idiotope is the actual antigen-binding site, and in others, may comprise variable-region sequences outside of the antigen-binding site.[1] Each antibody will present multiple idiotopes. The sum of the individual idiotopes is called the idiotype of the antibody. The antibody-idiotype is determined by gene rearrangement, functional diversity, palindromic nucleotides at sites of single-strand breaks, N-nucleotides, and somatic hyper- mutations.[1,3] Each antibody isotype has a unique structural and functional property that determine their idiotype.

Immunoglobulins with a shared idiotope are the same idiotype. This region binds to a part of the antigen that is called antigenic epitope, composed by 8-22 aminoacids.[1]

There are different regions where an antibody can recognize an antigen, as described above. The antigen-binding recognition is conducted by hydrogen bonds, Van der Waals force and hydrophobic and electrostatic interactions. These recognitions between foreign antigen and antibodies occur in proteins epitopes from the external region or also in sequences that are broken due to an intern folding of the protein (Fig. 3). In general, antigenic epitopes are formed by 5-15 amino acids sequences.[1,6]

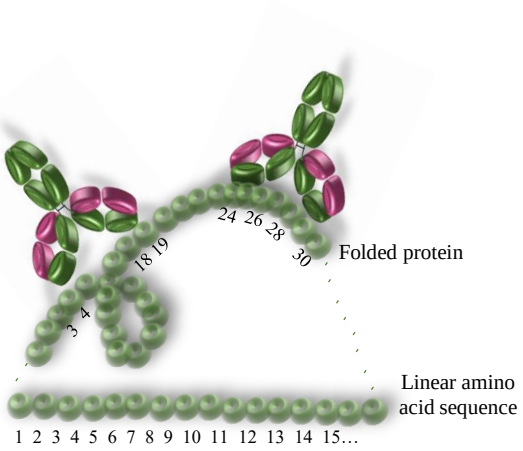

Figure 3 Illustration of an antibody recognition in a folded and non-folded protein region (not at real scale).

1.2 Autoimmunity

1.2.1 Autoimmune Diseases

The controlled series of cellular checkpoints regulating self-reactive receptors is responsible to avoid the autoimmunity. When it is broken, the consequence is the production of autoantibodies that destroy own proteins, nucleic

acids and their complexes, polysaccharides, nucleotides, DNA and so on, resulting in some cases, in autoimmune diseases.[1,3,15,16] The term autoimmunity refers to a physiological response that do not lead to immunopathology. The components responsible for the manifestation are genetic, environmental and regulatory.[16]

Adaptive immune response provides a key element of selectivity and memory but also carry a risk of inducing maladaptive immune responses including autoimmune diseases, allergy, and allograft rejection. These conditions occur when the immune system responds to a non-pathogenic antigen as if they were malignant, leading the production of autoantibodies that affects the organism functions.[17]

A special feature of autoimmune diseases is the high concentration of autoantibodies to many different endogenous antigens.[17] They are not necessarily specific for a manifestation of an autoimmune disease, since autoantibodies can also appear in the blood of healthy individuals or under some special situations, but in a majority of cases, this manifests as an autoimmune disease.[16]

Environmental factors have been attributed to cause autoimmune diseases, including a wide collection of agents as chemicals, virus, microorganisms, drugs, toxins, diet, stress and solvents. In addition, other factors including weight, puberty, increased linear growth and body mass index also affect the intensity of the immune response.[18] However, evidences has shown that the mechanism by which environmental factors induces autoimmune diseases include epigenetic modifications, reaction with the self-components to generate novel antigen molecules, molecular mimicry and many of viral infection, like *Borrelia burgdorfii* and Lyme arthritis, B4 Coxsackievirus, Cytomegalovirus or Rubella and type 1 diabetes.[16, 18-20]

More than 80 autoimmune diseases have been identified and the list continues to grow (Table 2), affecting 7-10% of the United States population.[19] Sex and gender disparities are notable for the manifestation and the majority exhibit female bias. Thus, in United States, the largest population of incidence of systemic lupus erythematosus (SLE), 78% of cases of the sickness are thought to be woman.

There are, in a world reference, 2.7 times of incidence of autoimmune disease in woman than men, being the fifth in the list of cause of women's death before the age of 65.[20]

Table 2 Principal human autoimmune diseases [19]

Autoimmune Disease	Affected organ/glandule	Consequences
Hashimoto´s Thyroiditis	Thyroid	Destruction/Under function
Grave´s disease	Thyroid	Stimulation/Over function
Diabetes Mellitus	Pancreas	Destruction of β cells
Addison´s disease	Adrenal Glands	Adrenal Insufficiency
Haemolytic Anaemia	Red Blood Cells	Anaemia
Thrombocytopenia	Platelets	Abnormal bleeding
Pernicious Anaemia	Intrinsic Factor	Autoantibodies
Multiple Sclerosis	Central Nervous System	Paralisys
Myasthenia Gravis	Neuromuscular Junction	Muscle weakness

Table 2 (Continuation) Principal human autoimmune diseases [19]

Autoimmune Disease	Affected organ/glandule	Consequences
Pemphigus Vulgaris	Epidermal Cells Junction	Severe Blistering
Rheumatoid Arthritis	Synovium, Glomerulus	Destruction
Systemic Lupus Erythematosus	Synovium, Skin, Joints, Tissues	Deformity, autoantibodies, inflammation of tissues
Goodpasture´s Syndrome	Basement Membrane	Glomerulonephritis
Sjögren´s Syndrome	Salivar and Lacrimal Glands	Glomerulonephritis
Primary Biliary Cirrhosis	Liver	Under function
Bowel Disease	Colon and Small Intestine	Inflammation
Psoriasis	Skin, mucosa	Inflammation
Sarcoidosis	Tissues	Granulomatous
Celiac Disease	Small intestine	Autoantibodies
Scleroderma	Nuclear Antigens	Fibrosis

All cited autoimmune diseases affects organs or tissues of the body. Hashimoto´s thyroiditis, rheumatoid arthritis, diabetes and systemic lupus

erythematosus are the most common of them, the first three affecting 1 in 100 people. In contrast, rare autoimmunity, as Goodpasture's syndrome affect 1 in a million people. All of them have in common autoantibodies production and dysfunction and damage of organs in long term.[21]

Autoimmune diseases can be generally divided into two categories: systemic autoimmune diseases such SLE that attack multiple organs and systems, and tissue specific like myasthenia's gravis and type 1 diabetes. Both categories involve chronic inflammation, causing multiple major organ damage and failure.[19,20]

1.3 Systemic Lupus Erythematosus

1.3.1 Pathogenesis, Prevalence, Genetic and Environmental Contributions

Systemic lupus erythematosus is a chronic, old and inflammatory autoimmune disease characterized by alternating periods of remission and disease activity. It involves nearly every organ of human body, as skin, heart, lungs and intestine. The DNA may act as both antigen and adjuvant, and the consequence is the production of antinuclear autoantibodies.[22-27] The excess of autoantibody-antigen form immunocomplexes, and develop an inflammatory processes.[28] Moreover, defective clearance of apoptotic cells mediate inhibitory signalling pathways, leading to the development of SLE.[29]

Interaction between B and T-cells leads to positive-feedback loop that causes amplification of the autoimmune response. After repeated times, the presence of exogenous autoantigens that initiated the response stop being necessary, all effects may be magnified, and the disease will become self-sustained for a period.[30]

SLE is substantially more common in women than in men, especially in the reproductive years (ratio of females to males is estimated at 9:1). Female predominance could also suggest a role for the X chromosome in the development of SLE.[31 -36] The strong female predominance is less pronounced in childhood-onset- and late-onset disease.[37] This suggests an influence of oestrogen hormones in the

development of autoimmunity, confirmed by the analysis of the disease activity during pregnancy, were the oestrogen hormone level increases.[38]

Genetic predisposition is clearly a major risk factor for SLE. A high incidence of this autoimmunity has been found in patients with African ancestry, and there are an excess prevalence among Asians, while Caucasians patients seems to be a minority. Although the underlying causes of these differences are not known, there are a variability in circulating sex steroids in these races.[39] Also, studies with monozygotic twins and first-degree relatives (mother, father, brother, sister) of SLE patients have a much higher risk of developing autoimmunity compared with the general public. Studies on monozygotic twins have determined a concordance rate of around 25–69%.[40]

Familial aggregation of SLE further supports a role for genetic susceptibility. Recent genome-wide association studies have identified associations with SLE including STAT4 (signal transduction and activator of transcription 4), IRF5 (interferon regulatory factor) and ITGAM (integrin alpha M). More than 20 susceptibility loci have been identified to date, and these generally confer an increased risk of SLE.[41] The immunoglobulin, T-cell receptor, MHC genes, due to its considerable heterogeneity, have soon been suspected of playing a distinct role in the etiopathogenesis of autoimmune diseases.[42]

The combination of environmental factors and genetic abnormalities associated with the defective clearance of pathogens contribute to the induction and perpetuation of SLE.[43] A number of occupational and environmental exposures have been implicated as enhancers in the development of this disease, and these exposures might explain a higher-than-expected occurrence in certain communities. However, to establish whether a true focus exists in a community is an inherently challenging, as there may be a small absolute number of definite cases, and it may be difficult to identify and quantify specific exposures. Furthermore, the multifactorial nature of SLE means that not all persons exposed will necessarily develop SLE, and that this infirmity can develop in those without exposure.[44]

Other contaminants, as trichloroethylene, is a known environmental contaminant that has been proposed as a trigger for the development of SLE. This compound is used as industrial solvent, and may be found in domestic cleaners, adhesives and typewriter-correction fluid. Exposure to this component has been linked with a number of auto-immune syndromes including lupus-like symptoms and scleroderma.[45] Finally, drugs such as hydralazine, procainamide, isoniazid and minocycline can cause a type of lupus named drug-induced lupus erythematosus (DILE), which is characterized by predominance of skin manifestations and usually resolves after the drug has been discontinued.[46,47]. However, the cause remains unknown.

1.3.2 Autoantibodies variety in SLE patients

An intriguing fact of the SLE manifestation is that they target nucleic acids or nucleic acid-containing complexes, which are highly conserved molecules, irreplaceable to the cell function such as replication, transcription and translation. The complexes are produced by the stimulation of B cells, with subsequent broadening of autoantibody production by epitope spreading. The produced autoantibodies in complex with chromatin deposit in basement membranes, generating inflammations in different parts of the body.[48] There are a diversity of 180 autoantibodies in SLE.[49] Between them, four classified autoantibodies are related with clinical manifestations (Table 3). These autoantibodies provides a crucial diagnostic and prognostic information for the management of the autoimmune disease, and they may be identified years before the manifestation of the disease, providing the advantage of an early diagnostic.[50] Why autoantibodies are developed against certain intracellular molecules is still not clearly understood.[51]

Table 3 SLE Clinical manifestations and its association with autoantibodies [49]

Clinical Manifestation	Autoantibodies
Glomerulonephritis	Anti-dsDNA
Sjögren Syndrome, Neonatal Lupus,Photosensitive Rashes, Primary Biliary Cirrhosis, Cutaneous Vasculitis	Anti-Ro/SSA (anti-TRIM21, anti-TROVE2)
Strokes, miscarriage, occlusive vasculopathy, livedo reticularis	Antiphospholipid
Puffy hands, Raynaud´s phenomenon, pulmonary hypertension arthritis	Anti-U1 RNP

1.3.3 Diagnosis

The etiology of SLE is enigmatic and the symptoms mimicry another illness, causing difficulty to diagnoses. Clinically, this heterogeneous disease may affect most organ systems. Some of the common manifestations also includes nonerosive polyarthritis, cutaneous hypersensitivity to sunlight, serositis, nephropathy and haematological abnormalities.[52,53] SLE patients may also present symptoms from the central nervous system, lungs, kidney and heart, including vascular manifestations as vasculitis, thrombosis as part of having a secondary anti-phospholipid syndrome, and Raynaud's phenomena.[54]

The standard case definition is a diagnosis by expert clinical assessment, usually a rheumatologist, which is impractical for large population-based studies.[55] In order to facilitate the diagnostic, the American College of Rheumatology (ACR) developed criteria to classify the disease, requiring at least 4 of 11 manifestations types (Table 4). Symptoms can vary from discoid rash to seizures, depending of the patient.[52]

Table 4 American College of Rheumatology Criteria to diagnose SLE in humans [52]

Criterion	Definition
Malar Rash	Fixed erythema, flat or raised, over the malar eminences, tending to spare the nasolabial folds
Discoid Rash	Erythematosus raised patches with adherent keratotic scaling and follicular plugging; atrophic scarring may occur in older lesions
Photosensitivity	Skin rash as a result of unusual reaction to sunlight, by patient history or physician observation
Oral and nasopharyngeal ulcers	Oral or nasopharyngeal ulceration, usually painless, observed by a physician
Nonerosive arthritis in at least two peripheral joints	Nonerosive arthritis involving two or more peripheral joints, characterized by tenderness, swelling, or effusion
Pleurisy and Pericarditis	Pleuritis—convincing history of pleuritic pain or rub heard by a physician or evidence of pleural effusion or Pericarditis (documented by EKG, rub, or evidence of pericardial effusion)
Profuse proteinuria and cellular casts	Persistent proteinuria higher than 0.5 g/day or greater than 3 if quantitation not performed, or cellular casts (may be red cell, hemoglobin, granular, tubular, or mixed)

Table 4 (Continuation) American college of rheumatology criteria to diagnose SLE in humans [52]

Criterion	Definition
Psychosis, Seizures	Seizures or psychosis—in the absence of offending drugs or known metabolic derangements (uremia, ketoacidosis, or electrolyte imbalance)
Hematologic disorder	Haemolytic anaemia (with reticulocytosis) or Leukopenia (less than 4,000/mm^3 total on two or more occasions) or Lymphopenia (less than 1,500/mm^3 on two or more occasions) or Thrombocytopenia (less than 100,000/mm^3 in the absence of offending drugs)
Immunologic disorders	Positive antiphospholipid antibody
Positive ANA	An abnormal titer of antinuclear antibody by immuno fluorescence or an equivalent assay at any point in time and in the absence of drugs known to be associated with "drug-induced lupus" syndrome

According to these symptoms, different SLE patients do not necessarily have any shared clinical outcomes, presenting the heterogeneity of patients with this disorder. Thus, the clinical presentation of SLE in terms of symptoms, severity and manifestation vary between individuals and even in the same patient over time, being a challenge to diagnose.

Another methods of diagnostic and prognosis of SLE includes the Systemic Lupus Erythematosus Disease Activity Index (SLEDAI), British Isles Lupus Assessment Group (BILAG), Systemic Lupus Activity Measure (SLAM), Lupus Activity Index (LAI) and the European Consensus Lupus Activity Measurement

(ECLAM). Between them, the SLEDAI is the easiest assessment tool (Appendix, Table A), comprising 24 features that are attributed to lupus, with a weighted score, given to any symptom that is present.[56]

Some of this methods are easy to incorporate into routine clinical care, providing the instantaneous status of the SLE disease activity.[57] However, these markers may not accurately predict the outcome of individual patients due to the heterogeneity of the disease. While the history and physical examination are most important in assessing flares, laboratory tests are helpful in different organ systems (hematologic, renal) that cannot be assessed clinically.[58]

More than 95% of SLE patients exhibit antinuclear antibodies (ANAs), the principal hallmarks of this disease manifestation.[52] Because that, the most commonly used laboratory assays for the SLE diagnostic is the detection of autoantibodies, although laboratory analysis are helpful in confirming the activity of the disease than to diagnoses. However, all assays requires careful validation to determine whether they perform adequately for human autoantibodies. A perfect test would be specific, sensitive, reflecting disease activity correlating with organ involvement and/or predict flares. [56]

Analysis of ANAs is the best semi-quantitative and poorly standardised method between laboratories. The precision and accuracy of the technique depends on the assay configuration, quality control procedures and professional qualification.[56] However, besides the 5 criterion presented, this is a manner to diagnose SLE nowadays (Table 5).

As presented in Table 5, different methods with varying are routinely used in clinical practice for detection of autoantibodies, including the two most popular, the enzyme–linked immunosorbent assay (ELISA) and the radiolabeled immunoprecipitation assay. However, these methods suffer from considerable drawbacks, as time-consuming and several steps of reaction, requiring radioactive, fluorescent and/or enzymatic labels. Moreover, cross–reactivity of the antibodies may cause erroneous diagnosis, and different assays detects particular antibodies

properties and even lose sensitivity. Some tests for specify SLE autoantibodies, and the clinical importance of this for pathogenesis or diagnosis is rarely fully understood. Also, due to the variety of symptoms that reflect the different target in the body, some assays lose the capability to detect specific autoantibodies, leading the assay to fail. [52-54]

Table 5 Based immunoassays used for the diagnosis and monitoring of SLE in humans [27,56]

Assay	Advantages	Disadvantages
ELISA	Automated, high potential to quantify, high sensitivity and high potential to define the IgG subclass and has the possibility to be polyspecific	Require purified antigen; detects low affinity antibodies; false positivity
Microarray	Can detect multiple antibodies at the same time; possible automatization; high sensitivity; economically competitive	Not widely available
Western Blotting	High selectivity	Expensive
IF-ANA	Economically competitive; high sensitivity	False positive; poor characterization of extractable antibodies
Ouchterlony double diffusion (ID)	Specific; cheap	False positive; slow
Pasive Hemaglutination	High selectivity	Requires purification
Double Immunodifusion(DID)	Economically competitive; high selectivity; multiple detection	Low sensitivity; requires high volume of serum sample

Table 5 (Continuation) Based immunoassays used for the diagnosis and monitoring of SLE in humans [27,56]

Assay	Advantages	Disadvantages
IFF rodent tissue	Can be isotypespecific; economically competitive	Anti-TRIM21 and anti-TROVE2 may be missed; not specific
Flow citometry	High sensitivity; automated; economically competitive	Proportionate just one result by time;
Immunoprecipitation (Farr)	High selectivity	Radioactive; expensive; intensive labour; false positive; technically difficult
Counterflow Immunoelectroforesis	High selectivity; economically competitive	Slow; not isotype specific

1.4 Principal Autoantigen in Systemic Lupus Erythematosus

1.4.1 Target of Autoantibodies

Before the diagnosis of SLE, autoantibodies can be detected, tending a predictable sequence, with an increased pattern accumulation, approximately 5 years before SLE arising in individuals.[57,59] These autoantibodies are produced against the Ro/SSA complex, composed by the tripartite motif 21 (TRIM21), Telomerase, Ro and Vault Domain Family Member 2 (TROVE2), and the Sjögren's syndrome type b (La) proteins, in patients suffering from rheumatic disorders, providing a crucial diagnostic and prognostic information for the management of the autoimmune

disease studied.[49,60-63] Although both antibodies reactivity were considered to form part of the Ro/SSA complex for a long time, nowadays it is established that their antigens are different, do not form part of a stable macromolecular complex, and are located in different cellular compartments.[64]

For easy of explanation, I divided in two sections the principal features of the TRIM21 and TROVE2 autoantigens in SLE patients, both proteins studied in this work.

1.4.2 TRIM21: Variants, Structure and SLE Relationship

Reported for the first time in 1988, the TRIM21 protein is a major autoantigen in autoimmune diseases such rheumatoid arthritis, SLE and Sjögren´s syndrome.[65] It is specific to humans and monkeys, and cytoplasmic ribonucleoprotein particles (hYRNPs) can be found on the cytoplasmic membrane or in small blebs during apoptosis, as a reaction to stimuli such as ultraviolet light B (UVB), 17-beta-estradiol, viral infection, tumor necrosis factor (TNF)-alpha and other cell apoptosis-inducing molecules.[63]

TRIM21 has an alternative splicing variant, being the first called TRIM21α and the other, TRIM21β. Structurally, the TRIM21α has a zinc finger encoding E3 ubiquitin ligase activity and a leucine zipper domain between the amino acids 211 and 232. Following, there are a coiled–coil region that is responsible to mediate oligomerization. At the C terminus of the protein ring–b–box coiled–coil region (RBCC), there is a well–conserved PRY–SPRY domain (or B30.2 domain), which commonly determines its function by acting as a targeting module.[66,67] This domain has been shown to bind normal IgG serum and anti-TRIM21α autoantibodies. When the protein are connected with an IgG, the structure contains C_H2 and C_H3 domains of one Fc heavy chain.[68]

The entire exon 4, comprising the C-terminal part of the coiled-coil domain, is spliced off in TRIM21β. So far TRIM21β has been detected only at the mRNA

level and to date there is no report showing the TRIM21β protein, with a predicted molecular weight of 45 kDa.[69]

TRIM21 intercepts antibody–pathogen bound, and neutralizes them by mediating their degradation. In addition, this protein initiates a signalling cascade, resulting in the transcriptional up-regulation of inflammatory cytokines and an antiviral state in the cellular environment. Also, has a RING–dependent E3 ligase activity and are believed to polyubiquitinate IRF3 and IRF8. It catalyses the formation of Lys63–linked ubiquitin chains and stimulates the transcription factor pathways of NF-κB, AP-1, IRF3, IRF5 and IRF7.[68]

Translocation of this protein to the proteasome produce the degradation of virus-antibody complexes, as well as release of the K63–linked polyubiquitin chain from TRIM21 by the proteasome-associated enzyme Poh1, triggering NF-κB activation. Its results in the production of proinflammatory cytokines, modulation of natural killer stress ligands and induction of an antiviral state. By increasing the amount of TRIM21 protein in cells, antiviral protection also increases, suggesting that drugs which up regulate TRIM21 might provide an effective treatment in the control of autoimmune diseases.[70]

The region where most autoantibodies recognize the TRIM21α are predominantly localized in the structurally stable regions. Epitope mapping studies showed that anti-TRIM21 antibodies react with the RING, coiled–coil and PRY–SPRY domains of TRIM21.[71,72] According the immune epitope database and analysis resource, the TRIM21 regions that mostly interact with epitopes of autoimmune globulins are underlined in scheme A (see Appendix, scheme A), sequences from the PRY–SPRY (that interacts with the Fc domain) and coiled-coil region.[73,74]

Understanding the structure of this protein could suggest the involvement in the SLE pathogenesis. However, the low solubility of the TRIM21 prevented the total x-ray definition of it structure. Indeed, from the entire family of this proteins, little is known about the molecular and structural organization of them.[75]

Analysis by bioinformatics identified that there are a high conservation and similarity (above 40%) between the proteins that has a ring, a b-box and a coiled-coil domains.[75] In TRIM21, the residues between the aminoacids 168-245 have been suggested to promote homodimer formation.[76] Nevertheless, the structure are not modeled, and the TRIM21 action in autoimmune patients are not described yet.

1.4.3 TROVE2: Variants, Structure and SLE Relationship

TROVE2, from Telomerase, Ro and Vault domain family, is a protein whose function is to bind to malformed 5SRNA fragments, marking it for degradation. This protein (60kD) formed by 538 amino acids.[77-82] TROVE2 has not the role structure defined for humans, but it is 78% similar to the *Xenopus laevis* (Figure 4). The structure is composed by two domains, the N-terminal and the Von Wilebrand factor A (vWFA). The N-terminal is formed by 353 amino acids, consisting of a repeated sequence of seven alpha helix called HEAT sequence. The diameter of the hole of the structure is between 10 and 15 Å and allows only single strands to be introduced in. This domain is also reported as horseshoe.[77,78,82] The vWFA is comprised between the amino acids 361 and 538, also known as metal ion dependent adhesion site (MIDAS), and acts as a binding site for divalent cations.[83] This domain is also present in other extracellular proteins and in cell adhesion proteins. There are 3 binding sites at the amino acids 378, 380, and 445, although the nature of them is not specified.[77,79]

There are five isoforms of TROVE2 protein. The called long-form is composed by 538 amino acids (from 1 to 538) and the short form is composed by 205 amino acids (from 1 to 205), with differences in the sequences from 195 to 205, that is replaced, considering the long-form, by KHKIFIGKKGG amino acids, missing the sequence from 206 to 538. Another isoforms, called 3, 4 and 5, are composed by 518, 534 and 525 amino acids, respectively, always starting in the amino acido 1. The type 3 isoform miss the sequence from 515 to 538, replacing it to DTVK. The type 4

replace the sequence from 529 to 538 to PCKIPY and finally, the type 5 isoform replaces the sequence from 515 to 538 to ALQNTLLNKSF amino acids.[84]

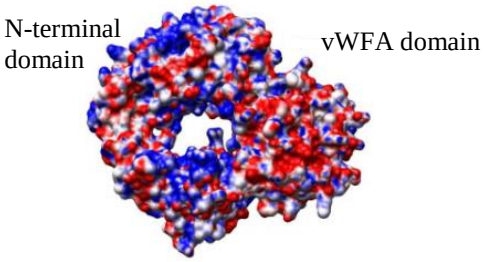

Figure 4 X-ray crystallography structure solved for TROVE2 protein from *Xenopus Laevis*.[83]

Most of the TROVE2 protein epitopes are discontinuous or conformational.[78,79] They are composed of two or more separated segments that, thanks to folding, are close together. Nevertheless, it has been found a larger epitope approximately at the third half part of the protein sequence, spanning from amino acid 140 to 325. This segment contains protein residues that interact with the YRNA and residues in the gap.[72]

TROVE2 protein is complexed with small RNA strands but remains to be seen how this union takes place. By codifying the TROVE2-RNA complex, the 3' ends of misfolded RNA chains binds to the central hole, and the rest of the chain is attached to the protein. The RNA binds to the ring around the hole and blocks the entrance to other chains. Thus, the connection between structure and function of the protein is that TROVE2 binds to the RNA strands causing rearrangements and correct folding. Also, the protein acts as a quality control of different non-coding RNA that have suffered any incorrect folding process or just any alteration, as commented above. It could be seen that this protein is important for the survival of the mammalian cells against the exposition to UV radiation, being capable to mark small chains of malformed non-coding RNA that have been modified by interaction with UV radiation.[77,81]

Antibodies of SLE patients principally recognize an epitope located between amino acids 169 and 180 in the TROVE2 protein.[78,80] This segment contains one serine and two arginine amino acid residues, which can be modified post-translationally (phosphorylation or citrullination), increasing the antigenicity of the epitope, and becoming more detectable by the antibody.[79] These amino acids are residing in a loop involved in binding to RNA. Indeed, there are three conserved residues in this sequence, which are capable of forming hydrogen bonds with the phosphate groups of RNA. Specifically, K170 and R174 residues are especially important for binding pre-5SRNA misfolded.[78] Antibody binding to this epitope causes blocking of pre-5SRNA binding. Other epitopes that are susceptible to be targeted by antibodies are between the amino acids 216-232 and 300-320 (outlined in the scheme B, see Appendix) which will be inside the HEAT repetitive part in the TROVE domain.[78,79]

As one target of the autoimmune response, a high number of anti-TROVE2 autoantibodies are found in SLE patients, ranging between 24% and 60%.[85] Patients with SLE have an epitope in the TROVE2 protein that can induce cell apoptosis, but the role function of this protein in SLE patients are not explained yet. These apotopes are probably between amino acids 82 to 244, and 393 to 538.[77,80-84]

As presented, SLE is an autoimmune disease with periods of flares and remissions, caused by a disorder in the immune system, and its diagnostic is based on the presence of established criteria to facilitate the management of the disease. However, these criteria are subjective. The analysis of antibodies to nuclear components (ANAs) are poorly standardised between laboratories and some of them miss the presence of autoantibodies against TRIM21 and TROVE2, the two serological hallmark present in SLE cases. Besides, although these proteins are the principal targets in SLE patients, TRIM21 do not has the entire structure defined, the mechanism of both proteins in SLE patients and healthy subjects is not elucidated, and the interaction between both proteins in the inflammation process related with SLE is not described yet. For this reason, we decide to research on the interaction

between these proteins with autoantibodies from SLE patients, map the region where autoantibodies exactly interact, to propose a model to the structure of human TRIM21α protein and finally, link the relationship between SLE flares and TRIM21 and TROVE2 proteins.

1.5 References

1. Goldsby RA, Kindt TJ, Osborne BA (2003) *Immunology* 5:16-18, 76-101.

2. Turvey SE, Broide DH (2009) *J Allergy Clin Immunol* 125:S24–S32.

3. Bellinger DL, Lorton D (2014) *Auton Neurosci*182:15–41.

4. Karsner HT (1949) *J B LLippincot & Co* 7:11–36.

5. Clark R, Kupper T (2005) *J Invest Dermatol* 125:629–637.

6. Wood P (2011) *Understanding Immunol* 2:22-42, 120-135 251–273.

7. Choo SY (2007) *Yonsei Med J* 48:11-23.

8. Holling TM, Schooten E, van Den Elsen PJ (2004) *Hum Immunol* 65:282–90.

9. Jefferis R (2012*) Arch Biochem Biophys* 26:159–166.

10. Kumagai I, Tsumoto K (2001) *Enc Life Sci* 1–7.

11. Lenvinson W (2016) *Microbiologia Médica e Imunologia* 59:510–511.

12. Palm W, Colman PM (1974) *J Mol Biol* 82:587–588.

13. Pumphrey RS (1986*) Immunol Today* 7:206–211.

14. Michaelsen TE, Frangione B, Franklin EC (1977) *J Biol Chem* 252:883–889.

15. Parkhomenko TA, Legostaeva GA, Doronin BN, Nevinsky GA (2012) *J Mol Recognit* 25:383–392.

16. Goodnow CC, Sprent J, St-Groth BF, Vinuesa CG (2005) *Nature* 435:590–597.

17. Qianjin L (2013) *J Autoimmun* 41:1–5.

18. Kieber-Emmons T, Monzavi-Karbassi B, Pashov A, Saha S, Murali R, Kohler H (2012) *Front Oncol* 2:1–12.

19. Moroni L, Bianchi I, Lleo A (2012) *Autoimmun Rev* 11:A386–A392.

20. Tan T, Hiang Y, Chang C, Zhou Z (2014) *Clin Rev Allergy Immunol* 47:234–243.

21. http://www.allergy.org.au/patients/autoimmunity/autoimmunediseases#sthash.0cha8i2N.dpuf. Consulted in february, 2016.

22. Kuhn A, Wenzel J, Weyd H (2014) *Clin Rev Allergy Immunol* 47:148–162.

23. Mathian A, Arnaud L, Amoura Z (2014) *Rev Med Interne* 35:503–511.

24. James W, Berger T (2005) *J Maxillofacial Oral Surgery* 10:1–1210.

25. Roberts TL , Idris A, Dunn JA, Kelly GM, Burnton CM, Hodgson S, Hardy LL, Garceau V, Sweet MJ, Ross IL, Hume DA , Stacey KJ (2009) *Science* 323:1057–1060.

26. Medrano-Campillo P, Sarmiento-Soto H, Álvarez-Sánchez N, Álvarez-Ríos AI, Guerrero JM, Rodríguez-Prieto I, Castillo-Palma MJ, Lardone PJ, Carrillo-Vico A (2015) *J Pineal Res* 58:219–226.

27. Petri M (2005) *Rheum Dis Clin North Am* 31:245–254.

28. Shirai T, Hirose S (2006) *Springer Semin Immunopathol* 28:79–82.

29. Nath SK, Han S, Kim-Howard X, Kelly JA, Viswanathan P, Gilkeson GS, Chen W, Zhu C, McEver RP, Kimberly RP, Alarcón-Riquelme ME, Vyse TJ, Li QZ,Wakeland EK, Merrill JT, James JA, Kaufman KM, Guthridge JM, Harley JB, (2008) *Nat Genet* 40(2):152–154.

30. P Lenert (2010) *Clin Exp Immunol* 161:208–222.

31. van Bavel CC, Dieker JW, Tamboer WP, van der Vlag J, Berden JH (2010) *Mol Immunol* 48:248–256.

32. Jacobsen S, Petersen J, Ullman S, Junker P, Voss A, Rasmussen JM, Tarp U, Poulsen LH, van Overeem Hansen G, Skaarup B, Hansen TM, Pødenphant J, Halberg P (1988) *Clin Rheumatol* 17:468–77.

33. Feng X, Zou Y, Pan W, Wang X, Wu M, Zhang M, Tao J, Zhang Y, Tan K, Li J, Chen Z, Ding X, Qian X, Da Z, Wang M, Sun L (2014) *Lupus* 23:327–34.

34. Mok CC, Lau SC (2003) *J Clin Pathol* 56:481–490.

35. Cervera R, Khamashta MA, Hughes GRV (2009) *Lupus* 18:869–74.

36. Alarcon-Segovia D, Alarcon-Riquelme ME, Cardiel MH (2005) *Arthritis Rheum* 52:1138–47.

37. Manfred R, Weinmann-Menke J, Scorletti E, Cavagna L, Schwarting A (2015) *Autoimmun Rev* 14:1005–1018.

38. Mok CC, Lau SC (2003) *J Clin Pathol* 56:481–490.

39. Moser KL, Kelly JA, Lessard CJ, Harley JB (2009) *Genes Immun* 10:373–379.

40. Deapen D, Escalante A, Weinrib L, Horwitz , Bachman B, Roy-Burman P, Walker A, Mack TM (1992) *Arthritis Rheum* 35:311–8.

41. O'Neill SA, Cervera R (2010) *Best Prac Res Clin Rheumatol* 24:841–855.

42. Cervera R, Khamashta MA, Hughes GRV (2009) *Lupus* 18:869–74.

43. Rahman A, Isenberg DA (2008) *N Engl J Med* 358:929–939.

44. Flanigan CM, Desai M, Shull KR (2000) *Langmuir* 16:9825–9829.

45. James JA, Kaufman KM, Farris AD, Taylor-Albert E, Lehman TJ, Harley JB (1997) *J Clin Invest* 100:3019–3026.

46. Janeway CA, Travers JrP, Walport M, Shlomchik MJ (2011) *Garland Science* 5th, New York.

47. Yaniv G, Twig G, Shor DB, Furer A, Sherer Y, Mozes O, Komisar O, Slonimsky E, Klang E, Lotan E, Welt M, Marai I, Shina A, Amital H, Shoenfeld Y(2015) *Autoimmun Rev* 14:75–79.

48. Arbuckle MR, McClain MT, Rubertone MV, Scofield RH, Dennis GJ, James JA, Harley JB (2003) *N Engl J Med* 349:1526–1533.

49. Menéndez A, Gómez J, Caminal-Montero L, Díaz-López JB, Cabezas-Rodríguez I, Mozo L (2013*) Sci World J* 832789:1–8.

50. Fritsch C, Hoebeke J, Dali H, Ricchiuti V, Isenberg DA, Meyer O, Muller S (2006) *Arthritis Res Ther* 8:R4.

51. Oke V, Wahren HM (2012) *J Autoimmun* 39:77–82.

52. Kurien BT, Scofield RH (2006*) Scand J Immunol* 64:227–235.

53. Hahn BH (1998) *N Engl J Med* 338:1359–1368.

54. Cojocaru M, Cojocaru IM, Silosi I, Vrabie CD (2011) *Maedica (Buchar)* 6:330–336.

55. Hu ZD, Deng AM (2014) *Clin Chim Acta* 437:14–18.

56. Egner W (2000) *J Clin Pathol* 53:424–432.

57. Zhiguo X, Christopher C, Zhiguang Z (2014) *Clin Rev Allergy Immunol* 47:174–192.

58. Stinton LM, Fritzler MJ (2007) *Autoimmun Rev* 7:77–84

59. Weisman M (2010) *Lupus* 19, 119–129

60. Hu ZD, Deng AM (2014) *Clin Chim Acta* 437:14–18.

61. Defendenti C, Atzeni F, Spina MF, Grosso S, Cereda A, Guercilena G, Bollani S, Saibeni S, Puttini PS (2011) *Autoimmun Rev* 10:150–154.

62. Hennig J, Ottosson L, Andrésen C, Horvath L, Kuchroo VK, Broo K, Wahren-Herlenius M, Sunnerhagen M. (2005) *J Biol Chem* 280:33250–33261.

63. Arbuckle MR, McClain MT, Rubertone MV, Scofield RH, Dennis GJ, James JA, Harley JB (2003) *N Engl J Med* 349:1526–33.

64. Sim S, Wolin SL (2011) *Wiley Interdiscip Rev RNA* 5:686–99.

65. Ben-Chetrit E, Chan EK, Sullivan KF, Tan EM (1988) *J Exp Med* 167:1560–571.

66. Vita R, Overton JA, Greenbaum JA, Ponomarenko J, Clark JD, Cantrell JR, Wheeler DK, Gabbard JL, Hix D, Sette A, Peters B (2014) *Nucleic Acids Res* 42:D405–412.

67. James LC, Keeble AH, Khan Z, Rhodes DA, Trowsdale J (2007) *Proc Natl Acad Sci USA* 104:6200–6205.

68. Keeble AH, Khan Z, Forster A, James LC (2008) *Proc Natl Acad Sci USA* 05:6045-6050. Gack MU, Full F (2015) *Proc Nat Acad Sci* 112:9797–9798.

69. Yoshimi R, Ishigatsubo Y, Ozato K (2012) *Int J Rheumatol* 2012:1–11.

70. Ottosson L, Hennig J, Espinosa A, Brauner S, Wahren-Herlenius M, Sunnerhagen M (2006) *Mol Immunol* 43:588–598.

71. Full F, Gack MU (2015) *Proc Natl Acad Sci USA* 112:9797–9798.

72. Reed JH, Michael JW, Gordont TP (2008) *Arthritis Rheum* 58:1125-1129.

73. Singh H, Raghava GPS (2001) *Bioinformatics* 17:1236–1237.

74. Henning *et al.* (2005) *J Biol Chem* 39:33250–61.

75. Reed JH, Clancy RM, Purcell AW, Kim MY, Gordon TP, Buyon JP (2011) *J Immunol* 187:520–526.

76. Espinosa A, Hennig J, Ambrosi A, Anandapadmanaban M, Abelius MS, Sheng Y, Nyberg F, Arrowsmith CH, Sunnerhagen M, Wahren-Herlenius M (2011) *J Biol Chem* 42:36478–366490.

77. Terzoglou AG, Routsias JG, Moutsopoulos HM, Tzioufas AG (2006*) Clin Exp Immunol* 146: 60–65.

78. Reed JH, Neufing PJ, Jackson MW, Clancy RM, Macardle PJ, Buyon JP, Gordon TP (2007) *Clin Exp Immunol* 148:153–160.

79. Millard TP, Ashton GHS, Kondeatis E, Vaighan RW, Hughes GRV, Khamastha MA, Hawk JLM, McGregor JM, McGrath (2002) *Br J Dermatol* 146:210–215.

80. Sánchez SH, Herrera D, Avalose E, Herrera R (2007) *Reumatismo* 59:292–298.

81. Lleo A, Selmi C, Invernizzi P, Podda M, Gershwin ME (2008) *J Autoimmun* 3:257–262.

82. Ramesh A, Savva CG, Holzenburg A, Sacchettini JC. (2007) *J Bio Chem* 18:14960–7.

83. The Uniprot Consortium (2015) *Nucleic Acids Res* 43:D204–D212.

84. Lim SS, Bayakly Charles G, Helmick GC, Gordon C, Easley K, Drenkard C (2014) *Arthritis Rheumatol* 66: 357–368.

85. Wolin SL, Reinisch KM (2006) *Autoim Rev* 5:367-372.

2. Objectives

Since the mechanism of action of TRIM21 and TROVE2 proteins in the human body are not completely elucidated, our goal is to present its function in SLE patients and healthy subjects. Autoantibodies, specially anti-TRIM21 and a TROVE2 are the serological hallmark of SLE patients. They are responsible for the formation of immunocomplexes, which are deposited in different regions in organs and tissues, generating severe symptoms. As the response of the adaptive immunity, these autoantibodies recognize certain epitopes of the protein and the target of these epitopes can help the development of new drugs with the capacity to block the reactive region, avoiding antigenic complex accumulation and complication of the disease. In addition, these data are contributing to the knowledge of the pathways involving TRIM21 and TROVE2 protein acting in the pathogenesis of this autoimmune disease. The mapping of the regions that interact with autoantibodies help us to predict a possible structure, once the structure of both proteins is not published yet.

The research in this thesis is presented into three chapters:

Chapter I: Structural basis for the Functional Mechanism of TRIM21α in Systemic Lupus Erythematosus. For that, serum samples from anti–TRIM21 SLE+ patients and samples from healthy subjects (control) were used. Measuring with a Quartz Crystal Microbalance with Dissipation sensor (QCM–D) and Dual Polarization Interferometry (DPI), information about the dry mass and the solvation sphere of the mechanism of interaction protein–antibody was obtained, allowing a better understanding in the actuation of the TRIM21α in SLE patients and health subjects. After that, a mapping was done using synthetic polypeptides, in order to localize if the immunodominant epitopes recognized by both antibodies was the same. Finally, the TRIM21α structure was modelled, relating its recognition mechanism and structure with its function.

Chapter II: Functional mechanism of the TROVE2 RNA–binding protein in SLE. Study of the molecular recognition of TROVE2 protein and autoantibodies, using the same strategy for study of TRIM21α. Also, a pathologic role for TROVE2 acting in the immune system was proposed, which involves the Ro/SSA complex formation by its interaction with TRIM21α. Knowledge about this synergy contribute to the controlling of interactions that potentially causes cellular damage.

Chapter III: Label-free piezoelectric biosensor for determination of circulating autoantibodies for Systemic Lupus Erythematosus Diagnosis. A new quantitative screening method was developed, based on the interaction fingerprint, for the discrimination of SLE patients and health subjects. The test quantifying the disease activity was adapted on a standard CD/DVD format, allowing high throughput sample analysis. The piezoelectric sensor is able to establish an interaction fingerprint pattern of circulating autoantibodies, distinguishing SLE patients from health donors. Furthermore, a statistical association of global disease activity with TRIM21-TROVE2 interaction was found. Thus, the piezoimmunosensor is capable to determine the biomarker concentration as well as the structural interaction profile.

3. Results

Chapter I

Structural basis for the Functional Mechanism of TRIM21α in Systemic Lupus Erythematosus

In this chapter, the molecular recognition of TRIM21α with autoantibodies in SLE patients was studied. Pre–steady–state analysis revealed an antibody bipolar bridging mechanism for SLE patients and healthy subjects. Mapping the dominant antigenic regions of TRIM21α in anti–TRIM21+ SLE patients and registering piezoelectric signals by a Quartz Crystal Microbalance with Dissipation (QCM–D) sensor, allowed to establish the correlation between antibodies and epitopes. With this data, was possible to identify, by *in silico* approach, the genetic predisposition and predict symptoms in positive anti–TRIM21 SLE patients. The achieved results were corroborated by Major Histocompatibility Complex (MHC) Class–II binding peptide prediction results, and TRIM21α structure homology–modelling.

1.1 Monitoring anti–TRIM21 autoantibodies

The interaction between TRIM21α protein and autoantibodies (antigenic complex formation) was monitored by QCM–D. For this purpose, recombinant human TRIM21α protein was immobilized onto the gold chip using 3–mercaptopropionic acid as a monolayer precursor and subsequent covalent EDC coupling (Scheme 1.1).[1] The immobilization result was fully analysed by X–ray photoelectron spectroscopy (XPS), polarization modulation infrared reflection adsorption spectroscopy (PM–IRRAS) and static water contact angle (SCA) measurements (Fig. 1.1 and 1.2, Table 1.1).

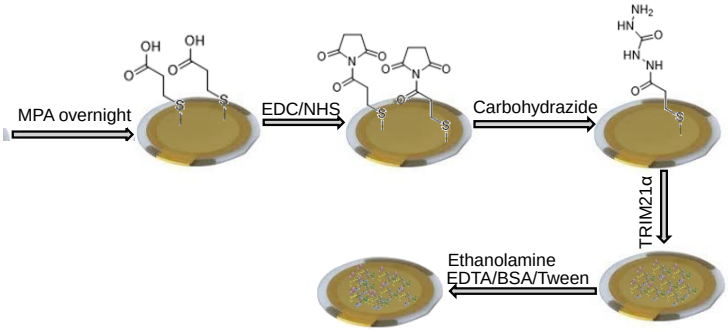

Scheme 1.1 Self-assembly monolayer steps

PM-IRRAS data corroborated the formation of self–assembled monolayer of TRIM21α with high structural order and surface homogeneity, being the calculated amount of protein of 267 ng/cm^2.

After the addition of MPA acid in the sensor chip, the sulphur percentage increases. Also, the EDC/NHS reaction and the addition of carbohydrazide induces an increase of the nitrogen percentage. As Figure 1.2 shows, the hydrophobicity increases as the monolayer is performed. Finally, the immobilization of the protein and the blockage process rendered a clear increase of carbon and nitrogen percentages, as expected after these immobilisation steps.

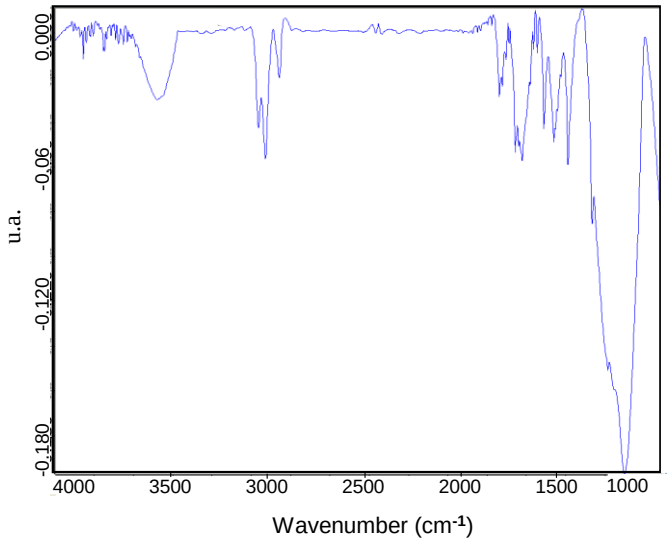

Figure 1.1 Polarization-modulation infrared spectroscopy (PM–IRRAS) spectra of the TRIM21α SAM in the 4000–800 cm^{-1} spectral range. The spectral bands revealed the presence of proteins, and the homogeneity and high-structural order in the gold surface was demonstrated by the high–defined peaks.

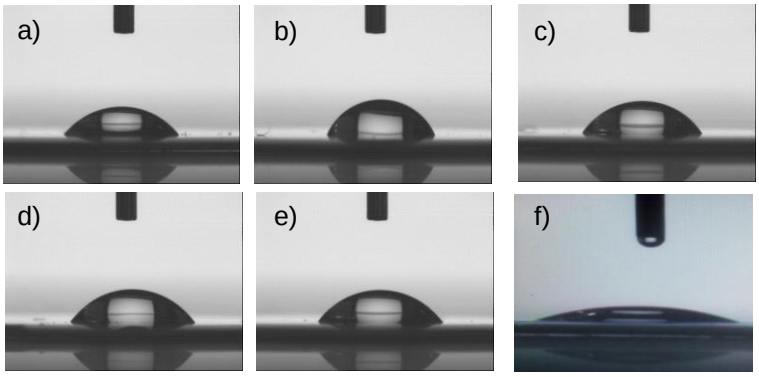

Figure 1.2 Static contact–angle measurement of a) cleaned chip (SCA 56.9 ± 1.02º), b) MPA (SCA 69.01 ± 0.18º), c) EDC/NHS (SCA 59 ± 0.63º), d) carbohydrazide (SCA 55.8 ± 0.31º), e) entire self-assembly monolayer (SCA 56.7 ± 0.79º), and f) the immobilization process of the polypeptides and blockage with D–glucamine (SCA 26.5 ± 0.3º). The reported values are the average of at least five droplets, and the error is less than ±1°.

Next, the chip saturation was investigated by analysing the evolution of the piezoelectric signal for different self–assembly monolayers with anti–TRIM21α autoantibodies, which were purified by affinity chromatography from a pool of 20 anti–TRIM21+ SLE sample from patients (SLE IgGs) and other of 8 healthy subjects (control IgGs).

Table 1.1 Percentage measured of the main elements by XPS during the TRIM21α immobilization, starting from the cleaning of the surface until the immobilization of the protein and blockage of free active sites.

QCM-D Chip	% Au	% C	% O	% S	% N
Cleaned	85	11	4	-----	-----
MPA	38	41	16	5	-----
EDC/NHS	19	52	23	2	3
Carbohydrazide	26	56	12	3	4
TRIM21α/blockage	8	64	15	1	12

As shown in Figure 1.3a and b, the dependence of the surface concentration of the antigenic complex as a function of anti–TRIM21α autoantibodies (IgGs) concentration was described using the Hill equation, which reflected two consecutive reaction steps.[2] A different biorecognition process for SLE patients and control subjects was observed. It is worth mentioning that the avidity for TRIM21α of anti–TRIM21α autoantibodies from SLE patients is higher than that exhibited by control IgGs, since lower concentrations can be detected in samples of SLE patients. Furthermore, using bovine serum albumin as negative control, the response was

negligible for all the concentrations under study, demonstrating the specificity of the TRIM21α–antibody biorecognition.

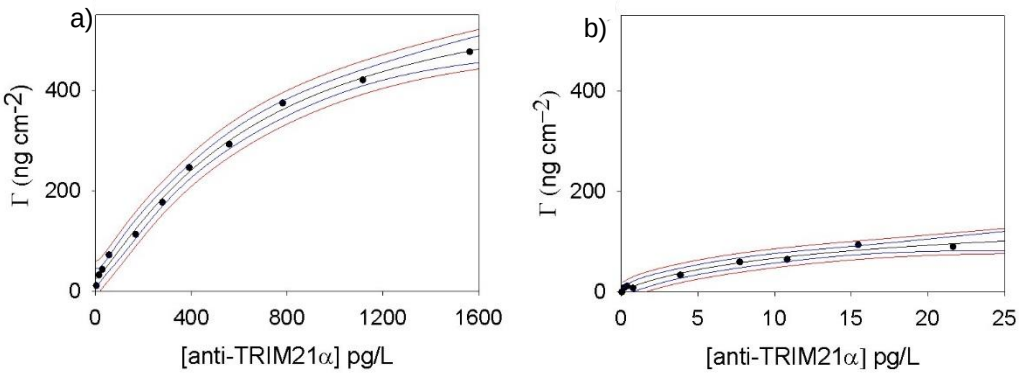

Figure 1.3 Calibration curve of human anti–TRIM21α antibodies from a) SLE patients and b) control subjects, with the prediction (blue) and confidence (red) bands.

1.2 TRIM21α:IgG complex at equilibrium

The dissipation factor (D) is related to the elasticity and viscosity of the molecular layer on a surface, therefore by measuring frequency (f) and D, information about the state of molecular immobilized layers, their wet mass and structural (viscoelastic) properties, can be obtained, as explained in Materials and Methods. In order to get more insights on the antigenic complex properties, the ratio between -Δf and ΔD from QCM–D measurements for the TRIM21α:IgG complex was calculated (Table 1.2). It is presented the dependence of the interaction mechanism with respect to the employed biomarker. This ratio is constant, ~13 Hz for SLE patients and ~7 Hz for healthy subjects. The difference was attributed to the structural changes occurring during the biorecognition process.

Different ratios of SLE and control IgGs lead us to attribute different structural properties to TRIM21α:IgG complexes, which may be the result of

conformational changes or a solvent effect occurred during the biorecognition process.

Table 1.2 -Δf/ΔD values for IgGs from SLE patients and healthy subjects.

SLE Patients				Healthy Subjects			
[IgG] pg/L	**-Δf (Hz)**	**ΔD**	**-Δf/ΔD (Hz)**	**[IgG] pg/L**	**-Δf (Hz)**	**ΔD**	**-Δf/ΔD (Hz)**
3	7	0.5	14	-	-	-	-
14	11	0.8	14	-	-	-	-
28	25	1.7	15	4	5	0.8	7
56	34	3.2	11	-	-	-	-
167	45	5.1	9	8	8	1.4	6
279	48	4.0	12	11	10	1.6	7
391	58	5.0	12	15	14	2.1	7
558	63	5.7	11	22	12	1.7	7
Average	-----	----	12±2	-----	-----	----	7 ± 1

In order to deeply investigate these proposed structural changes, the system was analysed by dual polarization interferometry (DPI), as this technique complements QCM–D measurements by probing the dry mass of the protein adlayer.[3] For that, a self–assembly monolayer similar to the one constructed for QCM–D measurements was prepared on a silicon oxynitride DPI chip (using carboxyethylsilanetriol as a monolayer precursor). Results showed similar dry

densities for SLE patients and control subjects (antigenic complexes around 0.26 mg mm^{-3}), suggesting a similar antigenic complex at equilibrium in both cases. Considering that TRIM21α forms a stable dimer, the change in thickness due to the biorecognition with IgG at equilibrium was estimated, and similar values (~13 nm) were obtained, indicating that autoantibodies may bind to with on one Fab bounded (considering typical IgG dimensions).[4] It is worth mentioning that the percentage change between antigenic complexes derived from SLE IgGs and control subjects determined by QCM–D and DPI was significantly different, 54 and 11%, respectively. Consequently, the higher change measured by QCM–D suggests that conformational changes in the protein hydration shells take place, corroborating the important role of water for the three–dimensional structure of these proteins, dynamic ensemble of conformations and their functioning.[5,6]

1.3 Conformational dynamics

The role of conformational changes in the TRIM21α biorecognition event was studied in real–time by QCM–D. We applied the $-\partial f/\partial D$ function that provides an unambiguous identification of the structural transitions of the adsorbed layer, being a tool to measure the conformational dynamics of proteins and, most importantly, to identify antigenic complexes which are formed during the molecular recognition. As shown in Figure 1.4, the function $-\partial f/\partial D$ (which is directly proportional to the Young's modulus for the measured adlayer) was found to be different for SLE patients and control subjects. In sera from SLE patients (Fig. 1.4a), we found a peak–shape function with peak intensity (~20 Hz), independently of the autoantibody concentration, being the peak position dependent on the concentration. Note that the time–to–start is always the same at all concentrations (zero seconds), suggesting that this parameter depends on the accumulation of a reaction intermediate by means of a two–state kinetics, which yields two different molecular entities during the autoantibody–TRIM21α interaction, the formation of a reaction intermediate (Int.

I) and the final product (PI). On the other hand, the aforementioned function for the interaction in healthy subjects (Fig. 1.4b) had the same characteristics than from SLE patients, with a constant (but lower peak intensity) about 8 Hz, indicating that both reaction mechanisms comprises a similar collection of elementary steps (Int. II and PII), and also confirming that the biorecognition mechanism is dependent on the selected autoantibody. It is important to emphasize that, according to the function -∂f/∂D, both intermediate states have different structural characteristics, but reaction products have similar conformations.

A detailed DPI analysis provides real–time measurements of thickness and dry mass of bound biological molecules onto films, at high resolution levels and without information of their hydration shells. As depicted (Fig. 1.4 c), the changes in thickness per molecule of IgGs showed how the autoantibody–TRIM21α interaction involves three and two reactive species for SLE patients and control subjects, respectively. In a first step, for SLE patients, autoantibodies initially targeted the TRIM21α protein with both Fab fragments bounded to the protein (aprox. 8 nm/molecule, Int. Ia), which changed to an orientation with only one Fab fragment bounded at intermediate times (aprox.14 nm/molecule, Int. Ib). At long times, the final product has an orientation intermediate between both cases (aprox. 13 nm/molecule, PI). In the same way, for healthy subjects, control targeted initially the TRIM21 α protein with only one Fab fragment (aporx.12 nm/molecule, Int. II), which changed to the above mentioned intermediate orientation at long times (aprox. 10 nm/molecule, PII or final antigenic complex).

Next, Figure 1.4d shows how the TRIM21α protein have multiple binding sites; it is simultaneously an antigen-binding fragment (Fab) receptor and an Fc receptor. This figure also shows how the half-life (t1/2) is 110 s for $F(ab')_2$ fragments obtained from SLE patients, being 2,474 s for Fc fragments. The piezoelectric response obtained in a 400 pg/L solution of SLE $F(ab')_2$ fragments is similar to that measured in 50 mg/L of Fc fragments (Fig. 1.4). Solutions with lower levels of Fc

fragments cannot be detected. Consequently, this figure show how F(ab')$_2$ fragments from SLE patients have more affinity for the TRIM21 α protein than the Fc fragments.

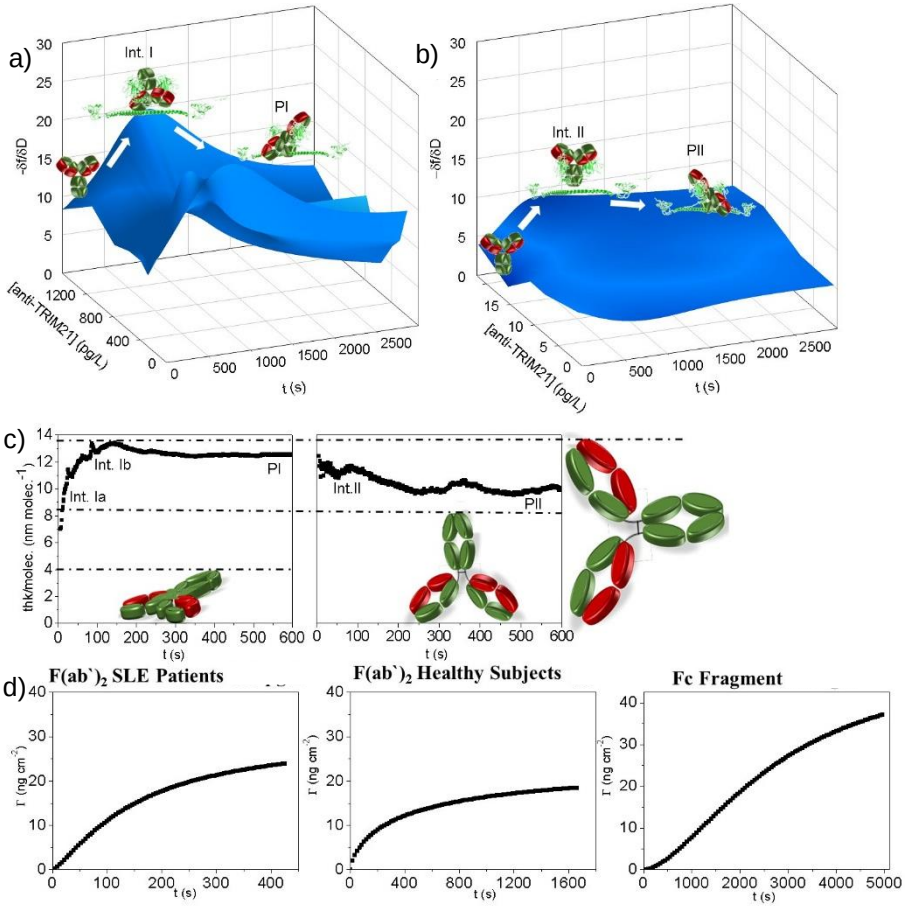

Figure 1.4 -∂f/∂D hypersurface representation according to antibody concentration for a) SLE patients, b) control subjects, and c) thickness per molecule (calculated from DPI measurements) of 300 mg/L of IgGs from SLE patients (left) and control subjects (right). d) F(ab')2 from SLE patients, healthy subjects and Fc measurements of QCM-D, respectively.

The same goes for F(ab')$_2$ fragments obtained from healthy subjects, since they also have higher affinity for the TRIM21α protein than the Fc fragments (t1/2 =

218 s for healthy F(ab')2 fragments at 7.5 pg/L). Hence, the response at higher affinity that is observed for patient and healthy IgGs is related to the Fab region, whereas the response at lower affinity is due to the Fc region. Thus, from the obtained data we suggest that anti-TRIM21 α autoantibodies of both groups are initially recognized by the Fab (first reaction) and then, due to the affinity of the protein by the Fc, the antibody conformation changes to a binding with both one Fab and one Fc linked simultaneously to the TRIM21α protein (second reaction).

1.4 Modelling the recognition

According to the above-mentioned experimental data, the TRIM21α–IgG molecular recognition mechanism in SLE patients and control subjects may involve two binding sites and therefore, two reaction steps. However, it is unclear whether these two steps correspond to consecutive or parallel processes. In order to deeply investigate the molecular recognition process, a conformational dynamic study was performed either by a L1 and L2 norm minimization, using the Akaike information criterion to select the molecular mechanism of protein–protein interaction (Table 1.3).

Table 1.3 Control parameters of the fitting of QCM–D data obtained from the IgG-TRIM21α biorecognition event

	Degrees of freedom	**Residual sum of squares ($ng^2\ cm^{-4}$)**	**Akaike information criterion**	**Second order Akaike information criterion**
SLE	63,800	159,265	23,899	23,899
Control	41,339	170,569	58,598	58,598

The kinetic parameters were fitted with 80,000 data points. The fitting was done considering three coordinates: time, surface concentration of antigenic complex and biomarker concentration in the bulk. The relative deviations of simulation kinetic parameters were lower than 3% in all cases.

The evolution of the piezoelectric signal in function of the reaction time was simultaneously modelled at different autoantibody concentrations for SLE patients and healthy subjects. For that, a two–step consecutive reaction model for autoantibodies from SLE patients was selected (Fig. 1.5a), where autoantibody–TRIM21α binds via Fab and antigenic complex simultaneously binds via their Fab and Fc region in a bipolar bridging mechanism.[7] On the other hand, the selected model when antibodies come from healthy subjects present subtle differences (Fig. 1.5b).

The reaction mechanism proposed for autoantibodies from SLE patients and healthy subjects considers a bivalent recognition process, although the second recognition step for healthy samples was fast. In both cases, these transitions embrace only minor conformational changes, which were identified by plotting the aforementioned thickness per molecule DPI parameter.

Figure 1.5 shows the good agreement between fitted curves and real curves, confirming that the proposed binding schemes predict the autoantibody–TRIM21α system behaviour correctly for a wide range of antibody concentrations (see Table 1. 4). Experiments with increasing concentrations of autoantibodies from control subjects fit to a bimolecular association with a rate constant (k_{on}) and dissociation rate constant (k_{off}) of 26.909 M^{-1} s^{-1} and 7,942 $\cdot 10^{-7}$ s^{-1}, respectively, yielding a kinetic dissociation constant (K_d) of 29 µM. However, for SLE patients autoantibodies, the first association constant corresponds to 128,800 M^{-1} s^{-1} whereas the dissociation constant is 17,070 $\cdot 10^{-7}$ s^{-1} (K_d = 13 nM), which results in a k_{on} and K_d similar to that reported by Keeble *et al.* for the TRIM21–mouse antibody association.[8]

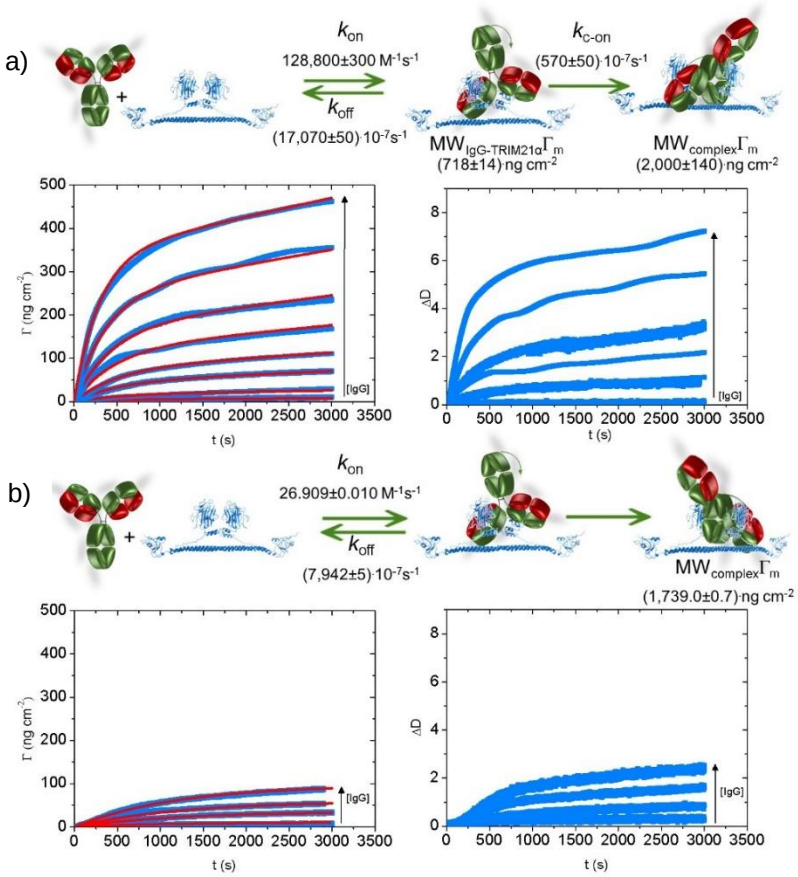

Figure 1.5 Real–time relaxation curves (surface concentration, Γ, and dissipation shift, ΔD, as a function of time) of IgG−TRIM21α interaction for different antibody concentrations. Values of association rate constants (k_{on}), dissociation rate constants (k_{off}) and molecular weight for the maximum surface concentration ($MW_{IgG\text{-}TRIM21\alpha}\Gamma_m$ for reaction intermediates and $MW_{complex}\Gamma_m$ for final antigenic complexes) were obtained from sera of a) SLE patients and b) healthy subjects. Red lines are the fittings from the kinetic parameters shown in the reaction schemes. Only one point out of ten measured points was taken for all plots.

Considering these data, we confirmed that the avidity of anti–TRIM21α autoantibodies for the TRIM21α protein is much higher than the avidity of control

autoantibodies. The $MW_{complex}\Gamma_m$ parameter is independent of the IgG origin, being around 1,800 ng cm^{-2}. As the immobilization strategy is identical in both studies, $MW_{complex}\Gamma_m$ can be considered invariable and therefore, the molecular weight of the antigenic complex can be also considered similar, regardless of the antibody origin. It is another proof that structures of autoantibody–TRIM21α antigenic complexes at equilibrium are structurally very similar regardless whether antibodies come from.

The measured affinity of anti–TRIM21α antibodies makes TRIM21α the highest–affinity Fc receptor in the body, showing higher association constant than bacterial protein A (apparent association constant equal to 8,020 M^{-1} s^{-1}), which may generate a massive immune response in SLE patients, causing a hyper–sensitivity. A large number of activated T–cells secrete large amounts of cytokines, the most important of which is interferon gamma, whose excess activates the macrophages.[9,10] The activated macrophages, in turn, over–produce proinflammatory cytokines such as TNF–alpha. This is particularly important as a part of the body's inflammatory response, which is a characteristic in SLE patients, whose levels are raised.[11]

Table 1.4 Equilibrium kinetics calculated from the fittings of QCM–D data obtained for IgG–TRIM21α biorecognition event*.

IgG	k_{on} $M^{-1}s^{-1}$	10^7 k_{off}	10^7 k_{c_on}	n	$MW_{IgG\text{-}RIM21\alpha}$ Γ_m	$MW_{complex}$ Γ_m
SLE	128,800±300	17,070±50	570±50	1.328±0.006	718±14	2,000±140
Healthy	26.909±0.010	7,942±5	--	1.35±0	--	1,739.0±0.7

We found that the final antigenic structure remains comparable between patients and control subjects, as presented in Figure 1.5. Here, the anti–TRIM21α serum may only accelerate the formation of the antigenic complex. In normal conditions, it may be released locally in undetectable levels and help the immune system defeat membrane antigens. They do not behave as superantigens in healthy subjects, given that the antibody affinity is much lower than in lupus patients. Thus, detectable amounts of anti–TRIM21α autoantibodies were found in healthy donors.[12]

Accordingly, to understand this disease, the undiscovered epitope that predicts our results might be located.

1.5 Linear epitope mapping

As commented before, autoantibodies can simultaneously bind TRIM21α via their Fc and Fab regions. Considering the immune epitope database, the undiscovered epitope may be located on the coiled–coil domain. Given that the RING domain is very hydrophobic, epitopes are not located on the B–Box domain and the PRY–SPRY domain interacts with the Fc fragment.[10] Accordingly, the amino acid sequence of the coiled–coil domain was screened for IgG–binding linear epitopes by probing 9 overlapping solid–phase synthetic polypeptides (Materials and Methods section, table 4.1) with the same pooled serum, from SLE and controls, in a QCM-D sensor.

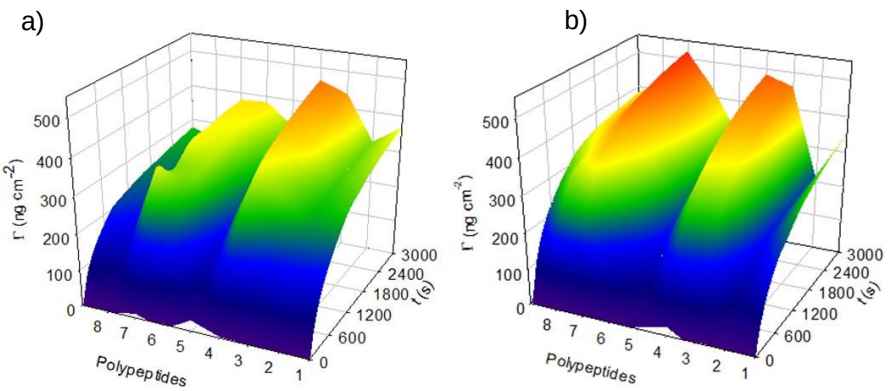

Figure 1.6 Real–time QCM–D measurements of the polypeptide–IgG biorecognition event from a) SLE patients and b) control subjects.

As presented in Figure 1.6a, SLE sera reacted strongly with polypeptide 3 and 4, weakly with the polypeptide 2 and 8, and the moderately with the others. It

should be noted that differences in the intensity of the reaction may reflect the affinity of the reactants, the relative amount of autoantibody present in the sera or a combination of both parameters. The reactive peptides (151–171 and 163–183 aminoacids) partially overlap adjacent reactive sequences and thus may together represent an unknown immunodominant linear epitope on the TRIM21α in SLE patients. Note that the $-\partial f/\partial D$ value for this immunodominant polypeptide corresponds to 22 Hz^{-1}, which is very similar to the measured using TRIM21α as a probe, 20 Hz^{-1}. Hence, it is possible to say that the conformational changes monitored during the TRIM21α:IgG interaction in SLE patients sera mainly correspond to changes in the conformation of the antibody, and not to conformational changes in the probe (TRIM21α or polypeptide).

In order to compare the recognition of the autoantibody–binding peptides of SLE and control antibodies, in the Figure 1.7 was presented the aligned sequences and the corresponding autoantibody–binding regions. For ease of discussion, we have highlighted 2 antigenic hot spots which was defined as antigenic regions that exhibit significantly different reactivity between SLE patients and control subjects. Many interactions that inhibit the binding are replaced by recognition that make positive contributions to the binding depending on the serum origin, which suggests possible associations between the antigenic hot spots and the location of a disease–associated polymorphism in the TRIM21 gene (11p15.4 OMIM 109092). Exon 2 encodes the hot spot #1 region (139–171 a.a.) and immunodominant linear epitope in SLE patients, while exon 3 encodes the hot spot #2 region (199–231 a.a.). The exon 3 also encodes the leucine zipper region of TRIM21α protein, which promotes TRIM21α dimer formation.[13] Consequently, the predicted polymorphisms should be located on exons 2 and 3.

The ProPred web–based algorithm was used to predict the motifs within the sequence of TRIM21α that have high affinity for a comprehensive panel of HLA–DR molecules, including all those expressed by SLE patients and control subjects.[14] The predicted results revealed that LRRKQELAE (a.a. 146–154, being expressed as

the HLA–DRB1*0806 and HLA–DRB1*0816 alleles) and VEIAIKRAD (a.a. 158–166, HLA–DRB1*1304 allele) sequences had higher affinity for any of the MHC class II molecules under evaluation. Interestingly, both sequences are located on the hot spot region #1, suggesting that this genetic region is related to the severity of SLE. Furthermore, the HLA–DRB1*1304 allele may also be related to this disease, given that it expresses the immunodominant linear epitope in SLE patients.

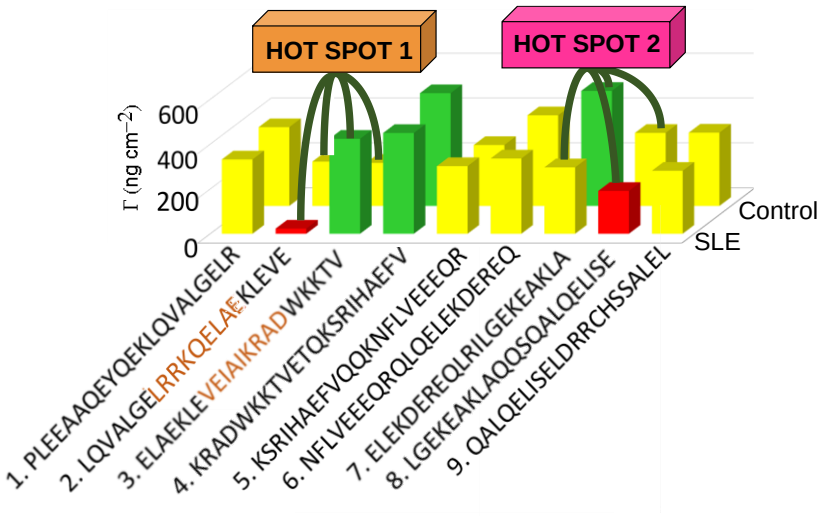

Figure 1.7 Linear epitope mapping for SLE patients and control subjects. Red, yellow and green bars show weakly (<166 ng cm^{-2}), moderate (166 ng cm^{-2} ≤ Intense ≤ 330 ng cm^{-2}) and strong (> 330 ng cm^{-2}) interactions between the protein and autoantibodies, respectively.

Confirming these data, the DRB1*13:04 allele frequency in worldwide populations is related to the reported prevalence of SLE. This allele has a frequency in the USA afroamerican population equal to 0.011, whereas it is 0.004 in the USA Hispanic population.[15] Thus, the associated haplotype DRB1*13:04–DQB1*03:01 has a frequency in the USA Afroamerican population equal to 1.17, being 0.65 in the USA Hispanic population. At the same time, the associated haplotype A*26:01–

B*08:01–C*03:04–DRB1*13:04–DQB1*03:01 has a frequency in the USA Afroamerican population about 0.14, being 0.09 in the USA Hispanic population. This percentage also agrees with the annual prevalence of SLE for black and white populations (present in 0.13 and 0.04% of the healthy population, respectively).[16] Both ratios between haplotype frequencies, 1.8 and 1.5 times, are in good agreement with the fact that African–American women are 1.5 times more likely to get lupus than Latin women. All these data should may suggest that SLE could be related to a specific haplotype associated to the allele DRB1*13:04, as shown in a Nature Versus Nurture study in which genetic and ethnic factors were found to be more important than socioeconomics in influencing disease activity.[17]

1.6 TRIM21α structure

Homology modelling and threading techniques were used to predict a preliminary model of the full TRIM21α structure (Figure 1.8a). The obtained results predict a homodimeric structure, similar to that indicated by Kuboshima et al. [13] The TRIM21α protein homodimerizes by forming interdigitating antiparallel helical hairpins that position the N–terminal catalytic RING domain at opposite ends of the dimer and the C–terminal PRY–SPRY domain at the centre, according to the TRIM25 structure. In addition, the homodimer core comprises an antiparallel coiled–coil with a distinctive, symmetric pattern of flanking heptad and central hendecad repeats, that appear to be conserved throughout the entire TRIM family. [18]

Figure 1.8a shows a good agreement between the proposed model and the experimental results. Real–time monitoring of the TRIM21α deposition shows that this protein is around 6 nm in height as illustrated in Figure 1.9. Furthermore, the reactive regions in control subjects are two different immunodominant linear epitopes (Fig. 1.8b), given that the above commented discontinuous reactive sections (163–183 and 199–219 a.a.) are distant in three–dimensional space. Both reactive

sequences are close to the flexible linker segments, so that these regions may play an important role in the functional mechanism of the TRIM21α protein.

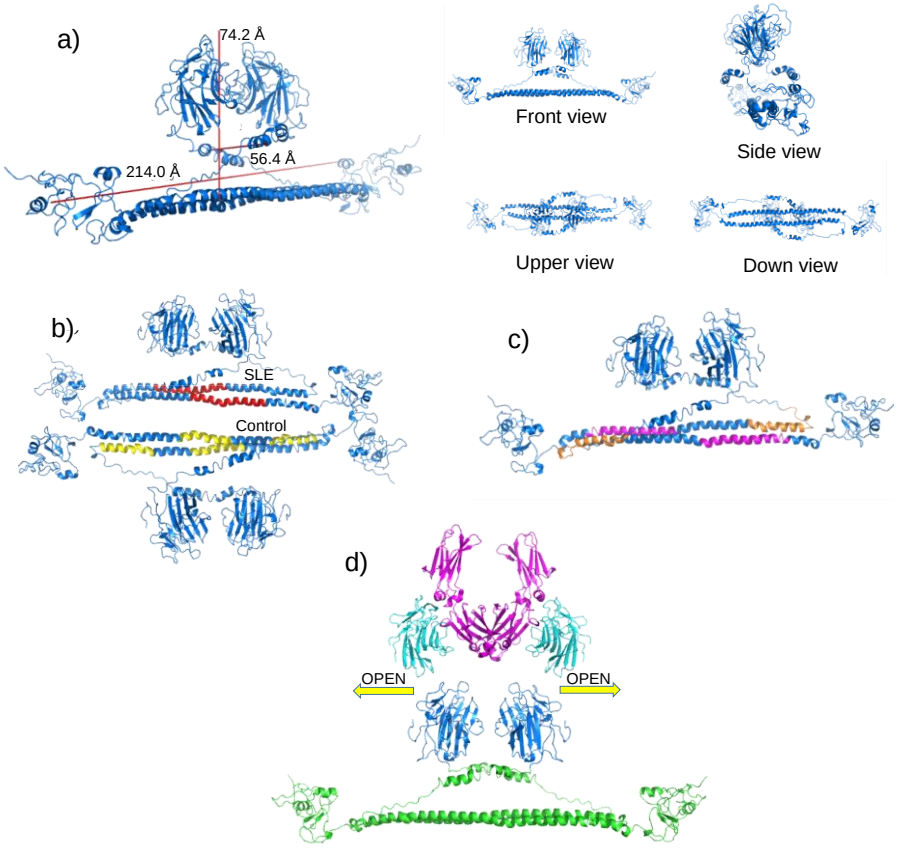

Figure 1.8 a) Preliminary structure of the TRIM21α homodimer with its different views. b) Different epitopes recognized by autoantibodies from SLE patients (red) and control subjects (yellow). c) Location of hot spot #1 (pink) and hot spot #2 (orange) in the TRIM21α structure. d) Scheme of the homodimer–IgG biorecognition. The PRY-SPRY domains open to interact with the Fc fragment of the antibody.

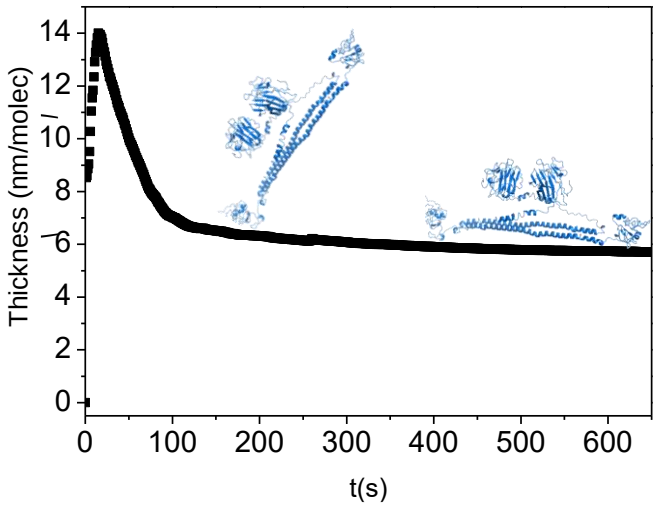

Figure 1.9 Thickness per molecule measured by DPI during the C–terminal–oriented immobilization of TRIM21α. The protein orientation depends on the surface coverage.

First, the protein is anchored in a vertical orientation (thickness/molecule about 14 nm/molecule). However, as the surface coverage increases, DPI monitors a restructuring of the monolayer, in which the TRIM21α molecule orientation changes from a vertical (14 nm molecule^{-1}) towards a flat-on manner (6 nm molecule^{-1}). The TRIM21α theoretical dimensions confirm the process of the protein deposition, about 21.4 x 7.4 x 5.6 (width x height x depth) nm.

Our homology–modelling also confirms that the SLE epitope is linear, and the two hot spots are located in regions that can reorganize the quaternary structure of the protein (Fig. 1.8c). This structure indicates that in the full–length TRIM21α dimer, the two catalytic RING domains will be separated by at least 24 nm at either end of the elongated dimer. In this tertiary structure, the two RING domains within one TRIM21α dimer probably could not cooperate during catalysis. However, the fold–back configuration of the TRIM21α subunits explains how the RING domains can approach the PRY–SPRY domains to enable polyubiquitylation, according to the TRIM25α structure.[17] For this approach, flexible linker segments of hitherto

unknown structure typically separate both the RING and B–box domains (L1, close to hot spot #1) and the coiled–coil and terminal effector domains (L2, the hot spot #2 involves the hinge region of this linker). Consequently, as commented above, polymorphism in these regions would provide a viable mechanism for autoinhibition, which would be consistent with recent researches, which show that the L2 linker plays an important role in high–order TRIM5α assembly.[19] This role is schematized in the Figure 1.8d, where the Fc–homodimer biorecognition is showed.

1.7 Discussion

In this chapter, we have demonstrated in vitro how the autoantibody bipolar bridging mechanism explains the TRIM21α molecular recognition. However, the interaction pattern associated to this binding depend on the antibody origin, SLE patients or healthy subjects. In SLE patients, TRIM21 behave as superantigens whereas in healthy subjects, the autoantibody affinity for this protein significantly decreased.

In bacterial pathogenesis, bipolar bridging of antibodies by superantigens blocks receptor binding, disconnecting antibody recognition from effector function. Thus, the detected autoantibody bipolar bridging so could affect autoimmune pathogenesis in several ways. First, bipolar-bridged complexes should contribute to the pathogenic deposition of immune complex in SLE. Second, bipolar-bridged autoantibodies associated with TRIM21α on the surface of apoptosing cells could inhibit cell clearance, for example by blocking access to so-called ‘‘eat me’’ signals on the cell surface. This one explains the defective clearance of apoptosed cells observed in diseased SLE mice.[20] Thus, the main difference between SLE patients and healthy subjects should be that the anti-TRIM21α autoantibodies from SLE patients may accelerate formation of these pathogenic bipolar-bridged complexes due its high-affinity.

The fine epitope mapping performed shows the existence of different induction pathways of human anti-TRIM21 autoimmunity, given that different

epitopes are found depending on the population under study. Hence, B cell responses against a specific TRIM21 epitope identify a subset of SLE patients. Finally, we show for the first time a preliminary model of the full TRIM21α 3D structure, showing that the flexible linkers may play an important role in the functional mechanism of the TRIM21α protein. Accordingly and given the pathogenic role of TRIM21α in systemic autoimmunity, knowing the biophysical nature of the interactions of this protein is crucial to understand the pathogenesis of SLE and to reach the ultimate goal of designing antigen-specific treatments.

1.8 References

1. Sung–Rok H, Suk–Jung C, Jeong HD, Hong S (2009) *Biosens Bioelectron* 24:1635–1640.

2. Rodríguez–Sevilla E, Ramírez–Silva MT, Romero–Romo M, Ibarra–Escutia P, Palomar–Pardavé M (2014) *Sensors* 14:14423–14439.

3. Escorihuela J, Gonzalez–Martínez MA, López–Paz JL, Puchades R, Maquieira A, Gimenez–Romero D (2014) *Chem Rev* 115:265–294.

4. Mallery DL, McEwan WA, Bidgood SR, Towers GJ, Johnson CM, James LC (2010) *Proc Nat Acad Sci USA* 46:19985–19990.

5. Tompa K, Bokor M, Verebélyi T, Tompa P (2014) *Chem Phys* 448:15–25.

6. Chaplin MF (2016) *Nature Rev Mol Cell Biol* 7:861–866.

7. James LC, Keeble AH, Khan Z, Rhodes DA, Trowsdale J (2007) *Proc Nat Acad Sci* 104:6200–6205.

8. Keeble AH, Khan Z, Forster A, James LC (2008) *Proc Nat Acad. Sci USA* 105:6045–6050.

9. Saha K, Bender F, Gizeli E (2003) *Anal Chem* 75:835–842.

10. Theofilopoulos AN, Kongouris S, Koko DH, Lawson (2001) *Arthritis Res* 3:136–141.

11. Harigai M, Kawamoto M, Hara M, Kubota T, Kamatani N, Miyasaka N (2008) *J Immunol* 181:2211–2219.

12. Weckerle CE, Mangale D, Franek BS, Kelly JA, Kumabe M, James JA, Moser KL, Harley JB, Niewold TB (2012) *Arthritis Rheum* 64:2947–52.

13. Kuboshima M , Shimada H, Liu TL, Nomura F, Takiguchi M, Hiwasa T, Ochiai T (2006) *Cancer Sci* 97:380–386.

14. Singh Z, Raghava GPS (2001) *Bioinformatics* 17:1236–37.

15. Gonzalez–Galarza FF, Takeshita LY, Santos EJ, Kempson F, Maia MH, da Silva AL, Teles e Silva AL, Ghattaoraya GS, Alfirevic A, Jones AR, Middleton D (2015) *Nucleic Acid Res* 28:784–788.

16. Lim SS, Bayakly AR, Helmick CG, Gordon C, Easley KA, Drenkard C (2014) *Arthritis Rheum* 66:357–368.

17. Ho KT, Ahn CW, Alarcón GS, Baethge BA, Tan FK, Roseman J, Bastian HM, Fessler BJ, McGwin G Jr, Vilá LM, Calvo-Alén J, Reveille JD (2015) *Rheumatology* 44:1303–1307.

18. Sanchez JG, Okreglicka K, Chandrasekaran V, Welker JM, Sundquist WI, Pornillos O (2013) *Proc Nat Acad Sci USA* 111:2494–2499.

19. Biris N, Yang Y, Taylor AB, Tomashevski A, Guo M, Hart PJ, Diaz-Griffero F, Ivanov DN(2012) *Proc Nat Acad Sci USA* 109:13278–13283.

20. Rhodes D, Trowsdale (2007*) Mol Immunol* 44:2406–2414.

Chapter II

Functional Mechanism of the TROVE2 RNA–binding Protein in SLE

SLE is a chronic autoimmune inflammatory disease characterized by the presence of B and T autoreactive cells. The disease comprised the production of antibodies towards the components of the Ro/SSA complex (TROVE2/TRIM21 and La proteins). These antibodies become the serological biomarkers for the disease. Particularly, specific antibodies against TROVE2 protein are present at high-levels ($\geq$ 100 U/ml) in patients with SLE. Nevertheless, the host-guest chemistry of the TROVE2 protein remains unknown. In this chapter, we found that the biorecognition mechanism of TROVE2 by autoantibodies is conserved regardless the serum origin, but the cell degradation pathways are different. Furthermore, we proposed a pathologic role for TROVE2 that involves the Ro/SSA complex formation by its interaction with TRIM21α.

2.1 Monitoring anti–TROVE2 autoantibodies

To monitor the antigenic complex formation, recombinant human TROVE2 protein was immobilized over a gold QCM–D electrode via self–assembly monolayer (SAMs).[1] The immobilization process was characterized step by step with X–ray photoelectron spectroscopy (XPS), polarization modulation infrared reflection adsorption spectroscopy (PM–IRRAS), and static water contact angle (SCA) and dual polarization interferometry (DPI) measurements.

The Table 2.1 presents the data obtained by XPS analysis, from the cleaning of the surface until the immobilization of the protein and blockage of possible free active sites. After the addition of MPA acid, the sulphur percentage increases. Next, due to the EDC/NHS linking reagent, the nitrogen appears and its percentage increases in the next steps due to the addition of carbohydrazide, in order to expand the nitrogen–terminal sites to react with the protein. Finally, the addition of the protein and the blockage process increases the carbon and nitrogen percentages.

Table 2.1 Percentage of the main elements during the TROVE2 immobilization

QCM-D Chip	% Au	% C	% O	% S	% N
Cleaned	85	11	4	-----	-----
MPA	38	41	16	5	-----
EDC/NHS	19	52	23	2	3
Carbohydrazide	26	56	12	3	4
TROVE2	30	47	11	3	9
TROVE2/blockage	19	54	12	2	12

The C–terminal–oriented immobilization of TROVE2 monitored by DPI at real-time is presented in Figure 2.1. The protein orientation depends on the surface coverage. Firstly, the protein is deposited in a vertical orientation (thickness/molecule about 9 nm/molecule). However, as surface coverage increases, steric effects also increase and DPI monitors a change in the TROVE2 immobilization from a vertical orientation towards a flat–on manner, 9 to 3 nm/molec. Considering theoretical data, the TROVE2 dimensions are about 8.5 x 5.5 x 2-3 (width x height x thick) nm, confirming the proposed deposition process.[2]

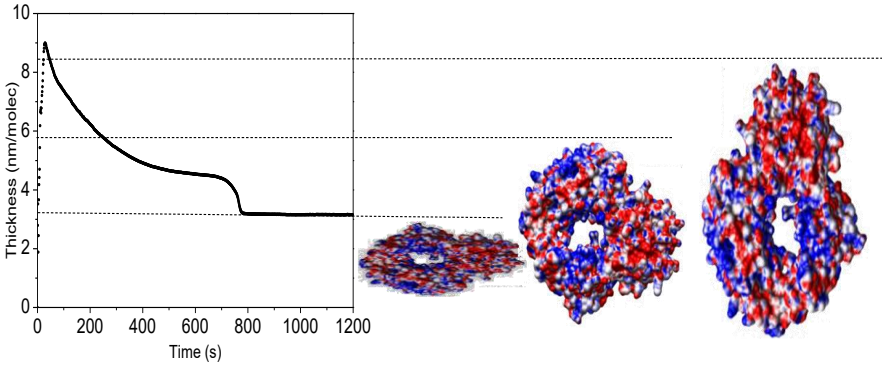

Figure 2.1 Thickness per molecule of the TROVE2 antigen over the DPI chip surface

The surface characterization showed that the immobilization of TROVE2 was correctly completed, generating a hydrophilic self-assembled monolayer of TROVE2 (SCA 56.7±0.8°) with high structural order and surface homogeneity. The amount of protein in the surface of the sensor was 267 ng/cm^2. The antigenic recognition was studied using monomeric fractions of human IgGs previously purified from a pool of 15 anti–TROVE2+ SLE patients, given that polyclonal B cell response is a natural mode of immune response.

The surface concentration of the antigenic complex increases as the human anti-TROVE2 antibodies from SLE patients also increases until saturation is reached

(Fig.2.2a). This progression can be described using the general Hill equation (R^2=0.99), which is based on a model that considers two reaction steps.[2] Herein, it is important to emphasize that the piezoelectric response using bovine serum albumin (BSA), as negative binding control, was nearly zero for all the range of concentrations assayed, so presenting that the piezoelectric response of the SLE IgGs system was free from unspecific interactions. Similarly, the presence of Fc receptors in the protein can be discarded, given that the evolution of the piezoelectric signal was zero using active human antibody Fc fragment as negative control (Figure 2.2c). It is possible to confirm that the response of the developed TROVE2 biosensor is only due to specific antigen-antibody interactions.

Next, to discriminate between SLE and healthy subjects, the recognition involving antibodies from healthy subjects and the cytosolic antigen was studied (Fig. 2.2b). The evolution of the surface concentration in solution of the antigenic complex was monitored according to the concentration of an IgG pool generated from sera of 8 healthy subjects (control IgGs). The obtained piezoelectric response was also adjusted with a nonlinear Hill model (R^2 = 0.99), considering two reaction steps. From these data we can draw two conclusions. Firstly, the control interaction with the TROVE2 protein is less intense than the corresponding to SLE IgGs. The avidity of anti-TROVE2 autoantibodies is higher than the avidity of control IgGs, since the concentration at surface saturation in sera form SLE patients (400 ng/cm^2) is significantly higher than in sera from healthy subjects (150 ng/cm^2). Secondly, the reaction mechanism is similar in both processes (two reaction steps), suggesting that samples from patients and control subjects have different epitopes and therefore, different avidities. Measurements with Fc fragments resulted in zero intensity in all the range of concentrations.

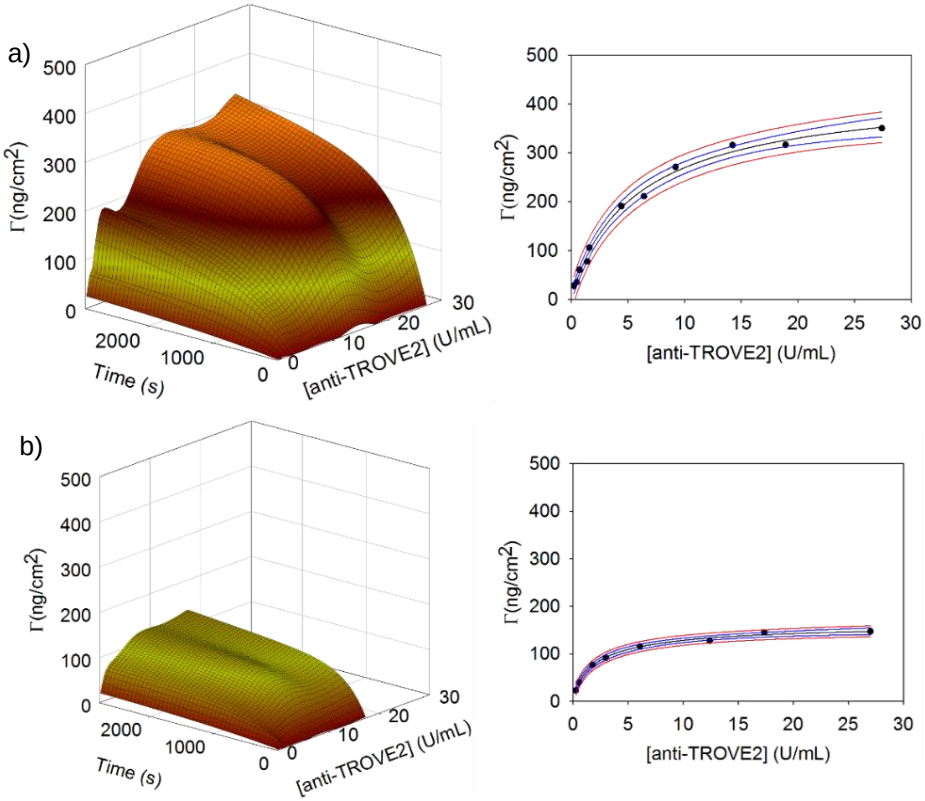

Figure 2.2 Response of the TROVE2-based QCM-D biosensor with respect to the concentration of a) SLE IgGs and b) Control IgGs.

2.2 Dynamic analysis of autoantibodies recognition

The role of conformational changes in the TROVE2 biorecognition was studied by QCM–D at real–time. Figure 2.3a shows the novel -∂f/∂D function according to the reaction time at different IgG concentration in the bulk. The function -∂f/∂D from both sera has the same general characteristics, with a constant peak intensity about 9 Hz. We must highlight that the time–to–start is always the same at all concentrations (zero seconds) so has the time–to–peak dependent of the

accumulation of an intermediate by means of two kinetic states. Consequently, two different species during the biorecognition process for both sera were identified, an intermediate (Int.) and a product (P). This two steps are consecutive. Both functions corroborate that the biorecognition mechanism has a similar collection of elementary steps, but is different depending on the antibody origin (SLE patients or healthy subjects).

To determinate the thickness and dry mass of bound biological molecules onto adlayer with high resolution, DPI analysis were performed, providing real-time measurements. As depicted in Fig. 2.3c, the changes in thickness per molecule of hIgGs showed how the autoantibody-TROVE2 interaction involves two and one reactive species for SLE patients and control subjects, respectively. Consequently, different epitopes must be involved in both biorecognition mechanisms, since their coordinate diagrams are different. In a first step, SLE IgGs targeted initially the TROVE2 antigen in a quasi-side-on orientation (≈ 12 nm/molecule, Int. I), followed by an increase of 1 nm (≈ 13.0 nm/molec, PI), connected both via a reaction intermediate with a "pure" side-on orientation (≈ 14.0 nm/molec, IntI). For healthy subjects (Figure 2.3d), control hIgGs targeted always the TROVE2 antigen in the same quasi-side-on orientation (≈ 12 nm/molecule, PII). In this case, only one process is monitored, but the QCM-D data show two reaction steps. One of these processes must mainly involve changes in the structuring of the surrounding water by the TROVE2 protein. Hence, the protein hydration shell dynamics may play an important role in the TROVE2–IgG molecular recognition of healthy subjects. A complete understanding of the TROVE2 functional mechanism requires a detailed picture of this hydration dynamics.

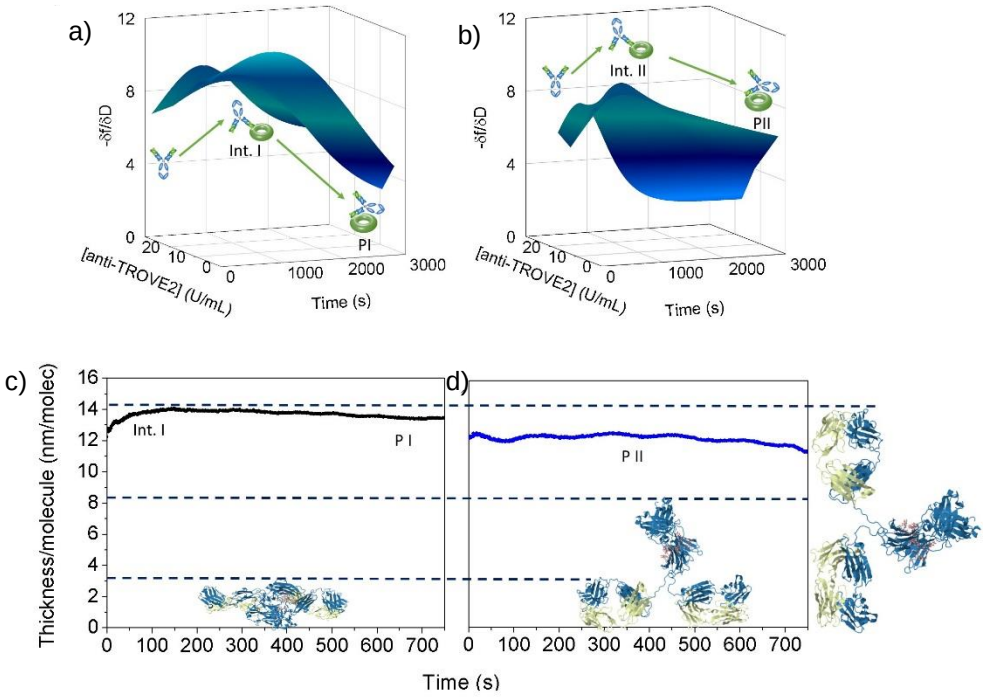

Figure 2.3 a)-∂f/∂D ratio for SLE patients ([anti-TROVE2] = 18.91 U/mL, left) and b) healthy subjects ([anti-TROVE2] = 12.39 U/mL, right). c) Thickness per molecule during the hIgGs:TROVE2 interaction ([SLE anti-TROVE2] = 4.43 U/mL, left, and d) [control anti-TROVE2] = 15.48 U/mL, right).

2.3 Modelling the recognition

In order to deeply investigate the molecular recognition process, a conformational dynamic study was performed either by a L1 and L2 norm minimization, using the Akaike information criterion to select the molecular mechanism of protein–protein interaction. The evolution of the piezoelectric signal according to the reaction time was simultaneously modelled at different autoantibody concentrations for SLE patients and healthy subjects. For that, a two–step consecutive

reaction model was selected, proposing for both autoantibodies a bivalent recognition process.

Figure 2.4 shows the good agreement between fitted curves and real curves, which confirms that the proposed binding schemes predict the autoantibody–TROVE2 system behaviour correctly. Experiments with increasing concentrations of autoantibodies fit to a first bimolecular association with a rate constant (k_{on1}) and a dissociation rate constant (k_{off1}) of around 1.1 L U^{-1} s^{-1} and $6.8 \cdot 10^3$ s^{-1}, respectively. The second association constant (k_{on2}) is about $3.8 \cdot 10^4$ s^{-1} and its corresponding dissociation constant (k_{off2}) $8.2 \cdot 10^4$ s^{-1}, yielding a kinetic dissociation constant (K_d) of 9 U mL^{-1}. According to these data, the avidity of anti-TROVE2 autoantibodies for the TROVE2 protein is high and practically independent on the serum origin. Hence, both epitopes may be similar.

The main difference in the IgG–TROVE2 binding between SLE patients and healthy subjects lies in the molecular weight of the involved antigenic complexes. Figure 2.4 shows how reaction intermediates are heavier than reaction products, $MW_{hIgG-TROVE2} < MW_{complex}$. As commented above, this difference is due to autoantibody–dependent modifications of the surrounding water by the TROVE2 protein during the biorecognition process.[3]

In a protein, the exchange of surface water is controlled by the exposure of the polar groups to the bulk solvent; longer exposure also correlates to greater flexibility[4]. Hence, the IgG–TROVE2 biorecognition may increase significantly the TROVE2 flexibility. This characteristic is best observed depending on the sera origin, $MW_{healthy\ subjects} < MW_{SLE\ patients}$. Sera from SLE patients involve more important structural changes in the surrounding water than sera from healthy subjects. Hence, the antigenic complex formed by anti–TROVE2 autoantibodies from SLE patients is more flexible than the same complex constituted by antibodies from healthy subjects.

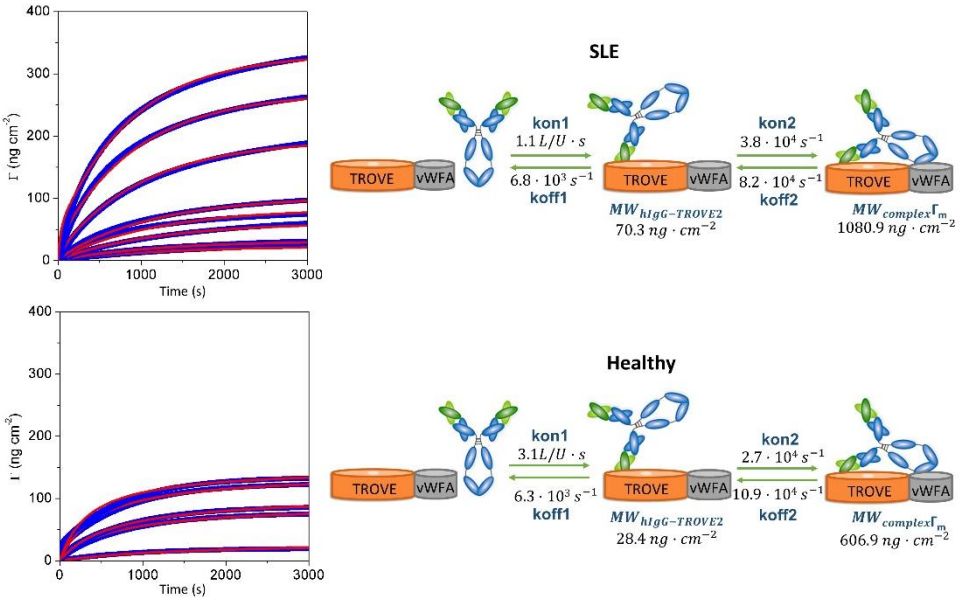

Figure 2.4 Real time relaxation curves (ΔΓ evolution as function of time) of hIgG-TROVE2 interaction for different antibody concentrations in solution sera from SLE patients and healthy subjects. Red lines are the fittings from the kinetic parameters shown on the reaction mechanism.

According to DPI results (Fig 2.3c), TROVE2–IgG biorecognition does not takes place by a bipolar interaction that involves only the $(Fab')_2$ fragment. Hence, we can only suggest that the TROVE2-IgG biorecognition occurs via an antibody bipolar bridging mechanism (Fab bridging the antigens and Fc receptors). Accordingly, and although Fc receptors (such as Fc-gamma receptors) do not exist on the protein surface, a representation of the Fab interaction with the TROVE2 protein, involving a conformational change in the protein that expose the Fc receptors on its surface is shown in Figure 2.5a. Herein, for the first time, the TROVE2 bound to autoantibody is revealed as a mechanism for antibody bipolar bridging.

2.4 MIDAS motif

The TROVE2 protein has a metal ion-dependent adhesion site (MIDAS) motif that binds to ligand (usually aspartate, sometimes glutamate) in a divalent cation–dependent manner. Subsequently, this motif could be related to the host–guest chemistry of the TROVE2–autoantibody system. For this, was studied how the divalent cation interaction regulates Fc–binding affinity. Figure 2.5a shows that the MIDAS motif is a high–affinity Fc receptor. The divalent cation at MIDAS increases the TROVE2 affinity by Fc fragments as increases its ionic radius; e.g. Mg^{2+} (x) < Ca^{2+} (1.3 x) < Sr^{2+} (2.3 x) < Ba^{2+} (10.5 x). Nonspecific interactions -negative binding control- are in the opposite direction, $Ba^{2+} \approx Sr^{2+} > Ca^{2+} = Mg^{2+} = 0$, given that the coordination geometry of this motif may be close in size to the calcium cation. The MIDAS motif of the TROVE2 protein provides mainly a calcium coordination site, being the Fc receptor exposed when the epitope–paratope binding takes place. Accordingly, it is important to emphasize that divalent cations such as magnesium, barium and strontium may also affect functions of the TROVE2 protein.

The MIDAS motif has the capacity of binding Fc fragments, depending on alkaline earth cations in solution. It may so have a key role in the intracellular antibody signaling, helping in the cascade effect of activating, or deactivating, the innate immune system.

Although the TRIM21α protein is a part of the Ro/SS–A ribonucleoprotein complex, the TROVE2–TRIM21α interaction remains unknown.[4,5] So, as the MIDAS domain has adhesive properties, we suggest that the TRIM21α:TROVE2 association could be also considered as a calcium–dependent adhesion system.

Figure 2.5b shows the monitoring of the TRIM21α–TROVE2 binding in the presence and absence of calcium ion in solution. The interaction between both proteins without calcium ion in solution reaches saturation at 122±3.0 ng cm^{-2}, beings a weak interaction. Nevertheless, the presence of divalent calcium ion in solution resulted in a similar maximum signal (136±3 ng cm^{-2}) when the TRIM21α

concentration was decreased 83%, from 300 mg L^{-1} to 50 mg L^{-1}. Furthermore, the stability of this complex is higher in the presence of calcium ion than without this cation.

As Figure 2.5c shows, the serum levels of total anti–Ro/SSA RNP complex, anti–TRIM21 and anti–TROVE2 are correlated in most cases (r=0.72), being statistically significant (P<0.0001, Figure 3.7 chapter III). However, the level of anti–TROVE2 subunit is the one that showed the highest influence, because the anti–TRIM21 influence is minimal. Hence, the TROVE2 protein concentration is directly related to the concentration of the Ro/SSA RNP complex, while the coupling of TRIM21 with this complex may be singular (Figure 5.2). Consequently, as the TRIM21α–TROVE2 binding is a calcium–dependent protein interaction, TRIM21α act in the Ro/SS–A ribonucleoprotein complex depending on the calcium intracellular level. This is why subsequent studies failed to confirm this association, because the intracellular calcium level was not considered.[6,7] Within a typical cell, the intracellular concentration of ionized calcium is roughly 100 nM, but is subject to increases of 10- to 100-fold during various cellular functions.[8]

In SLE patients, the cytoplasmic levels of TROVE2 antibodies, calcium, TRIM21α and TROVE2 are raised. Consequently, the link between all these species may be studied for a full complete understanding of the SLE disease. When TROVE2 is used for blocking the TRIM21α protein, Figure 2.5d shows how the TRIM21α–antibody biorecognition does not take place.

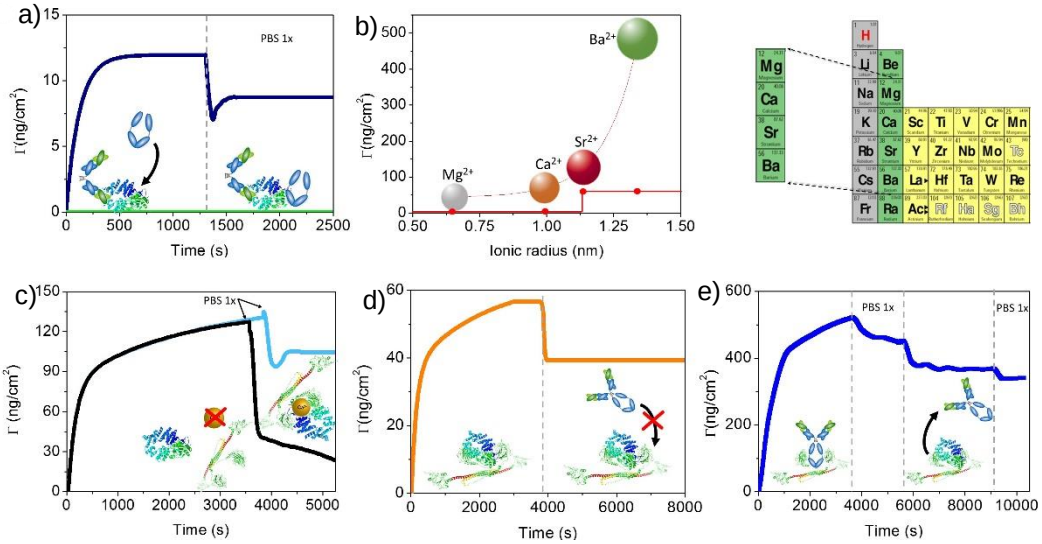

Figure 2.5 a) Surface concentration evolution of Fc fragments when TROVE2 was previously exposed to $F(ab')_2$ fragments comes from healthy serum and without previous $F(ab')_2$ interaction (green). b) Surface concentration of the Fc fragments according to the ionic radius of alkaline earth group divalent cations. Red line represents the nonspecific interactions with BSA. c) TRIM21-TROVE2 interaction in presence ([TRIM21α] = 50 mg/L, blue) and absence ([TRIM21α] = 300 mg/L, black) of calcium ion. d) Antibody recognition (12.5 U/mL) of TRIM21α previously blocked with TROVE2. e) TRIM21α blocking by control antibodies (12.5 U/mL) and subsequent TROVE2 recognition (50 µg/mL).

Furthermore, TROVE2 replaces antibodies when they block the TRIM21α PRYSPRY domain (Figure 2.5e). This one is due to that TROVE2 has a higher affinity for TRIM21α than for antibodies (Figure 2.5d). All these experimental evidences reveal how the TRIM21–PRYSPRY domain binds both TROVE2 and antibodies, having a higher affinity for the TROVE2 protein than for antibodies (Figure 2.5e).

2.5 Discussion

In this Chapter, the supramolecular chemistry of the TROVE2 biological system in SLE patients and healthy subjects has been elucidated, performing *in silico* and *in vitro* analysis. The circulating anti-TROVE2 autoantibodies are likely to undergo "autoantibody bipolar bridging" or the simultaneous binding of the autoantigen TROVE2 to both Fab and Fc domains. In addition to the vWFA domain, a new Fc binding site hidden in the TROVE2 tertiary structure was found, which facilitates the formation of TROVE2 cross-linked autoantibody aggregates. Consequently, anti-TROVE2 autoantibodies that undergo TROVE2-mediated bipolar bridging, resulted in their cross-linking and a similar block to Fcγ receptor and complement interaction. TROVE2-mediated bipolar bridging can occur by a single IgG bound by a single TROVE2 molecule, or, more likely, one TROVE2 molecule interacting with an anti-TROVE2 autoantibody that is bound by the discovered hidden Fc binding site of a second TROVE2 molecule. As the TROVE2 levels increase in SLE patients, it is likely that the resulting cross-linked bipolar-bridged immune complexes form very large protein aggregates.

We have demonstrated that subsequent studies failed to confirm the TRIM21-TROVE2 association probably because the intracellular calcium level was not considered. The TROVE2-TRIM21 binding might occur by means of calcium dependent protein-protein bridges, being located in the TRIM21 PRY-SPRY domain. Accordingly, the calcium-dependent association of TRIM21 with TROVE2 might mediate an inflammatory response in SLE patients through the intracellular immune signaling activated by this TRIM21 PRY-SPRY domain, affecting autoimmune pathogenesis.

Autoantibody bipolar bridging could affect autoimmune pathogenesis in several ways. First, bipolar-bridged complexes may contribute to the pathogenic deposition of immune complex in SLE because these large aggregates would not be cleared from the serum of SLE patients. Second, bipolar-bridged autoantibodies

associated with TROVE2 on the surface of apoptosing cells could inhibit cell clearance, for example by blocking access to so-called ‘‘eat me’’ signals on the cell surface.[9] This hypothesis could explain the defective clearance of apoptosed cells observed in diseased SLE mice.[10]

Given the pathogenic role of TROVE2 in systemic autoimmunity, these findings provide new insights about the pathogenesis of SLE disease. As a result, our findings might explain better the regulation of the TROVE2 physiological function and consequently, this information may be of great interest for understanding SLE disease.

2.6 References

1. Sung-Rok H, Choi SJ, Jeong HD, Hong S (2009) *Biosens Bioelectron* 24:1635–1640.

2. Rodríguez-Sevilla E, Ramírez-Silva MT, Romero-Romo M, Ibarra-Escutia P, Palomar-Pardavé M (2014) *Sensors* 14:14423–14439.

3. Fogarty AC and Laage D (2014) *J Phys Chem B* 118:7715-7729.

4. Kelekar A, Saitta MR, Keene JD (1994) *J Clin Ivest* 93:1637-1644.

5. O’Brien CA, Wolin SL (1994) *Genes Dev.* 8:2891-2903.

6. Yoshimi R, Ueda A, Ozato K, Ishigatsubo Y (2012) *Clin Dev Immunol* 2012:606195.

7. Boire G, Gendron M, Monast N, Bastin B, Ménard HA (1995) *Clin Exp Immunol* 100:489-498.

8. Rizzuto R, Pozzan T (2006) *Physiol Rev* 86:369-408.

9. Falati S, Edmead CE, Poole AW (1999) *Blood* 94:1648-1656.

10. Muñoz LE, Lauber K, Schiller M, Manfredi AA, Herrmann M (2010*) Nat Rev Rheumatol* 6:280-289.

Chapter III

Label-free Piezoelectric Biosensor for Determination of Circulating Autoantibodies for Systemic Lupus Erythematosus Diagnosis

In this chapter, a piezoelectric sensor to quantify specific circulating autoantibodies in human serum was developed. The sensor consisted on a quartz microbalance where TRIM21 and TROVE2 antigens were covalently immobilized to specifically detect autoantibodies for SLE diagnosis. The sensitivity of the biosensor, measured as IC_{50} value, was 1.51 U/mL and 0.32 U/mL, for anti-TRIM21 and anti-TROVE2 circulating autoantibodies, respectively. The sensor is able to establish an interaction fingerprint pattern of circulating autoantibodies, distinguishing SLE patients from health donors. Furthermore, a statistical association of global disease activity with TRIM21-TROVE2 interaction was found (n = 130 lupic patient samples, p-value = 0.0413). Thus, the piezoimmunosensor is capable to determine the biomarker concentration (related to the global SLE disease activity), as well as the structural interaction profile. The performances of the biosensor were compared with standard ELISA and multiplex DVD-array high-throughput screening assays. It showed good agreement between the different immunoassays, which corroborates the viability of piezoelectric biosensor for the clinical practice.

3.1 QCM-D-based anti-TRIM21 biosensor

In this study, we used a direct immunoassay format where the binding between the TRIM21 antigen and its autoantibody is label-free detected. The detection platform is based on TRIM21 immobilization onto gold coated QCM-D quartz crystals via a self-assembled monolayer. As Chapter I shows, recombinant human TRIM21 protein was immobilized onto the gold chip using 3-mercaptopropionic acid as a monolayer precursor and subsequent covalent EDC coupling (surface concentration 267 ng/cm^2, coverage percentage 100%).

Piezoelectric biosensor operates on the principle that a change in mass, resulting from the interaction between the autoantibody (biomarker) and its respective antigenic determinant (attached probe), can be measured label-free by direct detection (Figure 3.1a). Thus, the dependence of the apparent mass change on the bulk concentration of anti-TRIM21 autoantibodies generated from SLE patients was established next. As Figure 3.1b shows, the surface concentration of the antigenic complex increases as the bulk concentration of SLE IgGs also increases. The signals were fitted to the general Hill equation, producing a control curve to analysis the concentration-response curve.

Figure 3.1b shows how this curve achieves a very good experimental fit, R^2=0.99. Hence, it translates satisfactorily signal intensity to autoantibody concentration, being employed in the quantitative immunoassay. Using this fitting, the limit of detection (LOD) for anti-TRIM21 autoantibodies was calculated, 0.01 U/mL. This LOD was established according to the signal which was equivalent to the blank signal (0 ng/cm^2) plus 3 times the standard deviation (SD, 8.85 ng/cm^2) of the blank measures. The limit of quantification (LOQ) was 0.04 U/mL calculated from the blank measurements, also. Finally, the assay sensitivity calculated from the half maximal inhibitory concentration, IC_{50}, was 1.51 U/mL, with a dynamic range (DR, defined presenting the transition from 20% to 80% maximal signal) between 0.32 and 7.17 U/mL. Herein, it is important to emphasize that the developed biosensor

distinguished the studied biomarker from the negative binding control (BSA, signal equal to zero). Furthermore, the detection of anti-TRIM21 autoantibodies markers by the biosensor was consistent with ELISA results (IC_{50} 117 U/mL and LOD 1.2 U/mL), but label-free was about 120 times more sensitive (LOD 0.01 U/mL vs 1.2 U/mL). The use of this sensor was shown to provide good stability and sensitivity, so alleviating the need for labelled secondary antibodies.

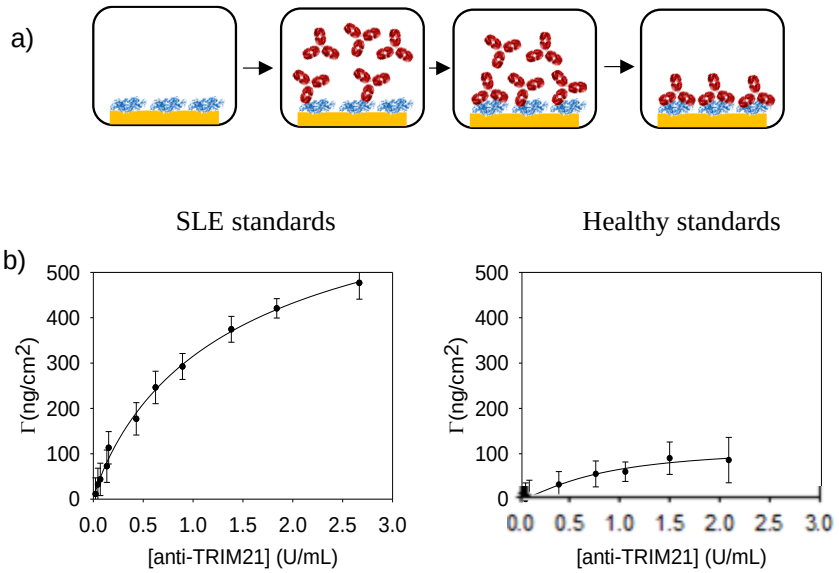

Figure 3.1 a) Scheme of the working format of the piezoimmunosensor; b) Calibration curves for anti-TRIM21 autoantibodies from SLE patients and healthy subjects.

In order to discriminate between SLE and healthy subjects (Figure 3.1b), the recognition event that involved only Igs from healthy donors was researched. As in the previous analysis, the evolution of the surface concentration of the antigenic complex was studied according to the bulk concentration of healthy IgGs (control IgGs). The obtained response was also evaluated via the general Hill equation (R^2= 0.95). However, a substantial change in the antibody selectivity is observed

depending on the standard origin, which shows that anti-TRIM21 autoantibodies from patients and healthy subjects have different selectivity (maximum surface concentration 766 ng/cm^2 for SLE standard and 110 ng/cm^2 for healthy standard).

The PRY-SPRY domain in the TRIM21 protein has the capability to recognize Fc. This is one reason why the developed QCM-D-based TRIM21 biosensor showed non-zero signal for health subjects (Figure 3.1b). Thus, the cut-off for this assay must be established in 110 ng cm^{-2}. This value is important for the anti-TRIM21 detection. The proposed cut-off value helps us to distinguish between positive (> 0.2 U/mL, pathological range) and negative (< 0.2 U/mL, normal range) samples.

The accuracy of highly sensitive biomarker methods is often drastically reduced by the presence of different circulating endogenous factors in samples, causing matrix effect. A commonly used method to remove this effect is the sample dilution, which works well with immunoassays exhibiting very high sensitivity.[1] Thus, a fit-for-purpose assessment of matrix effect was performed here for improving results and for demonstrating the applicability of the proposed piezoimmunosensor for the direct analysis of serum samples. Figure 3.2b shows how the signal due to non-specific interactions of the matrix (the sera pool without immunoglobulins G) of SLE patients (yellow bars) and healthy subjects (blue bars) decreases as the serum is diluted. The matrix effect of the QCM-D-based TRIM21 biosensor is below the cut-off value for serum samples diluted 1:100 (80 ng cm^{-2} from SLE patients and 107 ng cm^{-2} from healthy subjects). Consequently, the developed biosensor can directly estimate the concentration of anti-TRIM21 autoantibodies from a 1:100 blood serum dilution.

3.2 QCM-D-based TROVE2 biosensor

To quantify the anti-TROVE2 autoantibodies, the previous immunosensor was adapted for this purpose. Recombinant human TROVE2 protein was immobilized onto a gold QCM-D sensor via 3-mercaptopropionic acid as a

monolayer precursor and covalent EDC/NHS coupling (surface concentration 194 ng/cm^2, coverage percentage 91%). The immobilization process was characterized step by step in Chapter II, showing that the immobilization of TROVE2 was correctly completed. We generate a hydrophilic self-assembled monolayer with high structural order and surface homogeneity.[2]

Figure 3.2a shows how the surface concentration of the antigenic complex detected label-free by the developed piezoimmunosensor increases, as the concentration of SLE IgG also increases (0.01-1.5 U/mL). This progression can be described using the general Hill equation (R^2=0.99), being LOD 0.005 U/mL. This LOD is 400 times more sensitive than the reached by the commercial ELISA test (LOD 2 U/mL). Its LOQ resulted in a value of 0.019 U/mL, the IC_{50} 0.32 U/mL, with a DR from 0.07 to 1.46 U/mL. The negative binding control was nearly zero for all the range of concentrations employed, so presenting that the biosensor response was free from unspecific interactions. Furthermore, in this case, the presence of Fc receptors in the protein can be discarded, given that the evolution of the piezoelectric signal was zero using active human antibody Fc fragment as negative binding control. The response of the developed TROVE2 biosensor is only due to epitope-paratope specific interactions.

As the previous case, in order to discriminate between SLE and healthy subjects (Figure 3.2a) the recognition involving healthy IgGs was also studied. The obtained piezoelectric response was adjusted with a nonlinear Hill model (R^2 = 0.99), showing a substantial change in the autoantibody selectivity (maximum surface concentration 440 ng/cm^2 for SLE IgGs and 150 ng/cm^2 for healthy IgGs). The anti-TROVE2 autoantibodies have different paratopes depending on the standard origin. Hence, we must establish a cut-off value for this biosensor equal to 150 ng/cm^2 (110 ng/cm^2 for the QCM-D-based TRIM21 biosensor). This value facilitates to distinguish easily between a pathologic range (> 0.16 U/mL) and normal range (< 0.16 U/mL). In order to unify sensing criteria, the cut-off value for TRIM21 and TROVE2 piezoimmunosensors should be 150 ng/cm^2 in both cases.

Figure 3.2b shows how the signal due to non-specific interactions of the matrix (the sera pool without immunoglobulins G) in SLE patients (black bars) and healthy subjects (brown bars) decreases as serum is diluted. In both cases, the matrix effect was fully removed by diluting the serum 100 times (5.9 ng/cm^2). Hence, the developed QCM-D-based TROVE2 biosensor estimates correctly the concentration of anti-TROVE2 autoantibodies in a 1:100 serum dilution. TRIM21 and TROVE2 piezoimmunoassay can quantify label-free anti-TRIM21 and anti-TROVE2 autoantibodies in human serum, without previous purification steps.

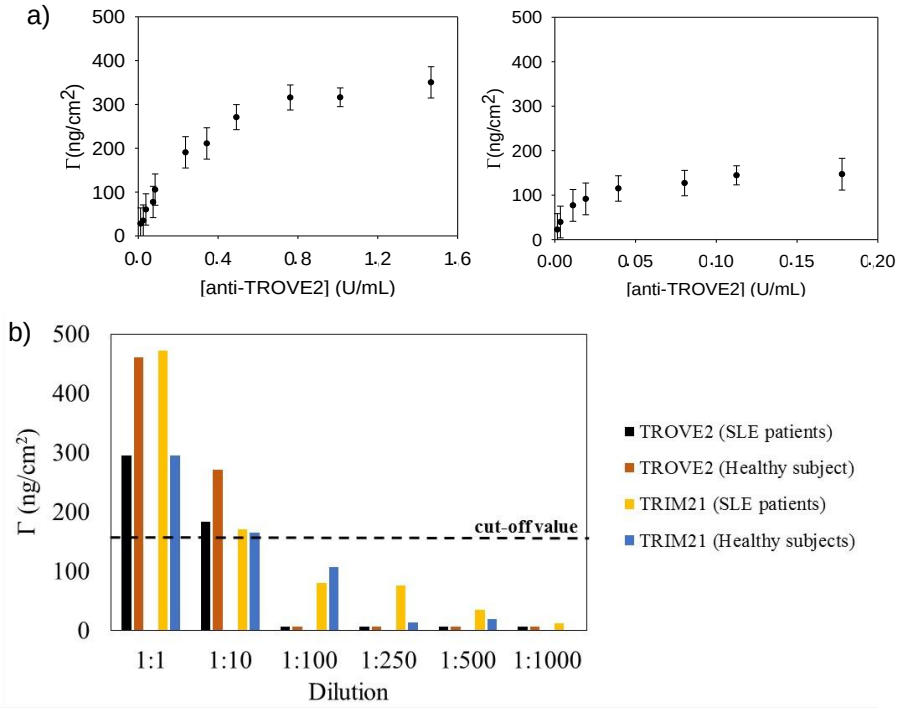

Figure 3.2 a) Calibration curves for anti-TROVE2 autoantibodies from SLE patients and healthy subjects. b) Effect of serum matrix on the analytical signal of the developed QCM-D-based assays.

3.3 Interaction fingerprint pattern

The main feature and advantage of QCM-D, compared with the conventional QCM, is that it in addition to measuring changes in resonant frequency (f), a simultaneous parameter related to the energy loss or dissipation (D) of the system is also measured. Thus, using both signals, the $-\partial f/\partial D$ function is calculated, providing the reaction path of the monitored interaction. Previous biosensors can so estimate these structural interaction profiles; that is, these piezoimmunosensors can simultaneously measure both the biomarker concentration (traditional sensor) and the interaction fingerprint pattern (innovative sensor).

As commented above, autoantibodies samples from patients and control subjects have a different recognition mechanism of the recombinant human TRIM21 protein. In view of that, the interaction fingerprint pattern was next established from the $-\partial f/\partial D$ function. For that, 80,000 data points with three coordinates (time, f, D) was measured at real time for each biomarker concentration (0.06-8.0 U/mL) during 3,000 s using the developed biosensor. Figure 3.3 shows how the TRIM21-IgG reaction path is different for SLE patients and healthy subjects. Thus, in SLE patients, the $-\partial f/\partial D$ function is a peak-shape function whose peak intensity does not depend on the bulk concentration of anti-TRIM21 autoantibodies, 19 Hz at 1000 s. However, the $-\partial f/\partial D$ function from healthy subjects has the same characteristics than from SLE IgGs, but with a constant peak intensity about 9 Hz at 600 s (8.8 Hz at 1,000 s), which is 2.1 times lower than in the patient group. Consequently, a novel interaction fingerprint pattern can be established for the fast identification of anti-TRIM21 circulating autoantibodies from SLE patients in human serum samples. This pattern represents the structural interaction profile of the sick antigenic complex and could be a selection criterion for further screening strategies. Moreover, it can be applied to detect false positive ($-\partial f/\partial D < 10$ Hz at 1000 s) and to improve the true positive rate ($-\partial f/\partial D = 19$ Hz at 1000 s) of the developed ultrasensitive immunosensor. The $-\partial f/\partial D$ function shows promise to fully leverage the wealth of information being generated by the protein conformational dynamics.

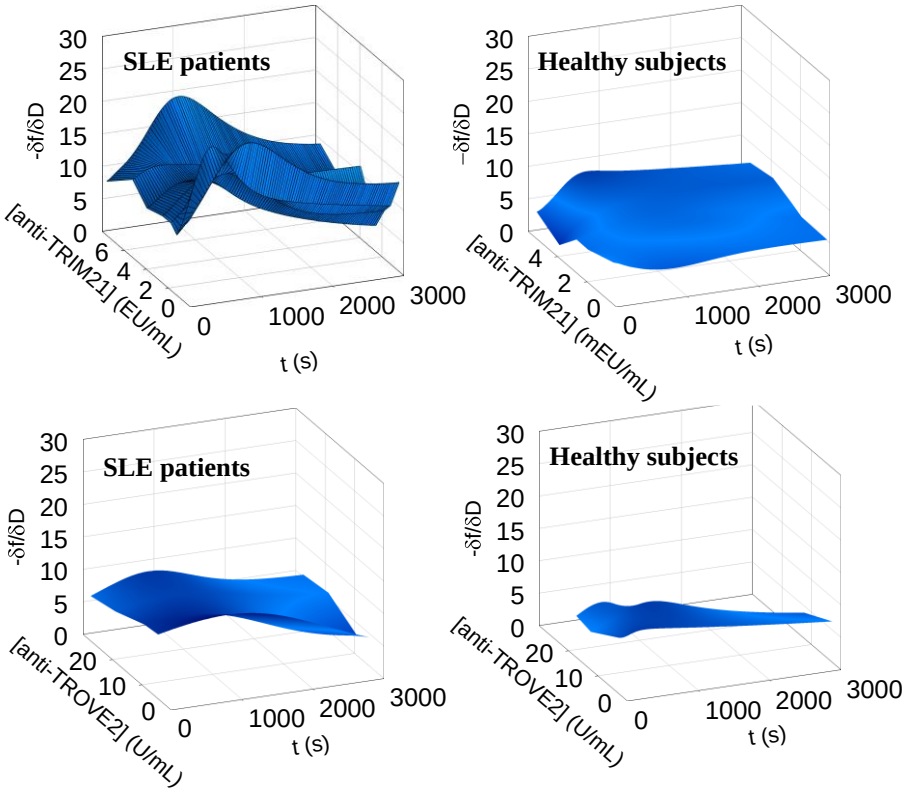

Figure 3.3 Interaction fingerprint pattern for the Ro subunit:autoantibody binding from sera of SLE patients and healthy subjects.

Following this step, the developed QCM-D-based TROVE2 biosensor allows also the TROVE2-antibody interaction fingerprint pattern to be calculated. Figure 3.3 shows how this pattern is not such a specific pattern of SLE. The reaction path of this interaction was found to be similar for SLE patients and control subjects, and independent on the bulk concentration of anti-TROVE2 standards (0.2-27 U/mL). It is a peak-shape function with a maximum value of 11 Hz at 1,000 s for silk autoantibodies and of 9 Hz at 300 s (8.6 Hz at 1,000 s) for healthy autoantibodies. Both values are very similar and consequently, it is not possible to differentiate easily

between SLE patients and healthy subjects through this pattern. The only feasible pattern for characterizing the SLE patient group is the TRIM21-antibody fingerprint.

3.4 Reusability

Reusability is one of the main issues found in biosensing. To estimate the piezoimmunosensor mean life, repeated analyses of anti-TRIM21 standards (1.5 U/mL) were carried out. After the regeneration step, the sensor chip was considered useful while the piezoelectric signal remained above 90% of the initial value. In a continuous work, the piezo signal remained constant for at least 30 assay cycles, being the useful life of the sensor.

3.5 Multiplex assay

As Hanly et al. established, there is a significant association between elevated global SLE disease activity index SLEDAI (which is a tool used to quantify the symptoms of patients with SLE) and the concentration of anti-Ro circulating autoantibodies.[3] Consequently, we used an ordinal regression model (n = 130 SLE patients, see Table B in Appendix) to evaluate the association of global SLE disease activity with the concentration in serum of anti-TRIM21 and anti-TROVE2 and the interaction between both.

No statistical association of activity index with the anti-TRIM21 and anti-TROVE2 concentration was found (p-value = 0.335 and 0.109, respectively). However, there was a statistical effect considering the TRIM21-TROVE2 interaction (p-value = 0.0413). Thus, the simultaneous measurement of both autoantibodies may become an important part of the overall assessment of SLE patients in clinical practice. For charactering fully SLE patients, it is necessary to measure simultaneously the individual concentration in serum of anti-TRIM21 and anti-TROVE2 autoantibodies, as well as the novel established interaction fingerprint pattern (to be considered to in the SLE management). Hence, a duplex immunoassay

should be developed, which would have the ability to detect both biomarkers (anti-TRIM21 and anti-TROVE2) concurrently in a single biological sample, along with negative and positive controls. As a first approximation, a microarray detection system based on the compact disc technology was used for transferring this test to the clinical practice.[4]

A non-competitive sandwich immunoassay for analysis of anti-TRIM21 and anti-TROVE2 circulating immunoglobulins was employed for proving the concept in this study (Figure 3.4a). For demonstrating the high-throughput screening, it required the integration of the larger number of single samples on the assay. In this work, 54 samples were analysed in a simple disc. To reach this goal, on the polycarbonate surface of standard DVDs was printed in a microarray format (54 arrays per disk of 2 x 4 spots), including spots for two different biomarkers (recombinant human TRIM21 and TROVE2) and positive (human immunoglobulin) and negative (BSA) binding controls, in triplicate.

Purified antibodies were tested by checkerboard titration in the proposed non-competitive assay. A wide interval of coating protein concentration, from 0.10 to 50 mg/L, was tested against serial dilutions of a calibration serum pool contained samples from 20 sera from anti–Ro+ patients with SLE (1/1 – 1/200 dilution). Thus, optimal coating protein concentrations and sera dilution were selected on the basis of obtaining good signal intensity (S/N > 60) in non-competitive format. The selected concentration for both proteins was found to be 40 mg/L and 1/100 sera dilution. The optimum time of primary antibody incubation was 15 and 30 min for the secondary antibody. Regarding detection antibody, the optimal concentration was obtained diluting the gold labelled secondary antibody 1/100 fold in PBS-T.

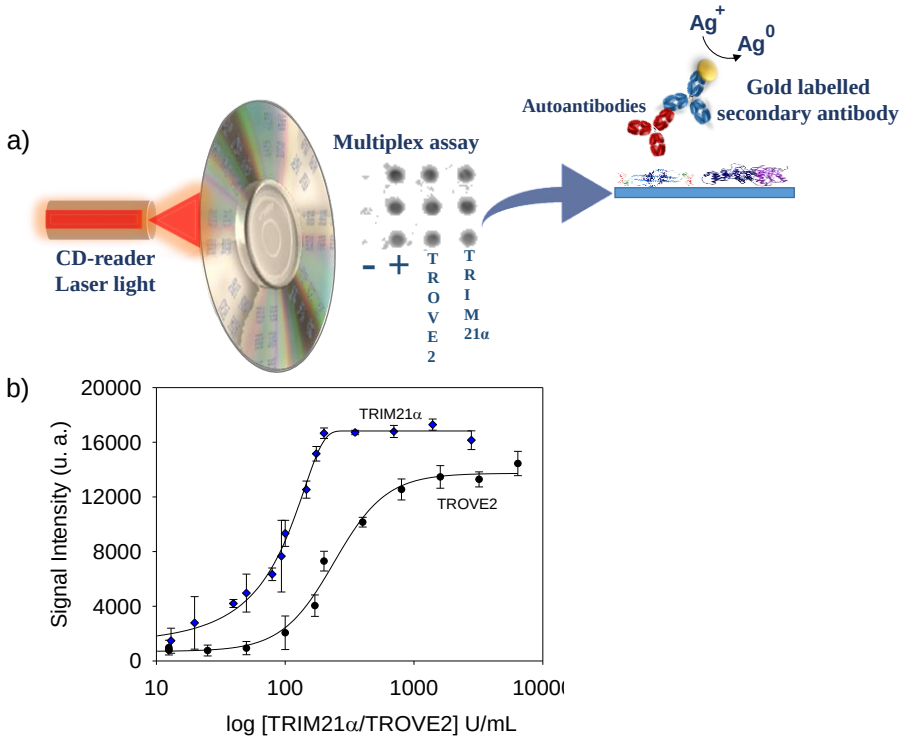

Figure 3.4 a) Scheme of the microarray detection system on a standard DVD. b) Calibration curves for anti-TRIM21α and anti-TROVE2 autoantibodies.

Under the optimized conditions, the sensitivity, limit of detection and working range of each probe were established. The calibration curves obtained for the simultaneous determination of the four integrated immunoassays are shown in Figure 3.4b. The standard curve for the anti-TRIM21 biomarker was fitted using the four-parameter Gompertz equation (R^2 = 0.997), because the diffusion of reactants greatly influence the assay response at these experimental conditions.[5] As can be seen, the LOD is 11 U/mL, LOQ 34 U/mL, IC_{50} 96 U/mL and DR from 35 to 152 U/mL for the TRIM21 immunoassay. On the other hand, for the anti-TROVE2 biomarker, the calibration curve was fitted from the four-parameters Hill equation

(R^2 = 0.995), providing a LOD equal to 58 U/mL, LOQ 107 U/mL, IC_{50} 228 U/mL and DR from 109 to 444 U/mL. Herein, it is important to emphasize that cross-reactivity were depreciable at these experimental conditions. The relative standard deviation values along the whole calibration curve were below 10%. It is also worth mentioning that the sensitivity of the multiplexed immunoassay is comparable to this obtained with ELISA (IC_{50} 117 and 42 U/mL for anti-TRIM21 and antiTROVE2 in ELISA assay, respectively), using the same antibodies and much higher than QCM-D-based label-free biosensor (ELISA plate≈DVD<QCM-D).

Regarding the assay quality, two controls were included in each array. The first one comprises the negative binding control, so monitoring the ability of the antibodies to specifically recognize the studied antigens. This control was nearly zero for all the range of assayed concentrations, showing how non-specific interactions are rejected. Furthermore, matrix effect was not detected at these experimental conditions. Finally, the second control is the positive binding control and aims to give information about the amplification step, this signal being used as an inter- and intra-disc internal calibrator.

We demonstrated the assay`s versatility for adapt it onto more simple and productive methods, facilitating the development of a point of care testing to monitor the global SLE disease activity. The developed multiplex immunoassay can be already incorporated into the accelerated monitoring protocols, providing a rapid, cost-effective mechanism to known simultaneously the concentration of anti-TRIM21 and anti-TROVE2 circulating autoantibodies in serum, without purification, only diluting it. Its central advantage is that it allows the serum concentration of anti-TRIM21/anti-TROVE2 autoantibodies to be easily monitored in a high-throughput screening mode.

3.6 Biostatistics

The statistical work developed with the obtained results confirms that serum levels of total anti-Ro, anti–TRIM21 and anti–TROVE2 are correlated in most cases (r=0.72). The correlation of the two subunits with the total anti–Ro protein concentration is statistically significant (P<0.0001), being the level of anti–TROVE2 subunit the one that showed the highest influence. Considering the interaction of TRIM21 and TROVE2 there is a statistical effect (P=0.0413, Figure 3.5). Probably, these levels can be related with the symptoms manifestation.

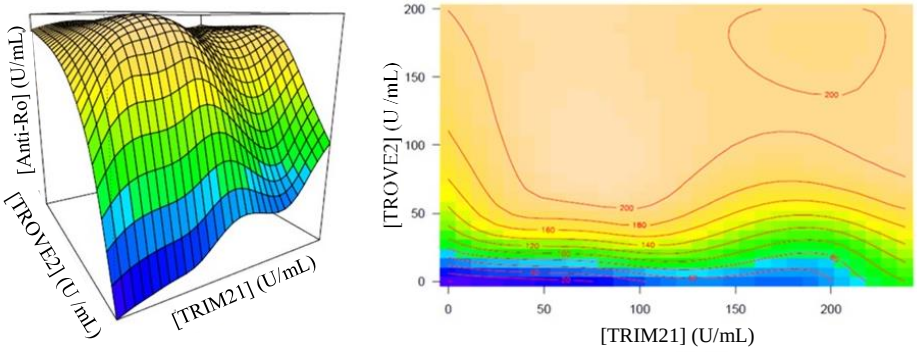

Figure 3.5 Correlation for serum levels of anti-TROVE2 and anti-TRIM21α with anti-Ro.

As presented, bioestatistical data showed a relation between anti-TRIM21/TROVE2 autoantibodies with total anti-Ro autoantibodies. In order to define the quantity of each autoantibody at the same time, the immunosensor was adapted to a simplified platform, containing both proteins, as presented. The simultaneous measurement of both autoantibodies may become so an important part of the overall assessment of SLE patients. The new immunoassay may have the ability to detect both analytes concurrently in a single biological sample.

3.7 Discussion

According to the results, label-free QCM-D technology provides an accurate, rapid and real-time approach to quantify anti-TRIM21/anti-TROVE2 autoantibodies. In usual immunoassay formats, such as ELISA plate tests or other immunoassays, the detection of these circulating antibodies is always indirect because one of the immunoreagents is labelled. However, in QCM-D approach the detection is direct, the corresponding superantigen is immobilized on the gold chip, and a direct piezoelectric signal is produced when the immune interaction occurs. Piezoimmunosensors combine the selectivity provided by immunological interactions with the high sensitivity achieved by the transducer. As a result, this sensitivity is here about 100 times higher than those obtained by traditional ELISA plate assay.

In addition to the biomarker concentration in human serum, the developed QCM-D-based biosensors enable simultaneous measurement of the structural interaction profile providing one of the clearest and quantitative characterizations of biorecognition interactions available today. Thus, the fingerprint of the TRIM21-antibody binding is a valid pattern of SLE, allowing this patient group to be fully reported.

As this work shows, the characterization of the SLE patient group may be realized measuring simultaneously the TRIM21-antibody binding fingerprint pattern (related to diagnosis) and the serum concentration of anti-TRIM21 and anti-TROVE2 (related to the SLE disease activity). For that reason, the ideal biosensor format for SLE diagnostic applications should be label-free, multiplex, and sensitive, enable direct measurement of the structural interaction profile and have enough throughput to be widely applicable into clinical practice. The multichannel quartz crystal microbalance array is so the best option for enabling easy transfer the detection of anti-TRIM21/TROVE2 circulating autoantibodies into clinical practice. Clinical and

laboratory settings may overcome reticence to its use, although they require more highly trained personnel.

Thus, in this work, ultrasensitive label-free QCM-D biosensors were developed for quantifying anti-TRIM21 and anti-TROVE2 autoantibodies in human serum, without previous purification. Their low limits of detection, about 100 times below than those obtained by traditional ELISA tests, may allow these circulating autoantibodies to be detected in advance of the SLE manifestation. Furthermore, the innovative QCM-D-based TRIM21 biosensor allowed a specific structural interaction profile in SLE patients to be monitored, which could be used to characterize clinically subjects with this model systemic autoimmune disease.

From a population of 130 SLE patients, a statistical association of global SLE disease activity with the TRIM21-TROVE2 interaction was found. Consequently, the full characterization of the SLE patient group might be realized by measuring simultaneously the TRIM21-antibody binding fingerprint pattern the serum concentration of anti-TRIM21 and anti-TROVE2 autoantibodies. To our knowledge, the QMC-D technology is the only tool that can measure simultaneously both parameters. We so preformed an innovative biosensor that can do these two things at once. In future, the developed piezoimmunosensors may be a cornerstone in long-term studies to monitor the stability of anti-TRIM21 and anti-TROVE2 autoantibody profiles over time, to determine their ability to predict clinical events and to examine the significance of a change in concentration of these circulating autoantibodies. If our preliminary results are confirmed, the developed platforms could be widely used in routine laboratories.

3.8 References

1. Ramakrishna N, Mehan VK (1993) *Mycotoxin Res* 9:53-63.

2. Stein AJ, Fuchs G, Fu C, Wolin SL, Reinisch KM (2005) *Cell* 12:529-537.

3. Hanly JG, Su L, Farewell V, Fritzler MJ (2010) *J Immunol Methods* 358:75-80.

4. Morais S, Tamarit-López J, Carrascosa J, Puchades R, Maquieira A (2008) *Anal Bioanal Chem* 391:2837-2844.

5. Avella-Oliver M, Gimenez-Romero D, Morais S, González-Martínez MA, Bueno PR, Puchades R, Maquieira A (2013) *Chem Commun* 49:10868-10870.

4. Materials and Methods

4.1 Serum Samples

Hundred sixty serum samples from patients with SLE, and 43 control samples (healthy subjects) were obtained from the Department of Rheumatology of the University and Polytechnic La Fe Hospital, Valencia (Spain). To develop a diagnostic tool with broad application to the heterogeneous pathogenesis of SLE patients, the calibration serum pool contained samples from fifty sera from anti–Ro+ patients with SLE (> 17 mg/mL). Control serum pool contained samples from eight sera from healthy subjects. Blood samples were collected by venepuncture of the patient's forearm vein, processed immediately following extraction, handled by standard procedures, and stored at −80°C in La Fe Biobank. All patients satisfy the SLICC-ACR2012 classification criteria.[1]

4.2 IgG Purification

Immunoglobulins type G (IgGs) were purified by affinity chromatography (GE Healthcare, HiTrap™ protein G HP). IgGs were eluted with glycine 0.05M (Sigma-Aldrich, for electrophoresis ≥ 99%) at pH 2.5 and immediately the pH was changed to 7.4 with phosphate buffer -Na_2HPO_4 (Scharlau, reagent grade) 0.023M and KH_2PO_4 (Scharlau, extra pure) 0.0018 M. Using ultrafiltration (Pall Corporation, Macrosep Advance Centrifugal Device, 30K MWCO), the sample was concentrated in a small volume and reconstituted with phosphate-buffered saline (1x PBS) -KCl (Scharlau, reagent grade) 0.0027 M, Na_2HPO_4 0.01 M, KH_2PO_4 0.0018 M and NaCl (Scharlau, synthesis grade) 0.137 M- at pH 7.4. Finally, the concentration of anti-TRIM21 autoantibodies were quantified by means of a human anti-SSA (Ro-52) ELISA kit (Signosis-Biosignal Capture). The optical density of each well was measured using a microplate reader (Wallac, Victor 1420 multilabel counter) at 450 nm.

4.3 Quartz crystal microbalance with dissipation monitoring (QCM–D)

QCM–D measurements were carried out using commercially available gold Q–sense sensors E1 (5 MHz, QSX 301, Biolin Scientific). Prior to the experiments, the sensor's surface was cleaned according to the manufacturer protocol. The frequency and dissipation variations were monitored using Q–Sense (Biolin Scientific) device equipped with a liquid flow cell setup. All experiments were carried out in the 1x PBS solution to dissolve protein and the resonance frequency was stabilized in 1x PBS. The flow rate was 50 µL/min at 25 ℃.

4.3.1 Self–Assembly Monolayer (SAM)

Unmodified piezoelectric chip was firstly cleaned by treating the chips with UV for 10 minutes. Afterward, the chip was immersed in a solution of 5:1:1 of mili–Q water, ammonia 25% (Scharlau) and peroxide 30% (Scharlau) at 75 °C. After that, the chip was rinsed with mili–Q water, and blown dry with high purity nitrogen. Finally, the chip were treated again with UV during 10 minutes. Self–assembled monolayer was conformed by treating the quartz crystal gold chip with 10 mM of MPA (3-mercaptopropionic acid, Sigma-Aldrich) overnight, and then the electrode was activated with 46 mM of EDC (-N-ethyl-N'-(3-dimethylaminopropyl) carbodiimide), purum grade-/NHS (N-hydroxysulfosuccin-imide 98%, Sigma-Aldrich) for an hour to produce carboxyl chip. After activation of SAM, following steps were proceeded for each scheme.

4.3.2 Immobilisation of TRIM21 and TROVE2 on hydrazine chip

Hydrazine chip was prepared by converting carboxyl group on SAM to hydrazide group by treating with 5 mM carbohydrazide 98 % (Sigma-Aldrich) before protein immobilisation. One hundred microliter of TRIM21α (recombinant human

RO-52/SS-A, Sigma) or TROVE2 (recombinant human RO-60/SS-A, long isoform, ProSpec) was added at the dose of 33 mg/L (around 267 ng/cm^2, saturation probe), and incubated for one hour to be cross-linked to the activated gold surface via its N-terminal amino group. Uncrosslinked residues were blocked by 1 M ethanolamine-HCl ≥ 98% (Sigma-Aldrich) and a blocking buffer containing 1 mM ethylenediaminetetraacetic acid (Riser), 0.25% bovine serum albumin (BSA, Sigma-Aldrich, ≥98% agarose gel electrophoresis), and 0.05% Tween-20 (Scharlau, synthesis grade). All reaction time was 1 h and sensor chip was cleaned using distilled water between reactions.

4.3.3 Immobilisation of the N–terminal polypeptides on carboxyl chip

After chip activation, it was rinsed with mili-Q water and the polypeptide sequences from TRIM21α (peptides&elephants) in a concentration of 33.3 ppm were added. Each polypeptide was terminated by an amino acid with a free amine group, and an amide group at its C-terminus. Those chips were blocked with 20 mg/mL of D-glucamine 95% (abcr) in 1x PBS, pH 9.75, and rinsed with mili-Q water. The relation of studied polypetides from TRIM21α protein is shown in Table 4.1.

4.3.4 Immobilisation of TROVE2 incubated with divalent cations

TROVE2 (33.3 mg/L) was incubated for an hour with a solution of 1 mM of magnesium, calcium (Panreac, Barcelona), strontium (Merck, 1000 mg/L solution) and barium chloride (MERCK, Madrid). After that, the protein was immobilized as previously described.

4.3.5 Calculation of the -Δf/ΔD ratio with the system at equilibrium

The -Δf/ΔD ratio shows the behaviour of the antigenic complex IgG-TRIM21α at equilibrium, highlighting the dependence of the interaction mechanism with respect to the employed biomarker. Certain approximations make the derivation of the -Δf/ΔD function more clear.

First, the dissipation (D) is quantified by means of the half-band-half-width, Γ and is defined as (Equation 1):

$$D = \frac{2\Gamma}{f_r} \qquad (1)$$

where Γ is half the bandwidth at half maximum of the resonance and f_r the real part of the complex resonance frequency. If we assume that the liquid is Newtonian with a density ρ_{liq} and a viscosity η, the equation 1 can be simplified as (Equation 2):

$$-\frac{\Delta f}{\Delta D} \approx \frac{\rho_f}{\rho_{liq} 4\pi\eta J'_f} \approx \frac{1}{4\pi\eta J'_f} \qquad (2)$$

where ρ_f is the average density of the film and J'_f the average value of the elastic compliance of the adlayer during the interval studied, which is directly proportional to the inverse of Young's modulus. Hence, the -Δf/ΔD ratio is an indicative value of this modulus; i.e. it shows the structural changes of the adlayer occurring during the protein-protein interaction.

4.3.6 Calculation of the instantaneous recognition of the proteins and IgGs though the -∂f/∂D function

-Δf *vs* ΔD plots are the most extended plots used to define mechanistic processes occurring at the sensor surface. These plots consists of discrete points representing the value of -Δf and ΔD at a particular time. Usually, -Δf *vs* ΔD plots provide an unambiguous identification of the structural transitions of the adlayer at equilibrium. However, the points (x, y) correspond to Δf(t), ΔD(t) so time is not an explicit parameter. This temporal information can be obtained from the novel -∂f/∂D function, which represents the punctual derivative of the resonance frequency with respect to the dissipation factor. It has the same meaning as the -Δf/ΔD ratio but it is measured point by point.

To calculate the -∂f/∂D function, motorization of the third harmonic due to its capacity to probe both the film on the chip and the bulk solution that is coupled to the surface, is carried out. After that, the –Δf(-t) and ΔD(-t) plots are represented. The processing of these signals take place representing the discrete-time signals as exponential functions. This exponential smoothing reduces irregularities (random fluctuations) in the original signal, so a clearer view of the true underlying behaviour of series is provided. Subsequently, both functions are derived with respect to time (-∂f/∂t and ∂D/∂t), dividing each other to obtain the expected -∂f/∂D function.

The derivative function is defined as the limit value of the ratio of the differences Δy/Δx as Δx becomes infinitely small. Thus, the -∂f/∂D function is described as the limit of the above commented -Δf/ΔD ratio (Equation 3):

$$-\frac{\partial \mathrm{f}}{\partial \mathrm{D}} = -\lim_{\Delta \mathrm{f} \to 0} \frac{\Delta \mathrm{f}}{\Delta \mathrm{D}} \approx \frac{\rho_f}{\rho_{liq} 4\pi\eta J_f'(t)} \qquad (3)$$

where ρ_f is the density of the film and $J_f'(t)$ the elastic compliance of the film at a given time when this one is in a liquid environment. Equation 3 can be further

simplified considering that the densities in soft-matter experiments usually are similar (Equation 4).

$$-\frac{\partial \mathrm{f}}{\partial \mathrm{D}} \approx \frac{1}{4\pi\eta J_f'(t)} \qquad (4)$$

The application of the Equation 4 requires films with a thickness of not more than a few nanometres in order to yield fair agreement with the full equation. Still, it holds quite generally that the shift in bandwidth is mostly affected by the elastic compliance of the film, rather than its viscous compliance. As commented above, the elastic compliance is the inverse of Young's modulus and therefore, the -∂f/∂D function is directly proportional to this modulus measured in real-time; that is, it defines the relationship between stress (force per unit area) and strain (proportional deformation) in an adlayer at a given time. So, the novel -∂f/∂D function is a measure of the instantaneous stiffness. Its value increases as the adlayer is more rigid. Furthermore, as time is an explicit parameter, it allows identifying reaction intermediates, as well as reacting products formed during the antigenic recognition. Also, it is possible quantify and separate the Young's modulus of all the species formed during biorecognition processes. Thus, the role of conformational dynamics in protein-protein interactions can be understood.

4.4 Characterization Techniques

4.4.1 Static Water Contact Angle (CA) Measurements

The wettability of the modified surfaces was determined by automated static water contact angle measurements (Krüss DSA German), WT-100 goniometer (volume of the drop of deionized water was 3.0 μL). The reported values are the average of at least two droplets, and the relative error is less than ±3°.

4.4.2 Infrared Reflection Absorption Spectroscopy (IRRAS)

IRRAS spectra were obtained with a Bruker Tensor 27 FT-IR spectrometer, using a commercial variable-angle reflection unit (Auto Seagull, Harrick Scientific, New York). A Harrick grid polarizer was installed in front of the detector and was used for measuring spectra with p-polarized radiation with respect to the plane of incidence at the sample surface. Single channel transmittance spectra were collected at 80° using 2048 scans in each measurement. The raw data were subtracted by the data recorded on a freshly cleaned reference Au surface, after which a baseline correction was applied to give the reported spectra.

4.4.3 X-ray Photoelectron Spectroscopy (XPS)

The XPS analysis of surfaces was performed using a JPS-9200 photoelectron spectrometer (JEOL, Japan). Survey and high resolution spectra were obtained under ultra-high vacuum conditions using monochromatic Al Kα X-ray radiation at 12 kV and 20 mA, and an analyzer pass energy of 50 eV for wide scans and 10 eV for narrow scans. The emitted electrons were collected at 10° from the surface normal (take off angle relative to the surface normal 10°). All XPS spectra were evaluated by using Casa XPS software (version 2.3.15). Survey spectra were corrected with linear background before fitting, whereas high-resolution spectra were corrected with Shirley background. Atomic area ratios were determined after a baseline correction and normalizing the peak area ratios by the corresponding atomic sensitivity factors (1.00 for C1s, 1.80 for N1s, 2.93 for O1s, 19.8 for au4d, and 1.68 for S2p).

4.5 Dual Polarization Interferometry

DPI measurements were carried out in an Analight Bio200 Dual Polarization Interferometer (Farfield Scientific Ltd., Crewe, UK) of a helium neon laser (λ=632.8 nm and 20 mW), a 1024x1024 element-imaging device, and a sensor chip clamped inside a thermostated (temperature control within 1 mK) block. The state of polarization of light was switched on a 2 ms cycle between transversal electric and magnetic modes using a ferroelectric crystal, before passing through the sensor. The interference pattern formed in the far-field was detected on the opposing side by the element-imaging device. Data acquisition and treatment were carried out by using Analight DAQ and Analight Explorer software packages (Farfield, United Kingdom), respectively. Solutions were flowed by a double-channel precision syringe pump (Harvard Apparatus PHD 2000 Infusion, Kent, UK) and the injections were carried out by using two high-performance chromatography valves connected in serie. During the entire experiment, solutions were injected in volumes of 250 µL and the flow was maintained at a constant rate of 20 µL min^{-1}.

4.5.1 Chip treatment

The activation of the DPI chip (FB100, Farfield, UK) was achieved by immersing the chip overnight in chromic mixture (100 g/L $K_2Cr_2O_7$ in 85% H_2SO_4). Then, the chip was rinsed with deionized water, dried with nitrogen and submerged in 20 % HNO_3 for 2 h. After rinsing with deionized water and drying with nitrogen, the activated chip was immersed in 1% of carboxyethylsilanetriol sodium salt (25% in water), cleaned with water and placed in an oven at 110 °C for 1 h. A phosphate buffered saline (PBS, 10 mM phosphate, 137 mM NaCl, 2.7 mM NaCl, pH 7.4) solution filtered through a 0.45 µm PVDF membrane and degassed by sonication was used as carrier. This protocol was also used to prepare the solutions injected unless otherwise stated. After treatment, the chip was mounted on the setup and an injection

of 0.2 M 3-(3-dimethylaminippropyl)-carbodiimide (EDC) and 0.05 M N-hydroxysuccinimide (NHS) in water followed by an injection of 5 mM of carbohydrazide in water were done.

TRIM21α or TROVE2 were immobilized by injecting a 33 mg/L solution of these proteins (100 µL). After that an injection of 2 mg/L of glucamine in PBS (pH 9.75) was made, in order to block the residual activated sites.

4.5.2 Determination of the Thickness per molecule

Equations 1 and 2 were used to calculate the thickness change per adsorbed molecule measured in real-time. For that, a special case where the captured ligand is unique is considered (Equation 5 and 6):

$$\Delta T = \frac{1}{N_T} \sum \Delta m_i \left(\frac{\Delta Thickness}{molecule} \right)_i \quad (5)$$

$$\left(\frac{\Delta Thickness}{molecule} \right)_1 = \frac{\Delta T}{\Delta m_1} \cdot N_T \left(\frac{nm}{molec.} \right) \quad (6)$$

where ΔT is the thickness change of the adlayer in nanometers, Δm is the surface concentration in nanograms per millimeter and N_T the surface concentration at saturation (nm molec^{-1}). The thickness per molecule of antigenic complexes, $\frac{\Delta Thickness}{molecule}$, can be so compared in real-time with the theoretical dimensions of the ligand, which allows the role of conformational dynamics during the protein-ligand interactions to be understood.

4.6 Prediction of TRIM21α structure

A preliminary model of the TRIM21α structure was predicted using homology-modelling by templating and threading methods using the servers LOMETS and SWISS MODEL.[2-5] The results given by SWISS MODEL were preferably used and only fragments that were not predicted by this server were taken from the results given by performing threading with LOMETS. Templates used for building the model were PDB ids 4CG4, 4AP4, 4TN3 and 2IWG. The different pieces obtained were manually modelled together and the final coordinates subjected to a mild energy minimization followed by a short molecular dynamics simulation with AMBER.[6]

4.7 DVD based immunoassay

Digital versatile disc provided by Media Range (16x speed high burner compatibility) were used to carry out the diagnostic assay. TROVE2 and TRIM21 proteins (40 mg/L in PBS1X buffer) were dispensed on the platform in microarray format by a noncontact nanoprinter (AD 1500 BioDot, Inc., Irvine, CA, dots of 25 nL, 20 arrays 3X3). The coupling reaction was carried out in an oven at 37 °C. Then, surfaces were rinsed with PBS-T and mili-Q water and dried by centrifugation. The assay consisted of dispensing 25 µL of the serum samples of SLE patients and health subjects diluted in 1/100 over the array, incubated 15 min at 37 °C. After that, the microarray was rinsed with PBS-T and mili-Q water and dried by centrifugation. Then, the DVD was incubated with 25 µL of Goat to human IgG (Abcam, gold small 1.4 nm) diluted in PBS-T (1/1000), also at 37 °C. Next, the assay was rinsed with PBS-T and mili-Q water, and dried by centrifugation. Silver enhancer solution (A and B, Sigma) was applied (25 µL in each matrix), reacting during 8 min. After that, the disc surface was rinsed with water and dried by centrifugation. After that, the disc

surface was rinsed with water and dried by centrifugation and the silver precipitated was measured by disc drive.[7]

4.8 References

1. Petri M *et al.* (2012) *Art Rheum* 64:2677–86.

2. Wu S, Zhang, Y (2007) *Nucleic Acid Res* 35:3375–3382.

3. Biasini, M, Biasini M, Bienert S, Waterhouse A, Arnold K, Studer G, Schmidt T, Kiefer F, Gallo Cassarino T, Bertoni M, Bordoli L, Schwede T (2014) *NucleicAcid Res* 42:W252–W258.

4. Bordoli L, Kiefer F, Arnold K, Benkert P, Battey J, Schwede T (2008) *Nat Protoc* 4:1–13.

5. Arnold K, Bordoli L, Kopp J, Schwede T (2006) *Bioinformatics* 22:195–201.

6. Case DA, Betz RM, Botello-Smith W, Cerutti DS, Cheatham TE, Darden TA, Duke RE, Giese TJ, Gohlke H, Goetz AW, Homeyer N, Izadi S, Janowski P, Kaus J, Kovalenko A, Lee TS,LeGrand S, Li P, Lin C, Luchko T, Luo R, Madej B, Mermelstein D, Merz KM, Monard G, Nguyen H, Nguyen HT, Omelyan I, Onufriev A, Roe DR, Roitberg A, Sagui C, Simmerling CL, Swails J, Walker RC, Wang J, Wolf RM, Wu W, Xiao L, York DM, Kollman PA (2010) *AMBER 11*, University of California (San Francisco).

7. Morais S, Tortajada-Genaro LA, Arnandis-Chover T, Puchades R, Maquieira A., (2009) *Anal Chem* 81:5646–5654.

5. General Discussion

According to the results obtained in this research, we suggested that an antibody bipolar bridging mechanism may contribute to the pathogenic accumulation of anti–TRIM21 autoantibody immune complex in autoimmune diseases. Interestingly, TRIM21 mostly can be found inside the cell, in the cytoplasm and in the nucleus.[1,2] Consequently, it is not possible for antibodies to be raised against TRIM21. Neutrophil apoptosis solve this paradox, given that apoptotic cells are widely believed to serve as the source of intracellular immunogen for antinuclear antibodies production, potentially via the generation of cryptic B and/or T cell epitopes.[3] Accordingly, both apoptosis and autoantibodies could be important factors associated with disease activity in the pathogenesis of SLE.[4] Furthermore, TRIM21 can translocate from the cytoplasm to cell surface during early apoptosis, independently of TROVE2 and La proteins in apoptotic or stressed cells.[5] Hence, the immune response should be due to the surface membrane expression of TRIM21 components during different phases of apoptosis, as described in apoptotic fetal cardiomyocytes.[6] Furthermore, Shusta *et. al.* found that after interaction with circulating autoantibodies, TRIM21 protein translocates to the plasma membrane.[7] Thus, we can conclude that the above mapped epitopes act as real apotopes (epitopes expressed on apoptotic cells), remaining accessible on the cell surface throughout early and late apoptosis. This role could explain the bipolar bridging mechanism described for the TRIM21 molecular biorecognition.

The fine epitope mapping shows the existence of different induction pathways of human anti–TRIM21 autoimmunity, given that different apotopes are found depending on the population under study. Hence, we suggest that B cell responses against a TRIM21 apotope exposed on early apoptotic cells identify a subset of SLE patients. The different patterns of human anti–TRIM21 autoimmunity are known to be strongly influenced by the HLA phenotype that controls the degree of intermolecular epitope spreading from TRIM21. Accordingly, we have shown that the SLE autoantibodies could be related with a specific haplotype associated to the allele DRB1*13:04. Consequently, the distribution of HLA class II alleles in the

subset of TRIM21 apotope–positive patients, in combination with an investigation of genes involved in the clearance of apoptotic cells and B cell tolerance, will hopefully lead to a deeper knowledge of anti–TRIM21 autoimmunity pathways and provide new insights for understanding the pathogenesis of SLE.

Furthermore, the preliminary model allows easily relating the NF–κB signalling activity to the functional mechanism of TRIM21. This protein can stimulate the NF–κB pathway via IκB kinase.[8] TRIM21 catalyses monoubiquitination of IKKβ in cooperation with the ubiquitin–conjugating enzyme UbcH5b.[8] Hence, according to Sanchez et al., we suggest that the TRIM21 binds to IKKβ via the PRY–SPRY domain, and the RING domain monoubiquitylates it through UbcH5b.[9] Thus, fusion of IKKβ with ubiquitin inhibits its function, suggesting a negative role of monoubiquitination in IKKβ.[9] Consistently, TRIM21 overexpression suppress IKKβ–mediated NF–κB activation and TRIM21α–deficiency displays hyperactivation of NF– κB in response to toll–like receptor stimulation.[10] When TRIM21 targets antibody–bound virus (incoming virus–antibody complexes in the cytoplasm), the PRY–SPRY domains of the homodimer away inhibiting the IKKβ recognition and its monoubiquitination. As shown in Figure 5.1, viruses so activate the IKKβ–mediated NF–κB pathway, according to Fletcher et al.[8]

In the cytoplasm, when TRIM21 targets antibody–bound virus, the PRY–SPRY domains of the homodimer is occupied, inhibiting the IKKβ and IRF3/7 recognition and monoubiquitination, leading the IKKβ degradation and the NF–κB activation (nucleus). On the other side, TRIM21 binds to IKKβ via the PRY–SPRY domain and the RING domain monoubiquitylates it through UbcH5b. This fusion inhibits its function, suggesting a negative role of monoubiquitination in IKKβ, leading the non-activation of the NF–κB factor. Similarly, the IRF3/7 binds to the PRY–SPRY domain of the TRIM21 protein and monoubiquitinates, preventing the activation of the NF– κB factor.

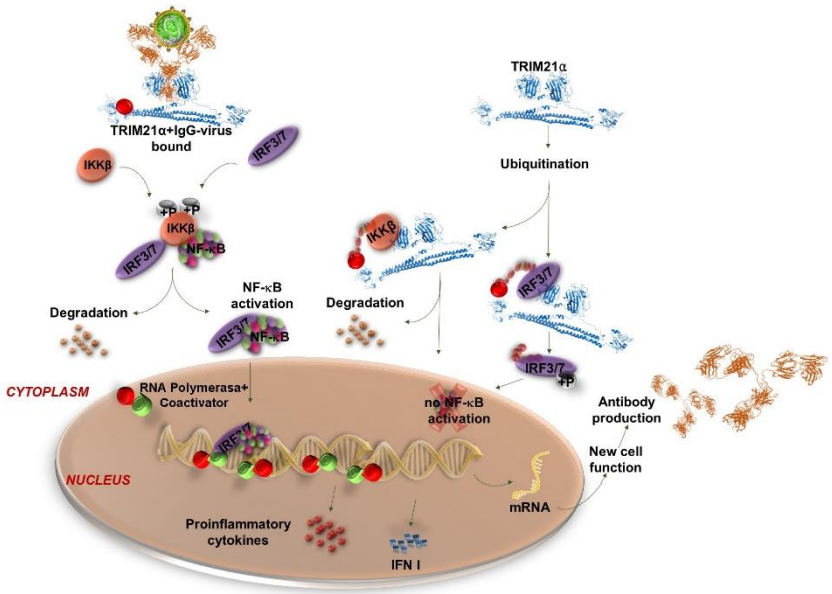

Figure 5.1 Integrative scheme of the TRIM21 functional mechanism.

In the same way, the PRY–SPRY domain of TRIM21 is known to be essential for binding of substrates, such as IRF3, IRF7, and IRF8.[11,12,13] Hence, the same structural mechanism can be considered in the polyubiquitination of these interferons, leading to a reduction in their levels by promoting degradation. We also present (Figure 5.1) how IRF binds to TRIM21 through the PRY–SPRY domain and the RING domain polyubiquitylates via an ubiquitin–conjugating enzyme, such as UbcH5b, in accordance with recent studies that suggest that IRFs potentially contribute to pathomechanisms of SLE.[11] The fact that TRIM21 malfunction is related to a polymorphism may explain the abnormal expression of interferon regulatory factors related to the pathogenesis of SLE.

On the other hand, anti–TROVE2 autoantibodies are key mediators in determining the clinical manifestations of SLE, however the precise cooperation of antibodies in SLE have not been unraveled so far.[14] Considering Lisi's results, anti–TROVE2 autoantibodies are cell-penetrating antibodies.[15] Hence, according to our

results and considering that anti–TROVE2 levels in SLE patients is elevated in comparison to healthy subjects, these autoantibodies induce the TROVE2 aggregation by means of a bipolar bridging mechanism. Consequently, they induce the inhibition of degradative activity of the TROVE2 autoantigen in SLE disease. This aggregation would so imply the accumulation of the Alu RNAs, stimulating intracellular RNA sensors to induce inflammatory responses (Figure 5.2). As a result, there is growing evidence that excess cellular RNA drives an interferon response that, by revving up the immune system, contributes to the initial lupus development.[16] Furthermore, it agrees with the fact that antibodies enter cells react with ribonucleoproteins, and potentially contribute to autoimmune disease by interfering with the functions of their targets.[17] These data also support the hypothesis that the inflammatory sequelae associated with anti–TROVE2 autoantibodies are due to the RNA–binding properties of TROVE2.[18] Furthermore, TROVE2 becomes self–aggregated by cell stress from lupic patients.[19]

Thus, Alu RNA accumulation will increase oxidative stress, which is associated with cellular Ca^{2+} deregulation, mitochondrial hyperpolarization (MHP) and necrosis.[20] The increase of intracellular level of calcium favors the TRIM21–TROVE2 binding through the PRY–SPRY domain. In the Chapter II, it is presented that antibodies have an inhibitory effect on the TRIM21 physiological function due to the Fc biorecognition via the PRY–SPRY domain. Consequently, TROVE2 may have the same inhibitory effect on the TRIM21 protein. This inhibition could easily explain the fact that the TRIM21 and IFN–α genes are overexpressed in SLE patients compared with healthy controls, given that TRIM21 is known as a negative regulator of type I IFN.[21] Elevated IFN–I expression is associated with severe disease, renal involvement (common in SLE patients) and autoantibodies against dsDNA and RNA-associated antigens, such as TROVE2, TRIM21, Sm/nRNP and SSB/La.[22] Thus, the levels of IFN–I are expected to enhance anti–TROVE2 autoantibodies in a positive feedback loop. Given the pathogenic role of TRIM21 and TROVE2 in systemic

autoimmunity, these findings might have important implications for the development of novel therapeutics for autoimmune diseases, such as SLE.

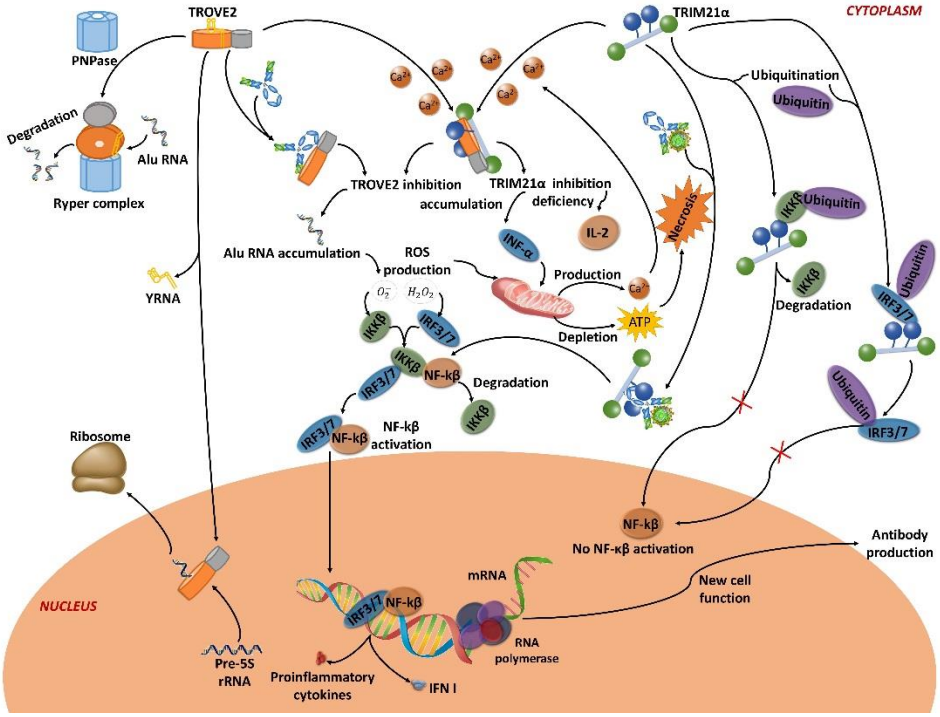

Figure 5.2 Scheme for the physiological function of the TROVE2 host-guest chemistry

This study has allowed developing a practical application. Thus, the QCM-based biosensor using immunoassay principles has been capable to discriminate between SLE patients and healthy people. The study has included serum samples from 145 SLE patients and 8 control subjects. Furthermore, the performances of the biosensor were compared with that obtained by reference methods, corroborating the viability of piezoelectric biosensor as a cost-effective *in vitro* assay for the early detection, monitoring or treatment of the SLE disease.

5.1 References

1. Foss S, Watkinson R, Sandlie I, James LC, Andersen JT (2015) *Immunol Rev* 268:328–339.

2. Defendenti C, Atzeni F, Spina MF, Grosso S, Cereda A, Guercilena G, Bollani S, Saibeni S, Puttini PS (2011) *Autoimmun Rev* 10:150–154.

3. Pan ZJ, Maier S, Bachmann MP, Kim-Howard XR, Keech C, Gordon TP, McCluskey J, Farris AD (2006) *Clin Exp Immunol* 143:237–248.

4. Su YJ, Cheng TT, Chen CJ, Chiu WC, Hsu CY, Chang WN, Tsai NW, Kung CT, Wang HC, Lin WC, Huang CC, Chang YT, Su CM, Chiang YF, Cheng BC, Lin YJ, Lu CH (2013) *J Transl Med* 11:2–7.

5. Ohlsson M, Jonsson R, Brokstad KA (2002) *Scand J Immunol* 56:456–469.

6. Yoshimi R, Ishigatsubo Y, Ozato K (2012) *Int J Rheumatol* 2012:1–11.

7. Shusta EV, Li J, Boado JB, Pardridge WM (2003) *Neuroreport* 14:1861–1865.

8. Fletcher AJ, Mallery DL, Watkinson RE, Dickson CF, James LC (2015) *Proc Nat Acad Sci USA* 112:10014–10019.

9. Wada K, Niida M, Tanaka M, Kamitani T (2009) *J Biochem* 146:821–32.

10. Yoshimi R, Chang TH, Wang H, Atsumi T, Morse HC, Ozato K (2009) *J Immunol* 182:7527–38.

11. Stacey KB, Breen E, Jefferies CA (2012) *PLoS One* 7:e34041.

12. Randow F, MacMicking JD, James LC (2013) *Science* 340:701–706.

13. Munir M (2010) *Sci Signal* 3:1–4.

14. Gatto M Iaccarino L, Ghirardello A, Punzi L1, Doria A (2016) *J Autoimmun* 69:1-11.

15. Lisi S, Sisto M, Scagliusi P, Mitolo V, D'Amore M (2007) *Panminerva Med* 49:103-108.

16. Hu X, Chakravarty SD, Ivashkiv LB (2008) *Immunol Rev* 226:41-56.

17. Feuerstein GZ, Liu T, Barone FC (1994) *Cerebrovasc Brain Metab Rev* 6:341-360.

18. Reed JH, Gordon TP (2016) *Rheumatol* 12:136-138.

19. Sánchez-Rodríguez S, Herrera-van Oostdam D, Avalos-Díaz E, Herrera-Esparza R (2007) *Reumatismo* 59:292-298.

20. Wang W (2016) *Mol Cell Endocrinol.* 426:91-100.

21. Manocha GD, Mishra R, Sharma N, Kumawat KL, Basu A, Singh SK (2014) *J Neuroinflammation* 11:24.

22. Kellner ES, Lee PY, Li Y, Switanek J, Zhuang H, Segal MS, Sobel ES, Satoh M, Reeves WH (2010) *J Neuroimmunol* 223:13-19.

6. Conclusions

Since the mechanism of action of the TRIM21 and TROVE2 proteins with autoantibodies was not described, the goal of this research was to establish the molecular recognition of both proteins with autoantibodies of SLE patients and healthy subjects.

Using a Quartz Crystal Microbalance with Dissipation sensor (QCM–D) and Dual Polarization Interferometry (DPI), was possible to compare the dry mass and the solvation sphere of the proteins and the immunocomplex (protein–IgG) interaction, which provided a better understanding of the recognition between the proteins and autoantibodies.

The $-\partial f/\partial D$ function provided an unambiguous identification of the structural transitions of the adsorbed layer, and can be used as a tool to measure the conformational dynamics of proteins. Most importantly, this function allows to identify antigenic complexes which are formed during the molecular recognition. By applying in measurements with the TRIM21α protein, the interpretation can be used as a fingerprint for the interaction between biomarker and antigen. In addition, the application of this novel function can be extended to other biological interactions.

It is possible to calculate the kinetic parameters involving the proteins and anti–TRIM21/TROVE2 antibodies, and the model demonstrated that the autoantibodies interact in an antibody–bipolar–bridging manner.

Interestingly, there are no reports in the literature explaining the interaction between anti–TRIM21/TROVE2 antibodies from samples of health donors and TRIM21-TROVE2 recognition. Thus, to locate the epitope correspondent to the recognition of health donors for TRIM21α, the correlation between epitopes recognized by the autoantibodies from both, healthy subjects and SLE patients, was studied. For that, were mapped the dominant antigenic regions of TRIM21α in anti–TRIM21+ patients and health subjects, registering the piezoelectric signals by a QCM–D sensor. The mapped encountered region allowed us to correlate the genetic predisposition and predict symptoms in anti–TRIM21 SLE patients, by finding the alleles involved in SLE manifestation. Thus, was encountered different epitopes for

SLE patients and healthy subjects in TRIM21α, by studying the autoantibodies interactions with sequences of synthetic polypeptides. This mapping helped the development of a predicted model of the structure of protein, once the entire structure was not published. In addition, was possible to present the conformation of the TRIM21α when interacting with autoantibodies.

Analysis of the TROVE2 interaction with different cations showed that depending of the cation, this protein can bind to another proteins. This was corroborated when proved the interaction of TROVE2 and TRIM21α with and without alkaline earth cations in the TROVE2 structure. The presence of calcium cation favors the binding of TRIM21α and TROVE2, through the MIDAS motif.

Finally, it has been developed a label free biosensor that can monitor the evolution of SLE anti–TRIM21/TROVE2+ patients. Interestingly, bioestatistical data shows that the level of autoantibodies TRIM21α/TROVE2 are related and it may be connected with the patient symptoms. The immunosensor, adapted to a more practical device, make easy monitoring in routine screening SLE patients.

Actually, the lupus diagnosis is realized in a subjective manner based on eleven AC/SLICC criteria. The developed biosensor can help to the prognosis and diagnosis of Systemic Lupus Erythematosus in an objective manner, although a future clinical validation is required.

7. Appendix

Appendix

Table A Systemic Lupus Erythematosus Disease Activity Index *

Criterion	Definition
Seizure	Recent onset
New Malar Rash	New onset or recurrence of an inflammatory type of rash
Psychosis	Altered ability to function in normal activity due to severe disturbance in the perception of reality. Includes hallucinations, incoherence, marked loose associations, impoverished thought content, marked illogical thinking, exclude the presence of uremia and offending drugs.
Alopecia	A patch of abnormal, diffuse hair loss.
Organic Brain syndrome	Altered mental function with impaired orientation or impaired memory or syndrome other intellectual function, with rapid onset and fluctuating clinical features
Mucous membrane	Recurrence of oral or nasal ulcerations
Visual	Cytoid bodies, retinal hemorrhages, serous exudates or hemorrhages in the choroid, optic neuritis
Pleurisy	Pleuritic chest pain with pleural rub or effusion, or pleural thickening.
Cranial Nerve	Sensory or motor neuropathy involving a cranial nerve

* Egner W (2000) *J Clin Pathol* 53:424–432

Appendix

Table A cont. Systemic Lupus Erythematosus Disease Activity Index *

Criterion	Definition
Pericarditis	Pericardial pain with at least one of rub or effusion. Confirmation by electro- or echocardiography
Lupus headache	Severe, persistent headache; may be migranous; unresponsive to narcotics
Low complement	Decrease in CH50, C3, or C4 level
Cerebrovascular accident	New syndrome
Increased DNA binding	More than 25% binding by Farr assay (to >the upper limit of the laboratory-determined normal range, e.g. 25%).
Vasculitis	Ulceration, gangrene, tender finger nodules, periungual infarction, splinter hemorrhages. Vasculitis confirmed by biopsy or angiogram.
Arhtritis	More than 2 joints with pain and signs of inflammation
Fever	More than 38 ºC after the exclusion of infection
Myositis	Proximal muscle aching or weakness associated with elevated creatine phosphokinase/aldolase levels, electromyographicchanges, or a biopsy showing myositis.
Casts	Heme, granular, or erythrocyte.
Thrombocytopenia	Fewer than 100,000 platelets
Hematuria	More than 5 erythrocytes per high power field
Proteinuria	More than 0.5 grams of urinary protein excreted per 24h
Pyuria	More than 5 leukocytes per high-power field
Leukopenia	Leukocyte count of < 3000/mm^3

* Egner W (2000) *J Clin Pathol* 53:424–432

Appendix

Scheme A TRIM21α aminoacid sequence *

```
         10          20          30          40          50
MASAARLTMM WEEVTCPICL DPFVEPVSIE CGHSFCQECI SQVGKGGGSV
         60          70          80          90         100
CPVCRQRFLL KNLRPNRQLA NMVNNLKEIS QEAREGTQGE RCAVHGERLH
        110         120         130         140         150
LFCEKDGKAL CWVCAQSRKH RDHAMVPLEE AAQEYQEKLQ VALGELRRKQ
        160         170         180         190         200
ELAEKLEVEI AIKRADWKKT VETQKSRIHA EFVQQKNFLV EEEQRQLQEL
        210         220         230         240         250
EKDEREQLRI LGEKEAKLAQ QSQALQELIS ELDRRCHSSA LELLQEVIIV
        260         270         280         290         300
LERSESWNLK DLDITSPELR SVCHVPGLKK MLRTCAVHIT LDPDTANPWL
        310         320         330         340         350
ILSEDRRQVR LGDTQQSIPG NEERFDSYPM VLGAQHFHSG KHYWEVDVTG
        360         370         380         390         400
KEAWDLGVCR DSVRRKGHFL LSSKSGFWTI WLWNKQKYEA GTYPQTPLHL
        410         420         430         440         450
QVPPCQVGIF LDYEAGMVSF YNITDHGSLI YSFSECAFTG PLRPFFSPGF
        460         470
NDGGKNTAPL TLCPLNIGSQ GSTDY
```

*Henning *et al.* (2005) *J Biol Chem* 39:33250–61.

Appendix

Scheme B TROVE2 aminoacid sequence*

```
        10         20         30         40         50
MEESVNQMQP LNEKQIANSQ DGYVWQVTDM NRLHRFLCFG SEGGTYYIKE
        60         70         80         90        100
QKLGLENAEA LIRLIEDGRG CEVIQEIKSF SQEGRTTKQE PMLFALAICS
       110        120        130        140        150
QCSDISTKQA AFKAVSEVCR IPTHLFTFIQ FKKDLKESMK CGMWGRALRK
       160        170        180        190        200
AIADWYNEKG GMALALAVTK YKQRNGWSHK DLLRLSHLKP SSEGLAIVTK
       210        220        230        240        250
YITKGWKEVH ELYKEKALSV ETEKLLKYLE AVEKVKRTRD ELEVIHLIEE
       260        270        280        290        300
HRLVREHLLT NHLKSKEVWK ALLQEMPLTA LLRNLGKMTA NSVLEPGNSE
       310        320        330        340        350
VSLVCEKLCN EKLLKKARIH PFHILIALET YKTGHGLRGK LKWRPDEEIL
       360        370        380        390        400
KALDAAFYKT FKTVEPTGKR FLLAVDVSAS MNQRVLGSIL NASTVAAAMC
       410        420        430        440        450
MVVTRTEKDS YVVAFSDEMV PCPVTTDMTL QQVLMAMSQI PAGGTDCSLP
       460        470        480        490        500
MIWAQKTNTP ADVFIVFTDN ETFAGGVHPA IALREYRKKM DIPAKLIVCG
       510        520        530
MTSNGFTIAD PDDRGMLDMC GFDTGALDVI RNFTLDMI
```

*Reed JH, Clancy RM, Purcell AW, Kim MY, Gordon TP, Buyon JP (2011) *J Immunol* 187:520–526

Appendix

Table B Anti-TRIM21/TROVE ELISA results of samples from patients (LES) and healthy controls (LESC)

Sample	TRIM21 (U/mL)	TROVE2(U/mL)
LES14_001	1.56	3.13
LES14_002	>200	>200
LES14_003	2.34	1.95
LES14_004	0.78	0.78
LES14_005	0.78	0.00
LES14_006	33.59	0.39
LES14_007	0.78	0.39
LES14_008	2.34	0.00
LES14_009	1.17	0.78
LES14_010	5.47	24.22
LES14_011	>200	56.25
LES14_012	5.08	5.47
LES14_013	3.13	0.78
LES14_014	16.41	39.84
LES14_015	1.17	0.78
LES14_016	1.95	3.91
LES14_017	1.17	3.13
LES14_018	1.95	42.00
LES14_019	1.17	2.34
LES14_020	3.91	16.00

Table B cont. Anti-TRIM21/TROVE ELISA results of samples from patients (LES) and healthy controls (LESC)

Sample	TRIM21 (U/mL)	TROVE2(U/mL)
LES15_001	1.87	2.17
LES15_002	2.45	52.00
LES15_003	0.52	1.94
LES15_004	210.56	200.00
LES15_005	210.33	200.00
LES15_006	1.62	5.86
LES15_007	38.33	68.44
LES15_008	1.68	6.59
LES15_009	3.38	13.11
LES15_010	110.06	83.66
LES15_011	0.67	0.47
LES15_012	1.27	-0.53
LES15_013	1.37	0.43
LES15_014	1.27	1.69
LES15_015	57.12	63.00
LES15_016	0.23	0.03
LES15_017	0.30	1.50
LES15_018	217.23	200.00
LES15_019	230.36	112.68
LES15_020	0.45	-0.45

Appendix

Table B cont. Anti-TRIM21/TROVE ELISA results of samples from patients (LES) and healthy controls (LESC)

Sample	TRIM21 (U/mL)	TROVE2(U/mL)
LES15_021	139.84	85.53
LES15_022	0.58	17.81
LES15_023	98.18	44.16
LES15_024	192.52	200.00
LES15_025	109.62	2.39
LES15_026	0.08	1.94
LES15_027	0.39	0.47
LES15_028	91.15	5.02
LES15_029	0.77	3.16
LES15_030	2.77	77.01
LES15_031	83.06	-0.60
LES15_032	73.35	0.51
LES15_033	0.42	0.47
LES15_034	0.14	1.91
LES15_035	230.09	149.12
LES15_036	122.05	18.56
LES15_037	145.04	-0.05
LES15_038	0.96	-0.38
LES15_039	0.01	-0.42
LES15_040	1.43	27.58

Table B cont. Anti-TRIM21/TROVE ELISA results of samples from patients (LES) and healthy controls (LESC)

Sample	TRIM21 (U/mL)	TROVE2(U/mL)
LES15_041	225.12	200.00
LES15_042	0.26	8.20
LES15_043	211.23	200.00
LES15_044	1.14	0.18
LES15_045	2.83	0.03
LES15_046	122.54	113.37
LES15_047	221.84	200.00
LES15_048	0.36	14.03
LES15_049	0.36	0.06
LES15_050	0.17	-0.23
LES15_051	238.74	97.20
LES15_052	0.52	2.57
LES15_053	0.23	0.10
LES15_054	-0.11	-0.56
LES15_055	0.14	57.49
LES15_056	103.05	1.72
LES15_057	0.33	-0.19
LES15_058	19.70	12.92
LES15_059	0.89	0.40
LES15_060	39.64	81.36

Appendix

Table B cont. Anti-TRIM21/TROVE ELISA results of samples from patients (LES) and healthy controls (LESC)

Sample	TRIM21 (U/mL)	TROVE2(U/mL)
LES15_061	0.05	-0.68
LES15_73	196.76	1.17
LES15_74	2.32	0.29
LES15_75	3.09	0.73
LES15_76	1.14	9.22
LES15_77	224.10	200.00
LES15_78	33.23	1.58
LES15_79	214.42	-0.49
LES15_80	215.82	200.00
LES15_81	1.21	-0.38
LES15_82	232.26	51.84
LES15_83	0.70	0.29
LES15_84	0.42	-0.27
LES15_85	74.72	11.57
LES15_86	229.29	200.00
LES15_87	205.76	78.89
LES15_88	2.51	4.77
LES15_89	2.51	0.58
LES15_90	0.14	-0.75
LES15_91	0.30	-0.71

Appendix

Table B cont. Anti-TRIM21/TROVE ELISA results of samples from patients (LES) and healthy controls (LESC)

Sample	TRIM21 (U/mL)	TROVE2(U/mL)
LES15_92	101.91	31.02
LES15_93	37.89	41.27
LES15_94	200.55	18.93
LES15_95	0.67	-0.82
LES15_96	-0.64	-0.90
LES15_97	0.86	-0.94
LES15_98	1.08	76.28
LES15_99	22.20	-0.53
LES15_100	0.42	200.00
LES15_101	181.60	10.61
LES15_102	16.37	29.02
LES15_103	0.80	14.21
LES15_104	68.86	0.25
LES15_105	1.87	-0.90
LES15_106	-0.33	-0.64
LES15_107	-0.39	-0.75
LES15_108	0.17	1.25
LES15_109	0.45	34.33
LES15_110	12.69	2.35
LES15_111	3.67	0.21

Table B cont. Anti-TRIM21/TROVE ELISA results of samples from patients (LES) and healthy controls (LESC)

Sample	TRIM21 (U/mL)	TROVE2(U/mL)
LES15_112	0.14	-0.71
LES15_113	0.26	2.97
LES15_114	0.67	13.59
LES15_115	0.92	13.84
LES15_116	134.56	200.00
LES15_117	230.90	200.00
LES15_118	206.18	7.36
LES15_119	70.17	0.47
LES15_120	40.13	-0.86
LES15_121	1.97	-1.01
LES15_122	1.11	4.55
LES15C_001	0.70	-0.71
LES15C_002	0.17	1.06
LES15C_003	0.17	-0.86
LES15C_004	0.26	-0.90
LES15C_005	0.83	1.06
LES15C_006	1.71	6.30
LES15C_007	1.97	2.28
LES15C_008	-0.11	-0.71
LES16C_009	0.55	0.51

Table B cont. Anti-TRIM21/TROVE ELISA results of samples from patients (LES) and healthy controls (LESC)

Sample	TRIM21 (U/mL)	TROVE2(U/mL)
LES16C_010	0.61	4.00
LES16C_011	-0.11	0.77
LES16C_012	0.64	0.69
LES16C_013	-0.02	0.51
LES16C_014	0.48	3.45
LES16C_015	-0.02	0.69
LES16C_016	0.48	0.43
LES16C_017	0.52	1.72
LES16C_018	1.97	2.64
LES16C_019	0.20	-0.49
LES16C_020	0.64	1.58
LES16C_021	0.64	0.21
LES16C_022	0.42	1.43
LES16C_023	0.86	2.83
LES16C_024	0.17	-0.79
LES16C_025	1.81	5.43
LES16C_026	2.03	1.02
LES16C_027	3.86	-0.01
LES16C_028	1.43	-0.45
LES16C_029	1.90	-0.82

Appendix

Table B cont. Anti-TRIM21/TROVE ELISA results of samples from patients (LES) and healthy controls (LESC)

Sample	TRIM21 (U/mL)	TROVE2(U/mL)
LES16C_030	1.24	-0.19
LES16C_031	2.13	0.80
LES16C_032	41.23	10.28
LES16C_033	0.96	3.30
LES16C_034	1.40	-0.64